The fate of residual sulphur from coal injection during ironmaking processes

A thesis submitted in partial fulfilment
of the requirements for the degree of

Doctor of Philosophy

Chay Anthony Davies-Smith

School of Engineering
Cardiff University
November 2023

Abstract

Coal injection is utilised in modern blast furnaces as a method of reducing the consumption of coke, the production of which is expensive and energy intensive. Sulphur is an impurity introduced into the blast furnace predominantly from the use of coke and coal. High levels of sulphur in steel can lead to increased brittleness in a heated state. However, removal of hot metal sulphur reduces the yield and incurs additional costs.

This study identified the routes through which sulphur from coal injection leaves the furnace and whether coal or process parameters can affect this.

A drop tube furnace was used to study the volatilisation of coal sulphur from four blast furnace injection coals. The greatest contributing factor to the volatilisation of coal sulphur was the burnout of the char. H_2S was measured as the major gaseous sulphur product during the partial combustion of the coal in the drop tube furnace.

The use of alternative solid fuels in a coal blend was shown to affect the char burnout and sulphur volatilisation in the drop tube furnace. The addition of H_2 and CO_2 to the gas atmosphere of the drop tube furnace was shown to affect the char burnout and sulphur volatilisation of the injected coals.

The relative sulphur fixation capacities of blast furnace charge materials across a temperature range of 150-900°C were studied using a synthetic blast furnace top gas containing 500 ppm of H_2S. The charged materials were shown to partially fix the gaseous sulphur, with fixation occurring predominantly at higher temperatures.

The raceway was suggested as the primary source of volatilised sulphur in the top gas. The increased volatilisation of blast furnace sulphur was shown to be beneficial for the lowering of the sulphur load of the furnace, which in turn can facilitate a reduction of the coke rate.

Publications, presentations, and posters

Publications

Davies-Smith, Chay A., Julian M. Steer, Richard Marsh, and David Morgan. “A Study of the Volatilisation of Coal Sulphur during Combustion under Conditions Similar to a Blast Furnace Raceway.” Fuel 330 (December 15, 2022): 125552. https://doi.org/10.1016/j.fuel.2022.125552.

Presentations

“The study of sulphur emission in the raceway region of a blast furnace”, The Fuel and Energy Research Forum’s 1st FERIA “The European Conference on Fuel and Energy Research and its Applications”, Monday-Wednesday 6th-8th September 2021, Jubilee Conference Centre, University of Nottingham, UK.

“Potential Issues for Consideration when Incorporating Alternative Injectants into a Blast Furnace”, The Fuel and Energy Research Forum’s Fuel Characterisation, up-grading and carbonisation/electricity generation and storage interest group seminars “Decarbonisation of the steel industry/decarbonisation of dispatchable power generation”, Wednesday 21st September 2022, The Roderic Hill Building, Imperial College London, UK.

Posters

“Trace element emission in the raceway region” The Materials Processing Institute’s 3rd Postgraduate Research Symposium on Ferrous Metallurgy, Tuesday 25th February 2020, Armourers’ Hall, London, UK.

Acknowledgements

Firstly, I wish to thank Tata Steel Europe and EPSRC for making this iCASE available and supplying the funding for my work.

I feel very fortunate having been able to undertake this PhD, as well as the rest of the studies that have brought me to this point. Whilst I wouldn't go so far as to describe my PhD study as a labour of love, I have to admit that I've thoroughly enjoyed my time studying at Cardiff University. Alas, after 11 years of flirting in and out of the University, my father's regular question of "when is it going to end?" finally has an answer.

There have been many people who have helped me along over the years, however, my family has been at the heart of my journey. First and foremost, I must thank my Mam and Dad, Sandra and Rob. Your love, emotional and financial support, as well as the gritty determination that you have instilled in me are infinitely valuable. I must thank my Nana, Marjorie. Once again, I wouldn't be here without your love and support. My late Grampa, Tom, I thank you for requiring me to develop unending patience and leaving my dear Nana with unrealistic expectations of how well a large garden can be kept! I think of you often. To my little brother, Cory, thank you for pushing me by being talented, hard-working, and successful. At least you left me the good looks.

To my academic supervisors, Prof. Richard Marsh and Dr Julian Steer, thank you for giving me the opportunity to study this PhD. Your support, guidance, and friendship have been immensely appreciated. I couldn't have asked for better mentors. Thank you especially for the painstaking work of reading my drafts and always providing constructive and encouraging feedback. I would also like to thank Mr Malcolm Seaborne, Mr Richard Griffiths, Mr Jeff Rowlands, and Dr David Morgan for their help with my various experiments throughout my PhD.

To my friends, your mercilessly mocking has always helped me to keep my head fitting through doors. I hope that your assistance on this matter continues for many years. Thank you for always being there for me.

Finally, I wish to thank my partner, Beth. Your love, encouragement, and support is ever present. You inspire me to be my very best.

Contents

List of Figures

List of Tables

Part I

Introductions, background, and a review of existing literature

Chapter 1

Introduction

1.1 The challenges of the steel industry

The steel industry faces many challenges in the global effort to reduce humanity's reliance on fossil fuels. The steel industry is heavily reliant on fossil fuels, particularly coal, which accounts for approximately 75% of the energy demand of the industry [10]. It is particularly difficult to replace carbon in the steel industry due to its major role as a chemical reductant of iron oxides. Iron and steel accounts for 8% of global final energy demand and 7% of energy sector CO_2 emissions [11, 12].

Great strides have been made in the improvement of existing technologies, with the energy required to make a tonne of steel dropping by 61% since the 1960s. However, it is argued that ironmaking has begun to reach the limits of efficiency and that an energy source other than coal must be utilised for further reductions using current technology [13].

European steelmaking faces many financial difficulties on account of stringent environment policies and emissions requirements, reduced demand following the 2007-2008 financial crisis, and the flooding of the market with cheap, surplus Chinese steel. In the UK, steel producers faced the additional pressure of some of the world's highest energy prices and high business rates. This has led to the sales and closures of several plants in the UK, most notably British Steel went to insolvency and in 2019 was sold to the Chinese firm Jingye [14].

In the UK, the steel industry is responsible for 13.5% of greenhouse gas emissions from manufacturing and 2.0% of total UK greenhouse gas emissions. The Climate Change Committee recommended for the 6th Carbon Budget that the UK Government should adopt a target that all iron-ore based steelmaking be near-zero emissions by 2035. In response, the UK Government published its Industrial Decarbonisation Strategy in March 2021 [14]. In this, it presented what it perceived as the two most feasible options for the decarbonisation of the steel industry:

1. Retain coking coal in steelmaking with Carbon Capture Utilisation and Storage (CCUS) to sequester emissions.
2. Use of electric arc furnaces with hydrogen replacing coal for use in direct reduced iron (DRI) processes.

In response, the UK steel industry highlighted that the UK Government must put in place a supportive policy framework so that the sector can continue to compete in domestic and international markets if costs of production rise, including further action on electricity costs, which currently hampers the industry's ability to invest in decarbonisation [14].

Until the implementation of mass decarbonisation within the steel industry, current measures used to reduce costs and emissions must be utilised to their full potential. Coal injection within the blast furnace has been used for decades as a way of reducing the demand for expensive and energy intensive coke. However, the utilisation of coal, which still retains the various volatile components that are removed during the coke making process, can lead to the increased addition of non-desirable elements into the blast furnace [15]. Sulphur is one such element. Whilst the coke making process does not remove all of the sulphur bound in coal, less thermally stable sulphurs are volatilised and removed from the solid coke product [4, 5]. Sulphur addition to the blast furnace leads to increased production of the toxic, environmentally polluting gases H_2S and SO_2. SO_2 is a component in the production of acid rain and is an indirect greenhouse gas due to its contribution to aerosol formation. H_2S oxidises in the atmosphere to SO_2, adding to these effects [16,17]. The addition of sulphur to the blast furnace also increases the requirements for desulphurisation processes. Whether within the blast furnace or externally, these processes are energy intensive, increasing fuel rates and CO_2 emissions. This thesis seeks to understand how sulphur entered into the blast furnace by the coal injection travels through the furnace, what factors affect the form in which it is removed from the furnace, and what savings can be made from this knowledge.

1.2 Hypothesis

Via the study of literature relating to the topic, it was deduced that the relative thermal stability of coal sulphur forms would play a role in the sulphur products leaving the raceway. Less thermally stable sulphur compounds, such as aliphatic organic sulphurs or pyrite, were thought to be more readily volatilised in the raceway region. Due to the relative levels of oxygen in different parts of the raceway, more readily liberated sulphur was believed to be combusted to SO_2, whilst sulphur liberated later in the raceway was believed to form H_2S or COS. More thermally stable sulphur compounds found in coal were expected to remain in the unburnt char when leaving the raceway.

By researching how these sulphur products could be expected to behave in the blast furnace, it was deduced that the volatilisation of coal sulphur to a gaseous sulphur product, such as H_2S, would overall be beneficial for the operation of the blast furnace as this could potentially leave the furnace via the top gas and reduce the sulphur load in the hearth of the furnace. It was believed that some gaseous sulphur could be fixed by the charge materials in the shaft of the blast furnace, however any gaseous sulphur leaving the furnace via the top gas would not have to be removed from the hot metal by the slag. It was therefore hypothesised that the use of coals or conditions that promoted the volatilisation of coal sulphur would allow savings to be made relating to the reduction in sulphur load and the related reduced need for the desulphurisation of the produced hot metal.

1.3 Aim and objectives

As described in Section 1.1, the need to reduce the costs and emissions of steelmaking are key to the future of the steel industry in the UK and Europe. The reduction of costs and emissions of blast furnace ironmaking are crucial to the short and mid term decarbonisation of the steel industry. Further insight into ironmaking processes, the challenges, and decarbonising, can be found in Chapter 2.

The aim of this thesis was to study the effect of sulphur from coal injection on blast furnace operation. In turn, this would potentially allow for better selection of coals and improvement of blast furnace operations in order to reduce operating costs and greenhouse gas emissions. Upon a thorough review of literature, the route of sulphur through the blast furnace was hypothesised. In order to validate this hypothesis and reach the described aim, the following objectives were produced:

- Confirm whether the initial form in which sulphur enters the blast furnace via the coal injection affects the sulphur products leaving the raceway.
- Identify if there are any coal properties which affect the formation of the

sulphur products leaving the raceway.

- Identify whether the utilisation of alternative fuel sources affects the formation of the sulphur products leaving the raceway.
- Identify how the sulphur products leaving the raceway may interact with the charged blast furnace materials.
- Identify how the findings of the study may be applied to industry to reduce costs and greenhouse gas emissions.

1.4 Thesis structure

This thesis is separated into four parts, consisting of a total of ten chapters.

- Part I: Introductions, background, and a review of existing literature. This Part consists of Chapters 1-3 and provides information on the challenges faced by the steel industry, introductions to ironmaking and coal sulphur, and a study of relevant literature, discussing new technologies, methods, and analysis.
- Part II: Experimental design and analysis. This Part consists of Chapters 4 and 5 and provides information on the materials used in this work, the experiments undertaken, and the analytical methods employed.
- Part III: Results. This Part consists of Chapters 6-8 and describes the results of the experimental and analytical work undertaken during this study.
- Part IV: Discussion and Conclusions. This Part consists of Chapters 9 and 10 and provides a discussion of the findings of this study and the possible industrial application of the knowledge gained. Further work is suggested.
- References are found at the end of this thesis.

Chapter 2

Ironmaking

2.1 Introduction

Iron is a very common element and is the fourth most abundant element in the Earth's crust. Iron could be considered the most important metal to human existence, with it accounting for approximately 93% of the tonnage of all metals used [15]. Most iron used globally is in the form of steel. Steel is an alloy of iron and carbon, containing up to 2% carbon [15].

World Steel reports that global crude steel production was 1,951 million tonnes in 2021, with China producing 52.9% of the total. Of this global total, 70.8% of this was produced by the blast furnace-basic oxygen furnace (BF-BOF) route, producing 1,353.6 million tonnes of pig iron. Steel made via electric arc furnace (EAF) route made up 28.9% of production. Global steel use was 1,834 million tonnes in 2021, this is predicted to grow to 1881.4 million tonnes in 2023 [18].

The BF-BOF route is the primary method globally of producing steel from iron ore [18]. To produce 1000 kg of crude steel, this route has an average consumption of 1370 kg of iron ore, 780 kg of metallurgical coal, 270 kg of limestone, and 125 kg of recycled steel. Comparatively, to produce 1000 kg of steel, the EAF has an average consumption of 710 kg of recycled steel, 586 kg of iron ore, 150 kg of coal, 88 kg of limestone, and 2.3 GJ of electricity [19].

In an integrated steelworks following the BF-BOF route, the blast furnace consumes 65-75% of the entire energy at the plant [15]. About 89% of a BF-BOF's energy input comes from coal, 7% from electricity, 3% from natural gas and 1% from other gases and sources. In comparison, for the EAF route, the energy input from coal accounts for 11%, from electricity 50%, from natural gas 38% and 1% from other sources [19].

Iron and steel accounts for 8% of global final energy demand and 7% of energy sector CO_2 emissions [11, 12]. In 2021, this equated to an average of 1.39 tonnes of CO_2 produced per tonne of crude steel. This has fallen from 1.49 tCO_2/t in 2016 and is predicted to fall to 1.03 tCO_2/t in 2030 [20]. In an industry heavily dependent on fossil fuels, coal in particular, major investment and advancement in technology is needed to decarbonise an industry crucial to the modern world. This will not happen overnight, however, and it is likely that the BF-BOF route will continue to be the major method of producing steel from iron ore for the foreseeable future. It is therefore crucial that efforts are made to minimise the environmental impact of the blast furnace until viable alternatives are implemented.

2.2 The blast furnace

As already stated, the blast furnace is crucial to the production of global steel, being used for 70.8% of steel produced in 2021 and being accountable for up to 75% of the energy consumption at an integrated steelworks [15, 18]. The blast furnace is a continuously operating counter-flow shaft furnace that chemically reduces and physically converts iron oxides into liquid iron (hot metal) [15].

Figure 2.1 shows a diagram of the blast furnace and indicates the various

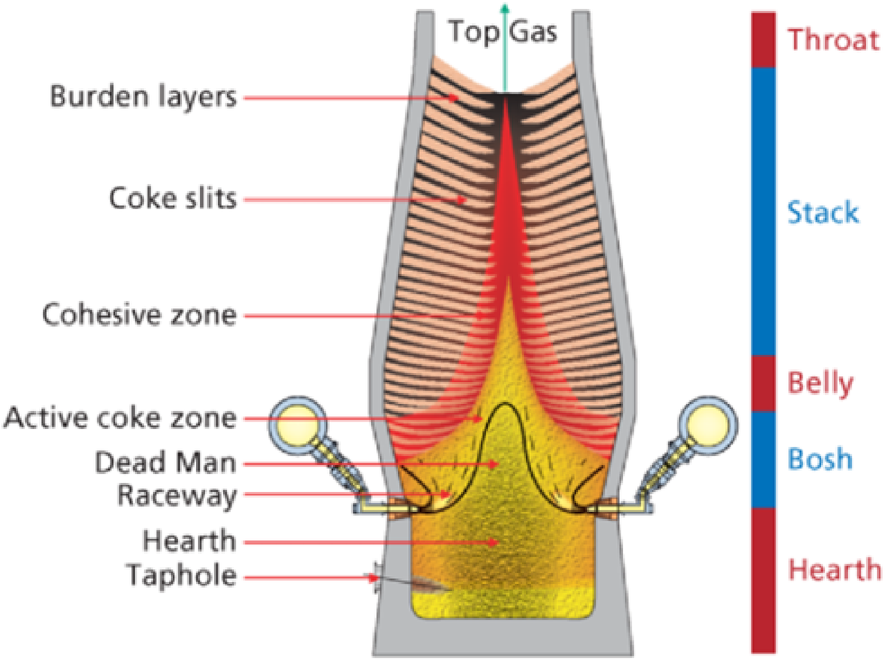

Figure 2.1: The blast furnace zones [1]

zones and features. During operation, coke and burden materials (pellets, sinter, lump ore, and fluxes) are charged in alternating layers at the top of the furnace and descend under gravity. Hot blast (usually air or oxygen enriched air between 1000-1300°C) is injected through the tuyeres, where it reacts with the coke and injected fuels (such as pulverised coal, natural gas, or oil) to form the raceway. The resulting gas has a high flame temperature of between 1900-2300°C. During this process, oxygen from the blast is used to combust carbon to form carbon dioxide via Equation 2.1. Under the presence of excess carbon at high temperature, the carbon dioxide is reduced to carbon monoxide via the reverse Boudouard reaction shown in Equation 2.2 [1,15].

$$C + O_2 \rightarrow CO_2 \qquad \Delta G = -406.12kJ \tag{2.1}$$

$$C + CO_2 \rightleftharpoons 2CO \qquad \Delta G = 172.47kJ \tag{2.2}$$

CO is the primary reducing agent in the blast furnace, reducing iron oxides via "indirect" reduction, shown in Equations 2.3-2.5. Indirect reduction is overall an exothermic process and occurs in the temperature region between 400-800°C [1,15,21].

$$3Fe_2O_3 + CO \rightarrow 2Fe_3O_4 + CO_2 \qquad \Delta G = -52.85kJ \tag{2.3}$$

$$2Fe_3O_4 + CO \rightarrow 3FeO + CO_2 \qquad \Delta G = 36.46kJ \tag{2.4}$$

$$FeO + CO \rightarrow Fe + CO_2 \qquad \Delta G = -17.13kJ \tag{2.5}$$

Indirect reduction occurs whilst the iron oxides remain in the solid phase. Unmelted iron ores will still contain non-reduced iron oxides. Once temperatures are great enough to melt the iron oxides, direct reduction of any remaining iron oxides by carbon can occur via Equations 2.6-2.8. "Direct" reduction is endothermic and occurs at temperatures greater than 1000°C. The energy required for direct reduction is provided by the combustion of coke [1,15,21].

$$3Fe_2O_3 + C \rightarrow 2Fe_3O_4 + CO \qquad \Delta G = 119.62kJ \tag{2.6}$$

$$2Fe_3O_4 + C \rightarrow 3FeO + CO \qquad \Delta G = 208.93kJ \tag{2.7}$$

$$FeO + C \rightarrow Fe + CO \qquad \Delta G = 155.34kJ \tag{2.8}$$

The cohesive zone, which can be seen in Figure 2.2, is a temperature zone of 900-1350°C and is the region where ore starts to soften and melt. Above the cohesive zone, the burden remains solid and is where indirect reduction occurs. Below the cohesive zone is the active coke zone, also called the dripping zone, where there is only coke and liquid iron and slag. Direct reduction occurs here and coke is consumed. Additional coke is consumed by carbon dissolving in the hot metal, which is called carburisation. Below this is the "dead man", or inactive coke zone, where stable coke piles up from the hearth, extending into the bosh. The liquid iron and slag accumulates in the hearth between the voids in the coke. The liquid iron and slag are removed by casting via the taphole [1, 15].

2.2.1 The ferrous burden

The ferrous burden contains the iron bearing materials. The iron burden is usually composed of sinter, pellets, or lump ore. These materials are produced from iron ores. The most common iron ores are haematite (Fe_2O_3), magnetite (Fe_3O_4) and goethite ($Fe_2O_3.nH_2O$) [1, 15].

Sinter does not transport well and is usually produced within the steelworks due to its role in the recycling of waste materials. In a sinter plant, iron bearing fines, coke breeze, fluxes, and recycled products, such as blast furnace dust, are agglomerated by the combustion of the coke upon a sintering belt. Sinter is made in three different types relating to the relative fluxes used: acid (CaO/SiO_2 ratio below 1.0), fluxed (CaO/SiO_2 ratio between 1.0 and 2.5), and super-fluxed (CaO/SiO_2 ratio above 2.5). Fluxed sinter is the most commonly used. Sinter will commonly contain in the region of 56-58% Fe [1, 15].

Pellets are usually produced near the iron ore mine. In contrast to sinter, they are easily transported and have a higher quantity of Fe, often in the region of 63-67%, and lower quantities of fluxing material. Pellets are generally produced in three main types: acid (CaO/SiO_2 ratio below 0.5), fluxed (CaO/SiO_2 ratio between 0.9 and 1.3), and olivine pellets (which use olivine - $(Mg,Fe)_2SiO_4$ as the fluxing additive) [1,15].

Lump ores are natural iron-rich materials, used directly from the mines. The use of lump ore is becoming more uncommon due to poorer performance in the blast furnace compared to sinter or pellets. However, lump ore remains a cheaper alternative and the charging of an iron burden containing 10-15% lump ore is sometimes viable [1,15].

For efficient blast furnace operation, the iron burden should contain over 58% Fe. It is becoming increasingly common to operate a blast furnace on a mix of sinter and pellets, or solely pellets. The type of iron burden has a large effect on the productivity, coke rate, and slag chemistry of the blast furnace. For example, blast furnaces using an iron burden of 100% pellets can operate at lower slag volumes due to the reduced amount of gangue and flux [1,15].

2.2.2 Coke

Coke is the carbonised solid product of high temperature coal pyrolysis. Metallurgical coke is produced by the heating of specially selected coking coals in the absence of oxygen up to temperatures of 1100°C. This produces a hard, porous material with a high amount of fixed carbon (see Section 5.1). As a product of coal, it also contains some of the mineral and sulphur components of the original coal. The process of coking produces coke oven gas (COG) as a valuable by-product. A hydrogen and hydrocarbon rich gas, this can be utilised in a range of applications on plant [9,15,22,23].

Coke plays an important role in ironmaking. First used in blast furnaces from the beginning of the 18th century, it is now crucial to the operation of modern blast furnaces where it fulfils three primary functions: it supplies heat; acts as a reducing agent; and supports the burden [15].

The coke and auxiliary reducing agents supply about 80% of the heat required for blast furnace operation [15]. The coke is the primary source of the carbon used in both the direct and indirect reduction of the iron burden, as described in Section 2.2. Coke is a hard, porous material. This allows it to maintain the burden permeability, which is crucial for the flow of gases throughout the furnace and the flow of liquid phases which first occur in the cohesive zone [9, 15, 22].

Coke use in the blast furnace has disadvantages, however. The production and consumption of coke is responsible for large amounts of CO_2 emissions. Coke constitutes a major portion of the production cost of hot metal. As previously eluded to, coke contains impurities in the form of sulphur and in its ash. Between 80-90% of the sulphur introduced into the blast furnace comes from the coke and auxiliary reducing agents. Due to the desulphurising operation of the blast furnace, for every 0.1% increase in coke sulphur content, coke consumption is increased by 0.5-1.8% and furnace productivity is reduced by about 2% [9,15,22].

The coke rate will vary with operating conditions, but rates between 300-400 kg/tHM (tonne of hot metal) are common [22, 24]. Methods to reduce the coke rate have been introduced to lower production costs and emissions, such as the use of pulverised coal injection (PCI) [15].

2.2.3 Pulverised coal injection

The cokemaking process is an expensive, energy intensive process. The idea of injecting fuel and smelting additives into the blast furnace via the tuyeres was formulated at the beginning of the 19th century as a method of decreasing the coke rate. However, its widespread adoption did not occur until after the Second World War [15]. During the 1960s, oil and natural gas were the prevailing injected substances, but as a result of the oil crises of the 1970s and 1980s, the use of pulverised coal was widely adopted [13, 15]. As of 2013, every blast furnace in Japan, the majority of blast furnaces in China, and 60% of European blast furnaces operated with pulverised coal injection (PCI). The average rate of PCI is 130-160 kg/tHM. However, PCI rates of over 200 kg/tHM have been achieved, allowing the coke rate to fall below 300 kg/tHM [15, 22]. The use of PCI allows the replacement of coke by supplying the carbon required for the reduction of iron oxides and by providing heat during it's combustion in the raceway, as discussed in Section 2.2.4. PCI reduces the consumption of coke, reducing the costs and emissions associated with the production of coke. This can also lead to an extension of the service life of coke ovens as they can operate at a lower production rate. PCI can lead to increased furnace productivity and allows greater flexibility during operation as parameters can be changed more rapidly than via charging materials to the top of the furnace [13, 22, 25].

The selection of coals for PCI is often a balance between cost and operational performance. The fuel ratio, defined as the ratio of fixed carbon to volatile matter, can be used to predict a coal's combustion behaviour. Coal combustibility usually increases with higher volatile matter content, but a higher fixed carbon content allows for a larger replacement of coke. Coal reactivity decreases with increasing coal rank as higher ranked coals have less volatile matter content, are less porous, and have less oxygen functional groups [15, 26]. The ability of coal to replace coke in the blast furnace is defined by the replacement ratio. The replacement ratio is based upon the carbon content of the coal, as such, higher ranked coals offer a higher replacement ratio. The blending of low and high volatile coals to receive the benefits of a high replacement and favourable combustion characteristic is a common practice [13, 15].

The use of PCI has some disadvantages that must be considered. Of particular interest to this study is the production of unburnt char and the introduction of sulphur into the blast furnace. When PCI is used, the coal combusts in the raceway region of the blast furnace. This produces CO_2 which reacts with the coke and produces CO via the reverse Boudouard reaction, as described previously by Equation 2.2. However, as the residence time of a coal particle in the raceway is often in the order of a few hundred milliseconds, not all of the injected coal may have undergone complete burnout. The unburnt residue, char, may have negative effects on gas permeability, slag viscosity, coke characteristics, and coke consumption [15, 22].

During the cokemaking process, much of the less thermally stable sulphur found in coal is volatilised and forms H_2S in the coke oven gas, leaving only the more thermally stable sulphur forms in the coke. The injection of coal can therefore lead to an increase in the amount of total sulphur entering the blast furnace, whilst also injecting the less thermally stable sulphur compounds found in the coal, which may volatilise under the conditions of the raceway. It is also possible that some component of the coal sulphur remains in the unburnt char. Identifying the fate of the sulphur injected by PCI is the main purpose of this research project.

2.2.4 The raceway

The raceway is the area of the blast furnace where the hot blast and PCI is injected via the tuyeres. The hot blast consists of air or oxygen-enriched air. The hot blast temperature is often between 1000-1200°C and the gas velocity is about 180-250 m/s. This creates a typical heating rate of around 10^5-10^6°C/s [25]. The number of tuyeres depends on the size of the blast furnace, often ranging between 12-42 tuyeres [15]. The raceway's location in reference to the rest of the blast furnace can be seen on Figure 2.1. Here, the combustion and gasification of the pulverised coal and coke occurs. The raceway has a length of between 0.7-2.0 m, produces temperatures of between 1400-2200°C, has a pressure of about 450 kPa, and has very short residence times [25].

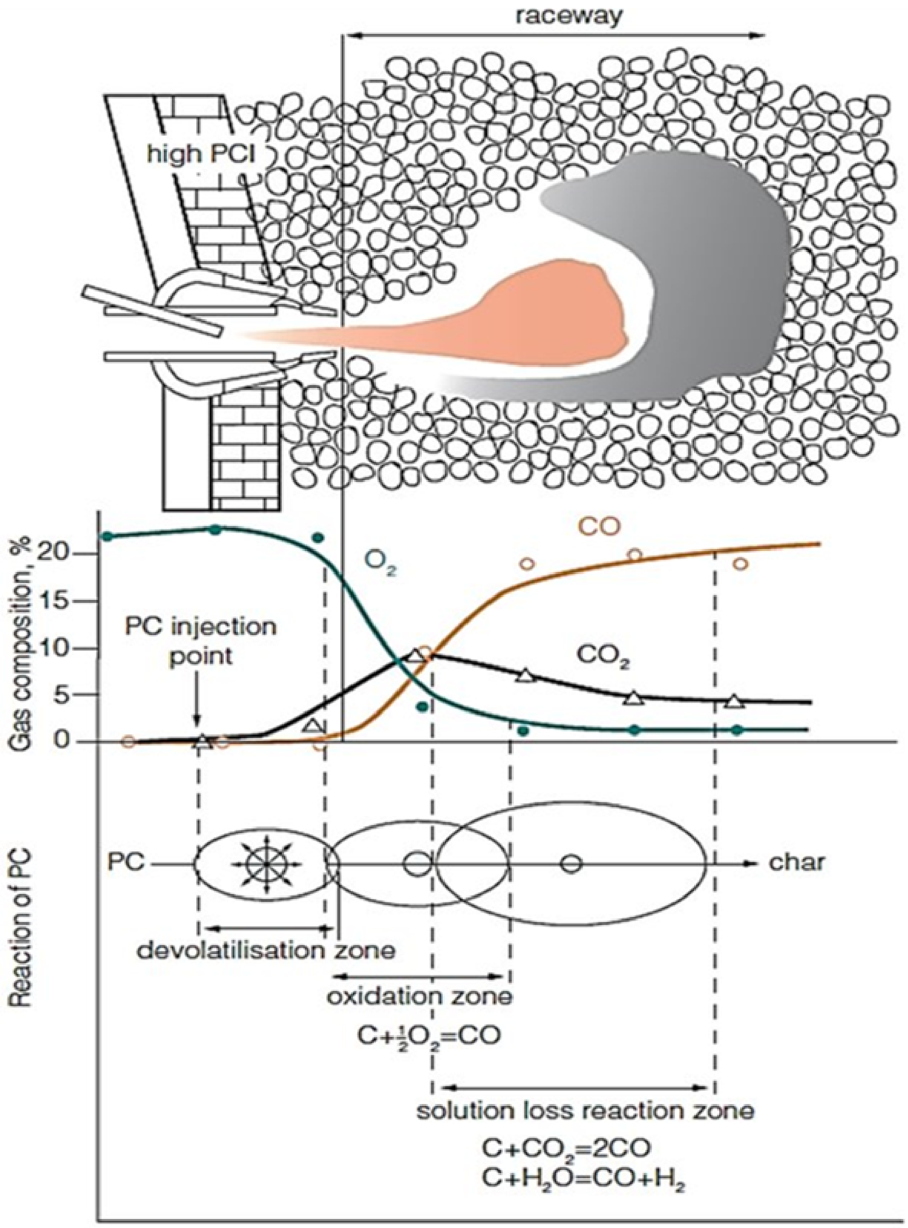

Figure 2.2: The overlapping reaction zones of injected pulverised coal throughout the raceway [2]

The combustion of the injected pulverised coal can be divided into overlapping stages. Figure 2.2 displays the overlapping reaction zones of the PCI in the raceway. In the first stage, the devolatilisation zone, the coal undergoes pyrolysis, gasifying the volatile components of the coal. In coals with higher levels of volatile matter, this rapid volatilisation can lead to the swelling of coal particles and the creation of large pores on the surface of the unburnt char [2]. In the oxidation zone, the volatilised component of the coal rapidly combusts, producing CO_2 and H_2O. This raises the temperature around the char particle, accelerating the ignition of the particle. The partial combustion of the char particle continues as the oxygen availability diminishes. This releases the majority of the heat required for the operation of the blast furnace. Lastly, in the solution loss reaction zone, the gasification of the residual char by CO_2 and H_2O occurs, producing CO and H_2. The overall extent of the combustion (burnout/combustion efficiency) is dependent on several factors: the coal properties, such as particle size and volatile matter; the blast gas composition and temperature; and the injection lance position and design [1, 2, 15, 25, 27] .

2.2.5 Slag

Slag fulfils an important role in the blast furnace operation. The slag is made up of unreduced ore oxides that reach the melting zone, fluxes, and fuel ash. Fluxes absorb the gangue of the iron ores and the tramp elements of the coke. Fluxing materials such as limestone or dolomite are rarely charged into the blast furnace in modern ironmaking, instead the use of fluxed sinter and pellets is more common and allows for increased productivity, reduced fuel consumption, increased furnace lining life, increased reliability and stability of furnace operation, and reduced silicon content in the hot metal. In modern blast furnaces, the produced slag volume is between 150-300 kilograms per tonne of hot metal (kg/tHM) depending on burden composition [1, 15].

The first liquid slag phases appear in the temperature range of 1100-1200°C. This is formed from partially reduced iron oxide and gangue form easily fusible eutetics with alumino-silicates, calcium oxide, and sometimes magnesium or manganese oxides [1, 15]. At this point, the burden as a whole remains solid and this initial "primary" slag is formed by the sintering of burden particles in the solid state. As the temperature changes as the burden descends through the furnace, the composition of this slag gradually changes to "bosh" and then "final" slag. As primary slag descends through the furnace, the content of MnO and FeO decreases due to direct reduction, whilst the content of SiO_2, Al_2O_3, and CaO increases as it is converted to bosh slag. In the hearth of the furnace, ash from the coke and injected fuel (primarily coal) passes into the slag. The sulphur content of the slag increases as the bosh slag is converted to final slag. The main constituents of final slag are SiO_2,Al_2O_2, CaO, and MgO, which constitutes to 95% of the mass of the final slag. The remaining 5% is made up of FeO, MnO, MnS, CaS, and alkali silicates. The sulphur content of the slag will vary between 1.0-1.5%. The slag plays a crucial role in the desulphurisation of the hot metal and is discussed in greater detail in Section 2.2.7 [15].

A key feature of slag is it's basicity. This influences the melting point, the viscosity/fusibility, and the desulphurisation capacity of the slag. Slag basicity B is calculated using Equation 2.9, however this is often simplified to Equation 2.10 or 2.11. CaO and MgO are the basic constituents of slag, whilst SiO_2 and Al_2O_3 are generally the acid constituents. Al_2O_3 has the potential to act as a base when the Al_2O_3 content is greater than 15% [15].

$$B = \frac{CaO + MgO}{SiO_2 + Al_2O_3} \tag{2.9}$$

$$B = \frac{CaO + MgO}{SiO_2} \tag{2.10}$$

$$B = \frac{CaO}{SiO_2} \tag{2.11}$$

Basic slag has a narrow fusibility range above the liquidus temperature. This means that the viscosity of basic slag increases sharply as temperature decreases. Basic slag can therefore hinder gas distribution and does not easily run out of the furnace when tapped, however it has a high desulphurisation capacity. In contrast, acid slag has a wide fusibility range, which means that its viscosity increases slowly with decreasing temperature. However, it has a relatively high viscosity above the liquidus temperature. It is better able to run out of the furnace when tapped, but also has a lower desulphurisation capacity than basic slag. Desulphurisation is a crucial role of the slag, however low viscosity of the slag is necessary to maintain sufficient gas permeability in the furnace, drainage of metal and slag through the coke, and free running of the slag during tapping. The desulphurising of the hot metal by the slag is the primary way in which sulphur is removed from the blast furnace. The basicity and volume of the slag are managed so that 80-90% of the sulphur entered into the blast furnace is removed via the slag [15].

Figure 2.3 is an example of a slag diagram that shows how varying quantities of SiO_2, CaO, and Al_2O_3 affects melting point of slag, in this case containing 10% MgO. It can be seen that the composition of the slag strongly influences the melting point of the slag, with percentage changes of composition resulting in changes to the melting point of hundreds of degrees. It is important that a slag composition is stable and that small changes to its composition do not result in significant changes to the slag's melting point, maintaining smooth furnace operation [15].

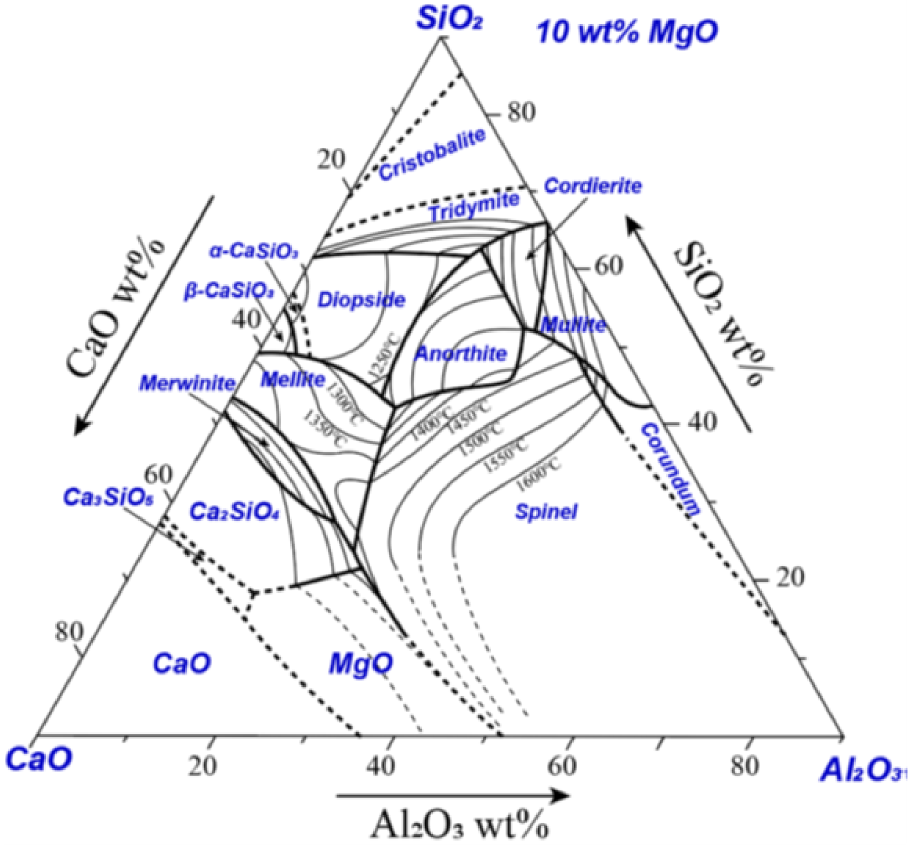

Figure 2.3: The SiO_2-CaO-Al_2O_3 slag system at 10% MgO [3]

2.2.6 Trace elements and impurities

A number of trace elements and impurities will be charged into the blast furnace during operation. These are often in the forms of oxides, carbonates, or silicates. Some of these elements will be removed from the furnace via the slag or top gas, whilst some will enter the hot metal. Elements with high recovery, i.e. elements that mostly enter the hot metal, include phosphorus, chromium, and depending on furnace conditions, manganese. Oxides containing calcium, magnesium, aluminium, and titanium transfer to the slag. The presence of oxides can affect the reduction of iron oxides by changing the partial pressure of

CO and therefore the CO/CO_2 potential [15].

Silicon enters the blast furnace in large quantities in the ore gangue and coke ash. Silicon is distributed in both the slag and the hot metal. Silicon can enter the hot metal by two methods, directly from the molten slag to the molten metal and indirectly where the silicon transfers from the slag or coke ash to the gas phase to form SiO, which then reacts with the liquid iron. The majority of the silicon enters the hot metal via the direct method. To facilitate low silicon levels in the hot metal, the use of a high basicity slag with low viscosity and low slag volume is encouraged. As SiO_2 affects the basicity of slag, high silicon content in the charge could reduce the desulphurisation capacity of the slag [15].

Some elements accumulate in the blast furnace by circulating through the high and low temperature zones. Elements such as lead, zinc, sodium, and potassium will transfer to the gaseous form in the blast furnace and ascend to lower temperature zones where they condense on the surface of the burden and the coke. They then descend with the charged materials to the hotter regions of the blast furnace, where they are once again volatilised to the gaseous phase [15].

2.2.7 Sulphur in the blast furnace

The fate of sulphur in the blast furnace is the focus of this research. Sulphur is an impurity introduced into the blast furnace via the coke, burden, and pulverised coal injection. Between 80-90% of the sulphur in the blast furnace is introduced via the coal and coke, the remaining balance is introduced via the ore materials and fluxes as sulphides and sulphates, such as FeS, FeS_2, CaS, $CaSO_4$, and $BaSO_4$ [15]. Sulphur in coal is discussed in greater detail in Chapter 3. The sulphur present in coke is the thermally stable component of the original coal sulphur that is not volatilised by the coking process, usually the more complex organic sulphurs and thermally stable inorganic sulphurs which are discussed in Chapter 3.

The sulphur in the hot metal cannot usually exceed 0.02-0.05% in order to satisfy quality requirements [15]. Increased sulphur in the hot metal can adversely affect the mechanical properties of the produced steel by increasing brittleness in a heated state (red-shortness) [22]. Sulphur enters the hot metal as iron sulphide from a number of sources:

By the decomposition of iron pyrite FeS_2, displayed in Equations 2.12-2.15 [15].

$$FeS_2 \rightarrow FeS + 0.5S_{2(g)} \tag{2.12}$$

$$FeS + 10Fe_2O_3 \rightarrow 7Fe_3O_4 + SO_2 \tag{2.13}$$

$$SO_2 + 2C \rightarrow 0.5S_{2(g)} + 2CO \tag{2.14}$$

$$[Fe] + 0.5S_{2(g)} \rightarrow [FeS] \tag{2.15}$$

Directly from the reduction of $CaSO_4$ in Equation 2.16, or via the reaction of CaS with FeO as in Equation 2.17 [15].

$$CaSO_4 + [Fe] + 3C \rightarrow [FeS] + CaO + 3CO \tag{2.16}$$

$$CaS + FeO \rightarrow CaO + [FeS] \tag{2.17}$$

CaS can be produced via Equation 2.18 or Equation 2.19 [15].

$$CaSO_4 + 4C \rightarrow CaS + 4CO \tag{2.18}$$

$$CaO + 0.5S_{2(g)} + C \rightarrow CaS + CO \tag{2.19}$$

Via the reaction of gaseous sulphur with FeO in Equation 2.20 [15].

$$FeO + 0.5S_{2(g)} + CO \rightarrow [FeS] + CO_2 \tag{2.20}$$

Or finally via Equations 2.21-2.22 [15].

$$CaS + SiO_{(g)} \rightarrow SiS_{(g)} + CaO \tag{2.21}$$

$$SiS_{(g)} + 3[Fe] \rightarrow [Fe.Si] + [FeS] \tag{2.22}$$

Note that [] means that the compound is concentrated in the hot metal.

Sulphur can also leave the blast furnace through the top gas as H_2S or SO_2, this usually makes up 2-5% of the sulphur balance. The production of H_2S and SO_2 from the decomposition of the sulphur forms found in coal and coke are discussed in greater detail in Chapter 3. A fraction of the sulphur from the blast furnace is removed from the furnace via the blast furnace flue dust. The majority of the sulphur introduced into the blast furnace is removed via the slag [15].

2.3 Direct Reduced Iron

Direct Reduced Iron (DRI) is an alternative method of producing iron from iron ore. About 8% of iron produced worldwide in 2021 was made via the DRI method [18]. The basic principle of DRI is that iron ore pellets descend under the force of gravity through a shaft furnace operating at high temperature whilst reacting with a reducing gas, most commonly a hydrogen rich syngas produced from natural gas. The MIDREX process, which reduces iron ore pellets in a shaft furnace using a syngas produced from steam reforming of natural gas, currently accounts for over 60% of DRI worldwide [28]. DRI technology has existed for over 50 years. However, processes are now being adapted to transition away from fossil fuel usage, replacing fossil fuel generated syngas with renewably produced hydrogen.

2.4 The future of ironmaking

Blast furnace ironmaking has existed for over seven hundred years [29]. It has proven to be an effective and profitable process throughout periods of massive change in human history. However, the future of blast furnace ironmaking is undoubtedly threatened by the global need to decarbonise industries in the fight against the climate change crisis. The steelmaking industry is one of the largest emitter's of CO_2 worldwide, making up to 7% of global anthropogenic CO_2 emissions and therefore has a major role to play in reaching climate change targets [11, 12]. This section will discuss some of the alternative technologies and adjustments to existing processes that are currently being researched and implemented to reduce greenhouse gas emissions from the ironmaking process.

2.4.1 Hydrogen and fossil fuel free steelmaking

The use of hydrogen to replace fossil fuels in carbon free technologies is a topic of great interest globally as a method of fighting the climate-change crisis that currently afflicts the Earth. Whilst hailed as a "silver bullet" by some political spin doctors aiming to appease climate concious voters, there are many challenges still to conquer with regards to the exploitation of hydrogen. It is however, almost infeasible to believe that hydrogen technologies will not be crucial to the de-carbonisation of many sectors, whether as a direct replacement for fossil fuels or as a form of energy storage. One of those sectors looks increasingly likely to be the steel industry, with several fossil fuel free processes using hydrogen currently being developed.

Hydrogen steelmaking will be seeking to use hydrogen primarily as a replacement for carbon monoxide in the reduction of iron oxides to iron. By comparing

Equations 2.23 and 2.24, it can be seen that a replacement of CO with H_2 is possible.

$$Fe_2O_3 + 3CO \rightarrow 2Fe + 3CO_2 \qquad \Delta G = -27.52kJ \tag{2.23}$$

$$Fe_2O_3 + 3H_2 \rightarrow 2Fe + 3H_2O \qquad \Delta G = 88.44kJ \tag{2.24}$$

As can be seen, when replacing CO with H_2, CO_2 is no longer produced and H_2O is produced instead [11].

Hydrogen steel production isn't an entirely new idea, with the only commercial hydrogen steel plant to date, Circored in Trinidad, produced over 300,000 tons of high-quality hot briquetted iron (HBI) over several months of successful operation using hydrogen to reduce fine ores in a two-stage fluidized bed process [11, 30]. This plant was decommissioned for economical, rather than technical, reasons.

Current research is heavily focussed on the use of hydrogen in DRI processes using a shaft furnace. HYBRIT is a project joint funded by SSAB, LKAB and Vattenfall in Sweden that aims to use green hydrogen and renewable energy to produce fossil fuel free steel, reducing Finland's and Sweden's CO_2 emissions by 7% and 10% respectively [31]. Their pilot plant in Luleå has been operational since 2020. SSAB aim to complete their demonstration plant in 2025 whilst converting their blast furnace in Oxelösund, Sweden, to an electric arc furnace. They aim to produce fossil fuel free steel on a commercial basis by the end of 2026 [32]. ArcelorMittal operates Europe's only commercial DRI-EAF facility in Hamburg, Germany, using the MIDREX process. Whilst initially designed to be operated on natural gas, this plant is currently being converted to run on 100% grey hydrogen with the intention of swapping to green hydrogen when economic conditions allow [33, 34]. Midrex Technologies and Paul Wurth have recently (October 11^{th}, 2022) announced an agreement with H2 Green Steel which aims to produce the world's first commercial 100% green hydrogen DRI plant in Boden, Sweden. This plant is scheduled to begin production in 2025 and produce steel with an estimated 95% reduction of CO_2 emissions compared to the traditional BF-BOS route [35]. It should be noted that the nature of Sweden's steel industry is inherently unique, facilitating an accelerated transition to hydrogen steelmaking that other countries will struggle to follow. It has strongly supported climate policy, relatively cheap electricity prices compared to other European countries, and an electricity supply produced largely from low carbon sources such as hydropower and nuclear [36]. The feasibility of transitioning to hydrogen steelmaking in Sweden and elsewhere around the world has been reviewed by several authors and is a topic that will have to be thoroughly addressed before green hydrogen steelmaking becomes a realistic alternative to the blast furnace - basic oxygen steelmaking route.

2.4.2 Blast furnace co-injection

As with all new technologies, a high level of capital investment and risk is involved in it's initial application. This will likely be one of the key limiting factors in the rate of transition to fossil fuel free steelmaking. In the case of green hydrogen steelmaking for example, further discussions around infrastructure, production, storage, cost, etc. must all be addressed before a transition can occur. It may be much more appealing in the short term for steel-makers to adapt their existing technology to reduce their greenhouse gas emissions. The co-injection of alternative fuels such as sustainably produced biochars, hydrogen, or hydrogen bearing compounds, e.g. natural gas or ammonia, into the blast furnace could be a method of reducing greenhouse gas emissions without requiring massive investment in brand-new plants and the redundancy of blast furnace ironmaking. In a world still yet unprepared for massive green hydrogen demand, the adaptation of current blast furnace operations could be considered the only feasible short-term option to reduce global ironmaking emissions. The co-injection of alternative fuels into the blast furnace is currently an area of intense research.

Natural gas has been used as a blast furnace injectant in countries such as Japan, Russia, and China. It isn't a new technology but can now be seen as a lower carbon alternative to coal. By replacing coal with natural gas, CO_2 emissions are reduced as a larger proportion of the iron ore reduction is undertaken by H_2 that has entered the blast furnace via the natural gas. Whilst producing lower CO_2 emissions, natural gas is still a fossil fuel and is non-renewable. The availability of natural gas is also affected by economic and political pressures, with Russia's invasion of Ukraine having caused a European shortage and increased wholesale prices. These factors considered, it is possibly unlikely that natural gas will develop as an alternative blast furnace injectant in Western Europe. Methane, the major constituent in natural gas, can be produced in renewable ways. Anaerobic digestion is commonly used to treat sewage or in the disposal of organic waste, by which methane is produced as a valuable product. This could theoretically be used as a renewable injectant in the blast furnace.

The effects of using natural gas as a blast furnace co-injectant with coal has been studied by Zhang et al. (2022). This was done by creating a numerical simulation to compare and analyse the differences of natural gas and pulverised coal mixed injection with pulverised coal injection on the thermal state, gas composition, and pulverised coal burnout in the tuyere and raceway of a Russian blast furnace. The simulations were conducted with natural gas injection rates of 47, 57, and 67 m^3/tHM and a pulverised coal injection rate of 181 kg/tHM. It was shown in the study that natural gas injection initially increased pulverised coal burnout by 1.52% compared to the simulation with only pulverised coal injection, but increasing the rate of natural gas injection from 47 to 67 m^3/tHM reduced the burnout from 70.11% to 68.31%. At higher injection rates, more CH_4 enters the furnace. The combustion of the CH_4 occurs intensely, consuming the oxygen and increasing the temperature close to the furnace wall. This results in less oxygen being available around the volatilising pulverised coal, slowing the rate of pulverised coal combustion. The water gas shift reaction, shown in equation 2.25, intensifies with increasing natural gas injection. The reaction is strongly endothermic and causes the average temperature of the raceway to drop. With the increasing natural gas injection rate, the molefraction of H_2 increases from 6.72% to 7.67%. The increase of the molefraction of H_2 will result in increased utilization of H_2 in the iron ore reduction reaction [37].

$$C + H_2O \rightleftharpoons CO + H_2 \tag{2.25}$$

It has been reported that the use of hydrogen within the blast furnace could lead to up to a 20% reduction in CO_2 emissions [11]. Several authors are currently focussing their research on this area.

Ren M et al. (2022) numerically studied the effects of hydrogen fraction in co-injection gas on combustion characteristics of the raceway in low carbon emission blast furnace. The simulation was based on an oxygen blast furnace with top gas recycling. The top gas recycling oxygen blast furnace (TGR-OBF) uses an oxygen blast to improve the partial pressures of the reducing gases CO and H_2, and as the TGR-OBF is nearly free of nitrogen, CO_2 can be separated and captured from the top gas with affordable costs. Following CO_2 separation, the remaining top gas is recycled into the furnace via the tuyere, which can help to control the over-heating problem introduced to the lower part of the furnace by the oxygen blast. The burnout rate of pulverised coal is improved by the oxygen blast and allows for a further increase of the coke replacement ratio. Recycled top gas is not the only suggested injectant gas for this process, with other H_2 rich gases, such as coke oven gas, also being suggested. The study investigates how varying the volume fraction of H_2 from 20% to 80% in the co-injection gas affects the coal-gas co-combustion characteristics. A high-volatile bituminous coal was used with an injection rate of 875 kg/h with a 23.33 Nm^3/h flow of N_2 at 300K used as a conveying gas. The oxygen-rich blast had a volumetric composition of 90% O_2 and 10% N_2 and injected at a rate of 1130.89 Nm^3/h at 298K. The co-injection gas volumetric composition varied between 80% CO and 20% H_2 to 20% CO and 80% H_2. It was injected at a flow rate of 1531.35 Nm^3/h at a temperature of 1173K [38]. It found that by increasing the hydrogen volume fraction in the co-injection gas, the preferential combustion of the gas is accelerated. This promoted the preheating of the pulverised coal, advancing the devolatilisation and char combustion processes, offsetting the oxygen grabbing effect of the co-injection gas preferential combustion over pulverised coal. This therefore shows that increasing the hydrogen fraction of a co-injectant gas can both encourage hydrogen-based reduction and pulverised coal burnout within the blast furnace [38]. The gasification of char by CO_2 in the char combustion stage is important to the burnout of coal particles. With an increasing H_2 volume fraction in the co-injection gas, it was seen that the gasification reaction rate of char with CO_2 changed very little, but the gasification with H_2O increased significantly [38].

Li et al. (2022) used a numerical model to study hydrogen co-injection in a 380 m^3 industrial blast furnace. This was done using a 3D CFD model with fixed flame temperature, bosh gas volume, and hot metal temperature. The PCI rate was set at 145 kg/tHM and remained constant for all hydrogen enrichment conditions. Hydrogen enrichment rate ranged from 0 to 10 Nm^3/s, corresponding to bosh gas concentrations of 3-49.5%vol H_2. To maintain a constant bosh gas flow rate, the hot blast rate was decreased with increasing hydrogen flow rate. As this decreased the physical heat coming into the furnace with the blast, oxygen enrichment in the blast was increased for raceway combustion to maintain constant bosh temperature [39].

It was found that as the hydrogen enrichment was increased, the coke rate decreased to a minimum, before again increasing. The productivity of the furnace increased with increasing hydrogen enrichment, but the rate of productivity increase slowed with increasing hydrogen enrichment. The utilisation factors of H_2 and CO were found to decrease with increasing hydrogen enrichment. An optimum hydrogen enrichment of 33.3%vol was therefore identified as an optimum enrichment rate in the conditions studied. It was identified that increasing hydrogen enrichment reduced the horizontal width and total length of the cohesive zone. The solid and gas temperatures were found to decrease sharply above the cohesive zone at higher hydrogen enrichment due to the endothermic reaction with H_2, a shorter residence time for heat exchange, and reduced gas volume per ton of hot metal. With increased hydrogen enrichment, indirect H_2 reduction rate increased, but slowed due to reduced temperature in the dry zone. CO indirect reduction decreased but remained more significant than the H_2 indirect reduction rate. The total carbon consumption due to chemical reactions decreased with increasing hydrogen enrichment [39].

Ueki et al. (2017) studied the effect of hydrogen gas addition on the combustion of pulverised coal using a drop tube furnace. Hydrogen addition was compared against non-addition at a range of flow rates. It was found that hydrogen addition initially enhanced the release of volatile matter from the injected coal and that the combustion of char was enhanced by the increase in coal particle temperature due to the rapid combustion of H_2 gas. The rapid release of volatile matter led to an increase in the formation of porous carbonaceous matrices in the char particle, which in turn, improved the combustibility of the remaining fixed carbon. However, it was found that at higher flow rates of H_2, the burnout (referred to as combustion ratio by Ueki et al.) of char particles was lower than under non H_2 gas addition. This was attributed to the excessive combustion of H_2 decreasing the O_2 concentration around the char particle, preventing char combustion. As such, it was concluded that an optimum H_2 flow rate was necessary to enhance the combustibility of of coal by H_2 gas addition [40].

Many other authors have produced studies on the effect of hydrogen or hydrogen rich gas, such as syngas or Coke Oven Gas (COG), co-injection. These studies produce similar conclusions to those studies already discussed. Gaseous injection of hydrogen results in an initial increase in burnout resulting from the increased devolatilisation of pulverised coal. Gaseous injection can lead to a decrease in raceway end-point burnout due to a reduction in available oxygen for combustion, however this is negated by reducing the PCI rate when increasing the gaseous injection rate. If not decreasing the PCI rate, it is possible to optimise the gaseous injection rate to maximise PCI combustion [41–44]. Gaseous co-injection can decrease the required coke rate and CO_2 emissions, whilst increasing hot metal productivity [45–47].

In addition to hydrogen or hydrogen rich fuels, other gaseous injectants, such as recycled process gases and syngases, have been investigated by various authors. Bailera (2023) studied the potential reduction of emissions by using a selection of syngases within air-blown blast furnaces, oxygen blast furnaces, and advanced oxygen blast furnaces. The syngases were produced from biomass and plastic gasification, CO_2 electrolysis, and by Reverse Water-Gas Shift. The gas produced from the CO_2 electrolysis (from the blast furnace top gas) was

CO and CO_2 rich, whilst the other gases had varying levels of CO, CO_2 and H_2. Each syngas showed the potential to be able to reduce net CO_2 emissions from the process [48]. J Li et al. (2022) investigated the co-injection of sintering flue gas as a method of desulphurising and denitrifying the gas. This was found to increase overall system efficiency by 24.88% compared to an ordinary blast furnace system [49]. Yeh et al. (2012) studied the combustion of pulverised coal with recycled blast furnace top gas (BFTG). It was found that the combustion of the BFTG raises the temperature of the injection environment, prompting an earlier start to coal devolatilisation, which in turn increased coal burnout [50].

The optimisation of process waste products has been commonplace within the steel industry for a number of years. Coke Oven Gas (COG) and Blast Furnace Top Gas (BFTG) are often used in power generation on sites. As already discussed, it is feasible to instead utilise these waste products within the blast furnace via co-injection. Another waste product that could be utilised is blast furnace dust (BFD), a material containing high quantities of both iron and carbon. If the issues arising from utilising these materials, which often have larger quantities of undesirable elements, can be addressed, then there are opportunities for large energy savings.

The use of biofuels as a co-injectant could allow a blast furnace operator to reduce their fossil fuel usage whilst utilising carbon from a sustainable source. Whilst not directly reducing the greenhouse gas emission of a blast furnace, the process would increase the utilisation of a “carbon neutral” resource, therefore reducing the net emissions of the process. A range of materials have been studied by various authors. For example, Ye et al. (2023) produced a feasibility analysis of plastic and biomass hydrochar for blast furnace injection. In this study, waste plastics and biomass underwent hydrothermal carbonisation (HTC) to upgrade the combustible waste to a high quality fuel, which is described as hydrochar.

To produce the hydrochars, 20 g of sample was added into a N_2 purged autoclave reactor with 60 ml of distilled water and held at 280 °C for 60 min. The process was shown to produce fuels of suitable quality for the partial replacement of bituminous coal with hydrochar for blast furnace injection [51].

An issue associated with using biofuels or waste materials is the introduction of harmful elements into the blast furnace. The HTC process was found to remove a significant portion of many of these elements, such as K, Na, Cl, and S. Another consideration of biofuel or waste material utilisation is its grindability. Many of these materials are flexible and fibrous and are not easily ground to a pulverised powder. The HTC process was shown to increase the grindability index of most of the fuels to levels comparable to coal. This would reduce the energy required to mill the materials. The hydrochars produced by the HTC had ignition temperatures in the temperature range of 228.9-337.9 °C with the higher temperatures comparable to bituminous coal. A lower ignition temperature could promote the combustion of anthracite in an injection blend but could introduce some safety concerns. Some of the hyrdochars were shown to be highly explosive materials, which is related to a high pore structure and low degree of graphitisation. This results in better detonation performance but also raises some safety considerations. The HTC process produces a more energy dense material than their corresponding raw material, with gross calorific value being increased for all hydrochars. The mass yields of the hydrochars ranged from 30.91% to 76.70%, resulting in energy yields of over 50% for all of the hydrochars. The use of hydrochar as a partial replacement for bituminous coal injection was calculated to reduce CO_2 emissions by 94.7 kg/tHM whilst also increasing the CO and H_2 volume, which would increase blast furnace smelting efficiency [51].

2.5 Chapter conclusions

The blast furnace is already a well understood technology with the process being continuously optimised since its inception centuries ago. The fate of the sulphur entered into the furnace via the coke and burden is well understood, with the interactions between sulphides, sulphates, slag, and the hot metal being managed to ensure the desulphurisation of the hot metal. The influence of coal injection on this is less well documented. The 2-5% of the sulphur balance that leaves the blast furnace through the top gas as H_2S or SO_2 could be the result of either the volatilisation of coal sulphur in the raceway or as a result of the thermal decomposition of sulphur compounds in the furnace. These sulphurous gases may react with the burden in the stack and therefore end up in the slag following the reduction and melting of the burden further down the furnace. There may also be additional factors that can determine whether sulphur is volatilised in the raceway or whether it remains in the unburnt char.

The blast furnace is, and will likely remain for the foreseeable future, the major technology used for ironmaking worldwide. With the decarbonisation of the steel industry a crucial challenge in the mitigation of anthropogenic climate change, the modification of blast furnace processes will help to bridge the step between traditional blast furnace operation and fossil fuel free steelmaking. The co-injection of alternative solid or gaseous fuels/reductants into the blast furnace is evidently an area of intense research with numerous studies being published within the last five years. There is however, very little research to date covering how these changes to blast furnace operation may affect blast furnace sulphur. As the purpose of this research was to identify the fate of sulphur introduced from pulverised coal injection, it would be advantageous to also study how future changes regarding co-injection may also affect this. The use of hydrogen rich gaseous fuels have been shown to increase the rate of devolatisation of co-injected pulverised coal whilst reducing overall raceway burnout, likely affecting the volatilisation of coal sulphur. The use of alternative solid fuels may bring different sulphur compounds or volatilisation accelerants or inhibitors with them when added to an injection coal blend, which would affect the volatilisation of sulphur in the raceway region.

Chapter 3

Coal sulphur

3.1 Introduction

Sulphur (chemical symbol **S**) is an abundant, non-metallic chemical element, atomic number 16. Historically known as brimstone, man's association with sulphur has existed for thousand's of years, with it referenced in many ancient writings, such as the Bible. In it's elemental form at atmospheric conditions, it is a yellow, crystalline solid. It is highly reactive and can form a range of organic and inorganic compounds, some of which are highly polluting [52]. Sulphur is found in varying quantities in fossil fuels. From mankind's exploitation of fossil fuels, many sulphur compounds are transformed into polluting sulphurous gases, such as SO_2 and H_2S [52].

3.2 Sulphur emissions from industry

The contribution of sulphur within industrial processes is of great interest within the research community as the world moves towards increased restrictions on the emission of polluting, sulphurous gases. The emission of sulphur dioxide (SO_2) has been shown to contribute to a number of detrimental environmental issues. Reactions between SO_2 and other atmospheric gases can lead to the production of sulphate aerosols and tropospheric ozone [52]. Sulphate aerosols contribute to fine particulate matter pollution [53]. SO_2 is also a well-known contributor to the formation of acid rain, which has devastated some natural environments. [52] The largest emitters of anthropogenic SO_2 to the atmosphere are coal power stations, smelting processes, and oil refineries [54].

Whilst consumption of coal and oil has decreased within Europe within the last twenty years, global consumption of coal and oil has increased [55]. As such, it could be reasoned that there is a corresponding increase in the emission of sulphurous gases such as SO_2 and H_2S. This doesn't appear to be the case, however, with calculated SO_2 emissions showing a decrease from 2005 to 2014 [56]. The major factor appearing to be the reduction in emissions from power plants. These reductions are attributed mainly to technological improvements, such as the addition of flue gas scrubbers to existing processes [53, 54].

This study will chiefly investigate the role of sulphur in the steelmaking industry, specifically, its role within the blast furnace. Globally, the iron and steel industry contributes 24% of all emissions from industrial sources (from figures published in 2013), 8% of global final energy demand, and 7% of energy sector CO_2 emissions [11, 12, 57]. China's steel production made up 52.9% of global steel production in 2021 [18]. A recent publication has reported that the steel industry in China contributes to approximately 20% of SO_2 emissions from key manufacturing industries in China (2017 figures) [58]. Chinese SO_2 emissions contribute about one third of global SO_2 emissions. By simply considering Chinese steelmaking, it is evident that the global steel industry is a significant emitter of SO_2 .

As well as the environmental concerns, sulphur within steel can adversely affect the mechanical properties of the steel, causing increased brittleness in a heated state (red-shortness) [22].

The use of high sulphur coals in steelmaking is becoming an ever more attractive consideration in the quest to cut production costs. Evaluating the impact that this would likely have on steel sulphur contents and on environmental emissions, it is easy to understand the need for further study into the mitigation of these negative effects.

3.3 Sulphur in coal

Sulphur is an undesirable, yet important component of coal. It can be found in varying amounts, from trace quantities to high quantities in excess of 10% of the coal mass [27, 59]. Sulphur compounds can be described as either organic or inorganic. These can then be defined further as a range of sulphur forms [4,5,60,61]. The distribution of sulphur forms is believed to correlate to a range of factors, including coal rank, maceral composition, and geological conditions [62–66]. Pyritic and organic sulphur often exist in varying quantities in most coals, whilst sulphates are usually found in more weathered coals and their relative quantity in coal is usually lower than pyrite and organic sulphur [23,63, 67,68] .

3.3.1 Organic sulphur

Organic sulphur compounds are a major component in most coals and can often account for over 50% of sulphur in coal [9, 62]. Organic sulphur is fixed within the chemical structure of the coal matrix [69]. This author has come across several methods of classifying organic sulphur compounds and that there is not one standardised method. This study will be defining organic sulphurs into three groups, which will be aliphatic sulphur, aromatic sulphur, and heterocyclic sulphur. These are explained in Sections 3.3.2, 3.3.3, and 3.3.4.

Compound name	**Sulphur bonding type**	**Chemical structure**
Dimethyl disulphide	Aliphatic	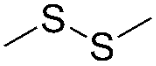
Dipropyl sulphide	Aliphatic	
Dibutyl sulphide	Aliphatic	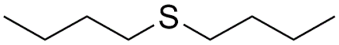
Benzyl methyl sulphide	Aliphatic	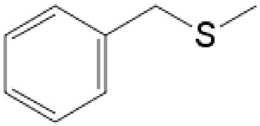
Dibenzyl sulphide	Aliphatic	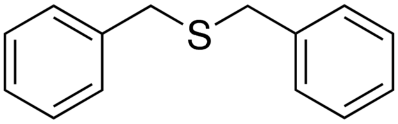
Dibenzyl disulphide	Aliphatic	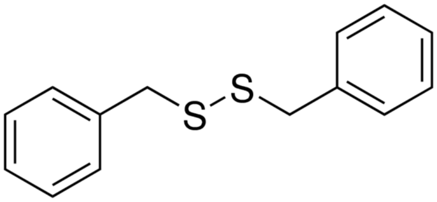
Dodecyl mercaptan	Aliphatic	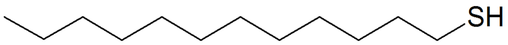

Table 3.1: Examples of aliphatic sulphur compounds found in coal

Compound name	**Sulphur bonding type**	**Chemical structure**
Thiocresol	Aromatic	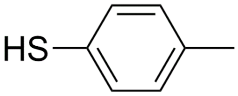
Thioanisole	Aromatic	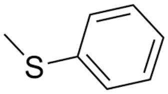
Diphenyl sulphide	Aromatic	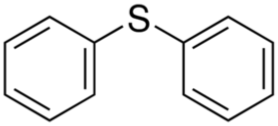
Thiophene	Heterocyclic	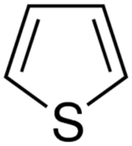
Benzothiophene	Heterocyclic	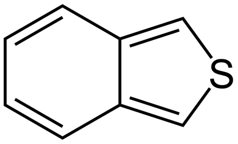
Dibenzothiophene	Heterocyclic	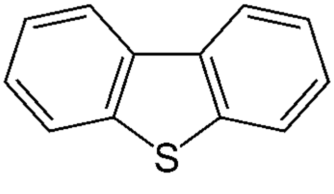

Table 3.2: Examples of aromatic and heterocyclic sulphur compounds found in coal

3.3.2 Aliphatic sulphur

In organic chemistry, hydrocarbons are divided into aliphatic and aromatic compounds. Aliphatic compounds describe the simple, chain hydrocarbons, such as alkanes, alkenes, and alkynes. Occasionally, it is possible to find cyclic aliphatic hydrocarbons (cycloalkanes, cycloalkenes, and cycloalkynes) [70, 71].

The bonding between carbon atoms in an aliphatic compounds can be described as aliphatic bonds, these differ to the bonding between carbon atoms in an aromatic ring structure, which are described in Section 3.3.3.

When describing a compound as an aliphatic or aromatic sulphur compound, it is important to note that it is not the presence of an aromatic ring structure within the molecule which defines the description, but the bonding of a sulphur atom directly to a carbon bonded within an aromatic ring, that results in the definition. i.e. a S-$C_{aliphatic}$ bond results in an aliphatic sulphur compound, whilst a S-C_{aryl} bond results in an aromatic sulphur compound.

Table 3.1 displays some examples of aliphatic sulphur compounds that can be found in coal [4,60,72]. As can be seen, it is not the presence of the aromatic rings in the likes of benzyl methyl sulphide and dibenzyl sulphide, but the presence of the S-$C_{aliphatic}$ bond that defines which group of organic sulphur compounds the compound belongs to.

3.3.3 Aromatic sulphur

Aromaticity differentiates aromatic ring structures from cyclic aliphatic compounds. An aromatic compound is a planar, monocyclic conjugated molecule with a p orbital on each atom and only if the p orbital system contains $4n+2$ π electrons, where n is an integer [70]. Aromaticity can be easily displayed by benzene and its derivative compounds. Aromatic compounds are planar ring structures where the p orbitals of the constituent atoms exist perpendicularly

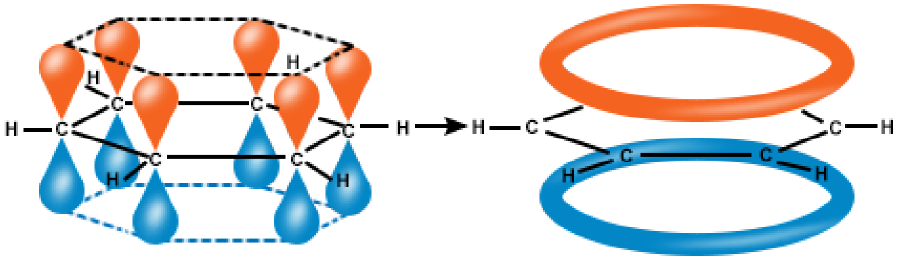

Figure 3.1: The delocalisation of p orbitals to form π electron clouds in benzene.

to the plane of the ring. Since all of benzene's six carbon atoms and six p orbitals are equivalent, it's impossible to determine three localised π bonds, in which a given p orbital overlaps with only one of its neighbouring p orbitals. Instead, each p orbital overlaps equally well with both neighbouring p orbitals. This leads to the six π electrons becoming delocalised and existing within two doughnut-shaped electron clouds, one above and one below the ring structure [70]. This can be seen in Figure 3.1. Aromaticity causes increased stability of the benzene molecule when compared to what may be expected for a cyclic triene [70]. Functional groups or substituents derived from an aromatic ring are referred to as aryls.

Following on from the explanation of the grouping of organic sulphur compounds described in 3.3.2, aromatic sulphur compounds can be identified by the presence of a S-C_{aryl} bond. The S-C_{aryl} bond is generally more stable than the S-$C_{aliphatic}$ bond [60]. Some examples of aromatic sulphur compounds found in coal are displayed in Table 3.2 [4, 60, 72].

3.3.4 Heterocyclic sulphur

A heterocyclic molecule is a compound with a ring that has one or more atoms other than carbon [70]. The definition of aromaticity (discussed in Section 3.3.3) doesn't prevent heterocyclic molecules also being aromatic. When referring to heterocyclic sulphur compounds in coal, thiophene and its derivative compounds are generally what are being referred to. Thiophene is an aromatic heterocycle. Many papers have shown aromatic heterocycles to have a very high stability. In coal, thiophenes are the most stable form of organic sulphur present [4,60,61,73].

Table 3.2 displays some examples of heterocyclic sulphur compounds found in coal [4, 60, 72].

3.3.5 Inorganic sulphur

Inorganic sulphur composes of the sulphides and sulphates found in the mineral matter of the coal. Inorganic sulphur in coal is usually further classified as either pyritic or sulphatic sulphur. If present, other inorganic sulphides, such as ZnS and PbS, are usually found in negligible quantities [23].

3.3.6 Pyritic sulphur

Pyrite and its dimorph marcasite (both FeS_2) are the dominant sulphide minerals found in coal. [23, 63, 67, 68] .

Pyrite is thought to have formed in coal in two stages: a syngenetic stage during peat formation, and a subsequent epigenic stage. Syngenetic pyrite is found along coal bands as separate framboids, framboid clusters, and individual euhedral crystals or clusters. Epigenetic pyrite can be found as large irregular grains, spheroidal aggregates, and clusters of framboids and euhedral pyrite crystals in coal fractures [63].

Pyrite has a specific heat capacity around only one third of that of coal, as such, it plays a significant role in the spontaneous combustion of coal [74].

3.3.7 Sulphatic sulphur

Sulphates do not usually comprise a significant proportion of sulphur species in fresh coal [23,67,68]. In fresh coal, gypsum ($CaSO_4.2H_2O$) and barite (Ba_2SO_4) can be found. In weathered coal, it is more likely to find hydrated ferrous and ferric sulphates, which are formed from the oxidation of pyrite [67,68]. Sulphates appear to form small inclusions within the coal in close association with pyrites and clay minerals [63].

3.4 Distribution of sulphur compounds in coal

The distribution of sulphur forms in coal has been studied by several authors [6, 61–66, 75]. It is evident that there are many influences on the distribution of sulphur in coal, including maceral content, coal rank, and marine influences.

3.4.1 Maceral sulphur composition

Macerals are not described in depth within this thesis. However, Table 3.3 provides a list of macerals and their corresponding maceral group.

It is generally accepted that the organic sulphur content of maceral groups generally follows the trend:

$$liptinite > vitrinite > inertinite.\ [65, 75]$$

A 1982 study investigated this further and found that the organic sulphur content of individual macerals generally followed the order:

$$sporinite, resinite \geq micrinite, vitrinite > pseudovitrinite \geq semifusinite \geq macrinite > fusinite.\ [75]$$

However a 1987 study produced its own variation:

$$sporinite > vitrinite > liptinites\ except\ sporinite > inertinite.\ [75]$$

Whilst other authors have concurred that sporinite generally contains the highest amount of organic sulphur, it has been shown to contain lower amounts of sulphur than vitrinite macerals in some coals [65, 66, 75]. It is not stated whether these studies consider huminites equivalent to vitrinites for the purpose of producing the trends.

Maceral group	**Maceral**
Vitrinite	Telinite
Vitrinite	Collinite
Vitrinite	Vitrodetrinite
Huminite	Textinite
Huminite	Ulminite
Huminite	Attrinite
Huminite	Densinite
Liptinite (exinite)	Sporinite
Liptinite (exinite)	Cutinite
Liptinite (exinite)	Resinite
Liptinite (exinite)	Fluorinite
Liptinite (exinite)	Suberinite
Liptinite (exinite)	Bituminite
Liptinite (exinite)	Alginite
Liptinite (exinite)	Exudatinite
Liptinite (exinite)	Liptodetrinite
Inertinite	Exudatinite
Inertinite	Liptodetrinite
Inertinite	Fusinite
Inertinite	Semifusinite
Inertinite	Inertodetrinite
Inertinite	Macrinite
Inertinite	Sclerotinite
Inertinite	Micrinite

Table 3.3: Subdivision of common macerals in coal [9]

It is not just the total amount of organic sulphur that changes per maceral, the type of sulphur also varies. Inertinites content has been correlated to increased aromacity, whilst it has also been shown that vitrinites contain comparatively more aliphatic compounds [64, 76]. There is some evidence to suggest inertinite macerals can contain more oxidised sulphur in comparison to other macerals [64]. It has been noted that coal rank does not appear to have an effect on the organic sulphur content of individual macerals when comparing coals of different ranks [65].

Vitrinite reflectance is a key figure in the analysis of coals. Lower vitrinite reflectance values have been found to correlate with higher levels of organic and total sulphur, especially in vitrinite abundant coals [66]. Higher vitrinite reflectance values corresponds with an increase in aromaticity within the vitrinite macerals [76]. Due to the role of vitrinite reflectance in establishing coal ranks, these considerations correspond with findings that higher rank coals contain higher proportions of aromatic and heterocyclic sulphur compounds [4, 6, 61]. Lower vitrinite reflectance values have been correlated with higher levels of calcium (and aluminium) within the vitrinite macerals, which may play a role in sulphur fixation in the coal [66].

As already mentioned in Sections 3.3.6 and 3.3.7, inorganic sulphurs exist as distinct inclusions within the coal structure. The association of inorganic sulphurs with coal macerals was studied in a 2005 paper. The study on Bulgarian lignite found that huminite and inertinite macerals were often associated or filled with pyrite and clay minerals. Large amounts of gypsum were found in close association with the clay and pyrite [63].

3.4.2 Coal rank and organic sulphur distribution

Organic sulphur distribution can be correlated to the rank of coal. It is well known, that as coal rank increases, aromaticity in the coal also increases [4, 61, 64, 73, 75]. It was first believed that organic sulphur was chiefly composed of aromatic heterocylces as it was believed that aliphatic compounds were generally too reactive to survive coalification [75]. The presence of aliphatic and non-heterocyclic aromatic compounds in coal has since been demonstrated in many studies, with the presence of aliphatic sulphurs being more common in lower ranked coals [4, 5, 61, 64, 69, 73, 75, 77–81].

As mentioned in Section 3.4.1, these changes in sulphur composition due to coal rank can be chiefly attributed to increased aromaticisation in vitrinite macerals, brought about by increased coalification.

3.4.3 Surface sulphur vs bulk sulphur

The distribution of sulphur forms is known to change from the surface of coal to its centre [6, 61, 63]. The proportion of oxidised sulphur species (sulphates, sulphonates, etc) has been found to be higher on the surface of pulverised coal, compared to the total coal bulk [6, 61].

3.4.4 Distribution of sulphur through a coal seam

With regards to coal seams, total, pyritic, and sulphatic sulphur values have been found to be highest near clay coal layers, whilst the highest organic sulphur levels have been found in the middle of the coal bed [63].

3.4.5 Marine influences on coal sulphur

The effects of marine influences on coal have been discussed by several authors. Seawater contains sulphate ions; the flooding of peatlands or paleoswamps by seawater likely contributed to the sulphur content of the produced coal. It has been displayed in several studies that marine influenced coals often have higher sulphur levels [9, 62, 63, 65, 68]. It has been suggested that marine coals may have higher organic sulphur levels. However, this appears to be disputed by some studies. It appears to be more commonly agreed that marine coals contain larger quantities of pyrite, however [9, 63, 65, 68]. Marine coals have been correlated with higher vitrinite and liptinite levels, as well as increased sulphur fixation within vitrinite macerals [65, 66].

3.5 Thermal reactions of sulphur in coal

The use of coal in thermal processes is key to many industrial applications. The pyrolysis and combustion of coal are topics researched by many authors. This section will examine the work of these authors. References to organic sulphur groups which have not been described in Section 3.3 will be made. Clarification

Group name	**Description**	**Bonding structure**
Thiol/mercaptan	R can represent an alkyl or aromatic structure.	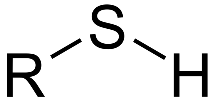
Sulphoxide	R and R’ can either be alkyl or aromatic structures.	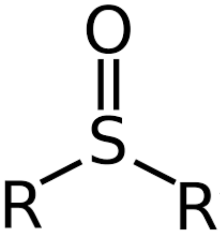
Sulphonic acid	R can represent an alkyl or aromatic structure.	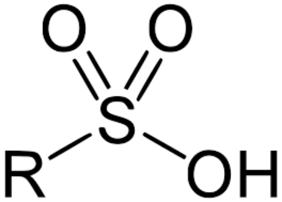
Sulphone	R and R’ can either be alkyl or aromatic structures.	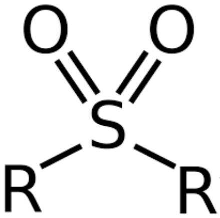
Sulphide/thioether	R and R’ can either be alkyl or aromatic structures.	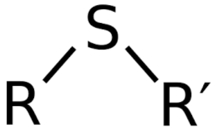

Table 3.4: Group names of organic sulphur compounds in coal

of these groups can be found in Table 3.4.

In the blast furnace, the high heating rate and low residence times of the raceway results in the partial combustion of the injected coal. The initial devolatilisation stage of coal combustion in the raceway, described in Section 2.2.4, are comparable to flash pyrolysis conditions. In the mostly reducing atmosphere of the blast furnace, the pyrolysis of unburnt coal char will occur.

3.5.1 Pyrolysis

Coal pyrolysis is the thermal decomposition of coal at temperatures excess of 300°C in the absence of oxygen whereby gas, tar, and char are formed. It is the basic process of coking (carbonisation) and the starting reaction of combustion, gasification, and hydrogenation [9].

Davidson's 1993 literature review of organic sulphur in coal summarises the findings of the few studies at the time. Since then, there appears to have been an influx of studies into the subject. Evidence was presented for several key findings. Pyrite in coal was found to decompose at temperatures greater than 500-550°C. Aliphatic sulphur compounds were identified as the least thermally stable and decomposed readily at temperatures under 400°C. Thiophenic sulphur remained stable at temperatures under 400°C and showed very little decomposition at temperatures greater than that. The transformation of unstable sulphur forms (aliphatics and pyrites) to more stable thiophenic sulphur was theorised [75].

Calkins (1986) investigation into organic sulphur-containing structures in coal using flash pyrolysis was covered by Davidson's report. Figure 3.2 was produced by Calkins. It identifies the conversion rate of sulphur model compounds to H_2S under flash pyrolysis. This corresponds to the relative stability of the sulphur molecules within the coal, showing that the compound stability increases in the order:

aliphatic → aromatic → heterocyclic.

The study suggests that the organic sulphur found in coals is mainly aliphatic or heterocyclic, with only a small proportion being non-heterocyclic aromatics. Low ranking coals appear to have higher amounts of aliphatic sulphur, whilst higher ranking coals have higher amounts of heterocyclic sulphur. Calkins identified 550°C as the temperature at which pyrite in coal pyrolyses [4].

Gu et al. (2016) studied the release of organic sulphur compounds during pyrolysis under inert (He and N), H_2, and CO_2 atmospheres. The study found that organic sulphur compounds can be fractured from the coal matrix under pyrolysis. It was found that pyrolysis under a CO_2 atmosphere results in an increase in volatile sulphur compound yield compared to a N_2 or He atmosphere. The increased reactivity of the CO_2 atmosphere also caused organic sulphur compounds to be volatilised at lower temperatures. A CO_2 atmosphere saw thiophenic sulphurs released mainly between 300 and 400°C, and also between 500 and 600°C. The second peak was believed to be caused by the decomposition of of more complex thiophenic structures. The maximum release of SO_2 in the CO_2 atmosphere occurred 100°C below that of the N_2 and He atmospheres. The effect of kaolin addition (5% mass) to the coal was also studied. Kaolin was found to have a catalytic effect on the emission of volatile organic sulphur compounds under pyrolysis in all atmospheres [73].

Gu et al. (2017) studied volatile sulphur emission from high-pyrite coal under pyrolysis in H_2, N_2, and CO_2 atmospheres. The mechanism of emissions were found to be different under different atmospheres. In H_2, most coal sulphur was hydrogenated/reduced to H_2S with inorganic sulphur being the main source. For most organic sulphur compounds, an H_2 atmosphere resulted in the most emission of gaseous sulphur compounds. In N_2, H_2S was produced with a dominant peak around 600°C, corresponding mainly to organic sulphur decom-

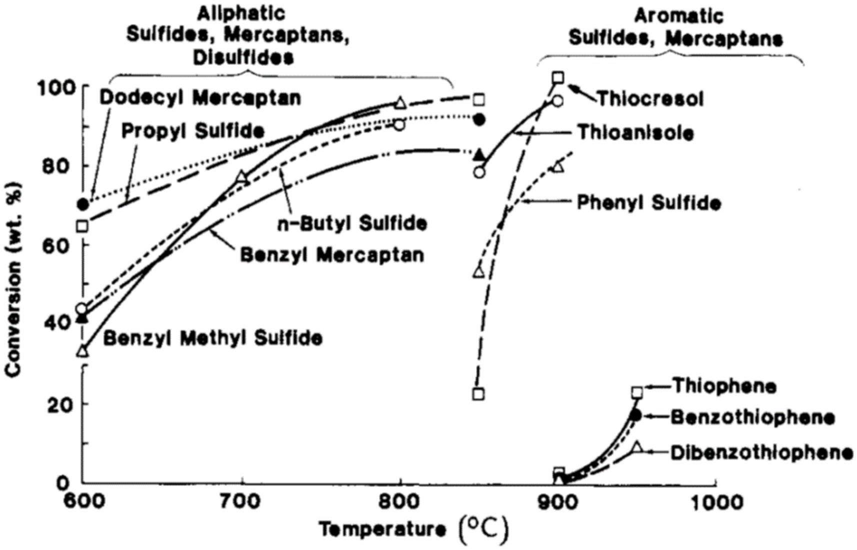

Figure 3.2: Flash pyrolysis behaviour of model sulphur compounds [4]

position. In CO_2, coal sulphur was mainly converted to SO_2/SO as CO_2 acts as an oxidising agent. Very little H_2S could be detected under the CO_2 atmosphere, Equations 3.1 and 3.2 suggest reaction mechanisms to explain this [77].

$$H_2S + 3CO_2 \rightarrow H_2O + SO_2 + 3CO \tag{3.1}$$

$$H_2S + CO_2 \rightarrow COS + H_2O \tag{3.2}$$

Sulphonic acids were found to decompose under 500°C and sulphoxides above 500°C. Above 800°C, char gasification in CO_2 resulted in further decomposition of sulphur compounds and lower total sulphur retention in the char. Thiophenic structures were found to be released in CO_2. Pyrite was found to be more readily decomposed in CO_2, compared to N_2. Equations 3.3 and 3.4 describe the possible decomposition reactions of pyrite in CO_2 [77].

$$FeS_2 + 2CO_2 \rightarrow Fe_{1-x}S + 2CO + SO_2 + xFe \tag{3.3}$$

$$2Fe_{1-x}S + 2CO_2 \rightarrow Fe_{1-y}S + 2CO + SO_2 + (1 + y - 2x)Fe \tag{3.4}$$

Liang et al. (2016) studied the effect of circulating ash on sulphur conversion characteristic in the coal polygeneration process. High-sulphur bituminous coal was pyrolysed in N_2, the remaining char and ash was then combusted. The study found that above 500°C, intensive decomposition of pyrite occurred, accompanied by an increase in sulphide and organic sulphur contents in the char. This suggests interconversion of different sulphur forms through the pyrolysis process. The increase in sulphides content was believed to be produced mainly by the decomposition of pyrite to iron sulphide. The increase in organic sulphur was believed to be produced from the reaction of active sulphur from pyrite decomposition with the organic matrix present in the char [82]. The presence of different sulphur forms on the char surface was investigated. Sulphur present on the char surface was mostly thiophenic, increasing with an increase in temperature, whilst the sulphoxide and sulphone content decreased. The deoxygenation of the sulphoxides and sulphones was believed to be responsible for the increase in thiophenic sulphur. No pyrite was found on the surface of the coal or respective chars. The total sulphur found on the surface reached a minimum at 600°C before increasing again with increasing temperature. This indicated that greater quantities of sulphur were transferred from the bulk to the surface under high temperatures [82]. The presence of CaO and Fe_2O_3 significantly affected the distribution of sulphur between the solid and gaseous phases under pyrolysis, being converted to CaS and FeS respectively. At 600°C, only 3.68% of the total sulphur was released to the gaseous phase, whilst 30.88% of the total sulphur was found to be retained in the circulating ash. MgO, NaOH, and KOH showed little effect on sulphur retention in the char [82].

Liu et al. (2010) examined the behaviour of sulphur compounds during the pyrolysis of high-sulphur coals under H_2, He, and a 2% O_2/He blend. The study found that internal and external hydrogen didn't show hydrogenation ability temperatures below 400°C. At temperatures higher than 400°C, indigenous hydrogen and indigenous oxygen in coals can react to form H_2S or SO_2. The similar tendency between H_2S and SO_2 evolution indicates that after the breakage of C-S bonds, S containing radicals react indiscriminately with indigenous hydrogen and oxygen. Pyrite was found to decompose at 540°C in H_2. Further decomposition peaks at 800 and 890°C were attributed to the reduction of FeS and FeS_{1-x} respectively. In He, SO_2 emission was thought to be as the result of the decomposition of organic sulphonic acids and inorganic sulphates, the peak emission being between 200 to 400°C being attributed to the sulphonic acids. In the 2%O_2/He blend, pyrite was found to easily oxidise to SO_2 around 400°C. Thiophenic structures in the coal matrix could be partially oxidised in this atmosphere. The differences displayed between results from deashed coals indicate that the mineral matter shows some contribution to sulphur fixation within the coal [78].

Liu et al. (2014) studied the sulphur release and transformation behaviours of sulphur-containing model compounds during pyrolysis in N_2 and a 4% O_2/N_2 blend. The order of sulphur release from the model compounds was found to be:

$$Dibutylsulphide > 2 - methylthiophene > tetradecylmercaptan >$$
$$benzothiophene > phenylsulphide > dibenzothiophene.$$

The decomposition temperatures of all sulphur compounds was found to be lower during pyrolysis in the oxidative 4% O_2/N_2 blend than in pure N_2. The maximal SO_2 evolution temperature of all model compounds was found to be lower than the peak CO_2 evolution temperature, indicating that oxygen can break C-S bonds more easily than C-C bonds. The model compounds were shown to produce several SO_2 emission peaks across a temperature range. Dibutylsulphide, tetradecyl mercaptan, 2-methylthiophene, and benzothiophene all displayed an emission peak around 500°C. This indicated that those compounds can transform to the same sulphur-containing compounds (which are more stable than the model compounds) during pyrolysis in the oxidative atmosphere [72].

Marinov et al. (2003) conducted the pyrolysis of low rank coals in a flow of water vapour. Several emission peaks were detected across the temperature profile of Katrishte coal, using AP-TPR. The peak at 325°C was attributed to alkyl and aryl thiols. The 435°C peak related to aryl-alkyl sulphides. The complex peak at 645°C were thought to be related to pyrite, diaryl sulphides, and less complex thiophenic structures. A shoulder peak at 740°C was attributed to more complex thiophenic structures. Above 950°C, the increase in measured signal was attributed to the reduction of inorganic sulphate groups [83].

Miura et al. (2001) undertook analysis on the formation rates of sulphur-containing gases during coal pyrolysis in inert atmospheres. The CAPTO method was used to distinguish sulphur forms. The study found that aliphatic sulphurs decomposed below 500°C and that aromatic sulphurs decomposed between 400 and 700°C, irrespective of coal type. The decomposition of thiophenic structures was judged to be strongly dependent on coal type with some coals showing decomposition of thiophenic sulphurs at temperatures above 500°C, whilst others showed very little decomposition under 900°C. Pyrite was judged to decompose at 590°C. Sulphurs of all forms in the coal were judged to decrease monotonically with increasing temperature, suggesting that transformations between sulphur forms in the solid phase were negligible [5].

The effect of heating rate on the pyrolysis products was investigated. Fig-

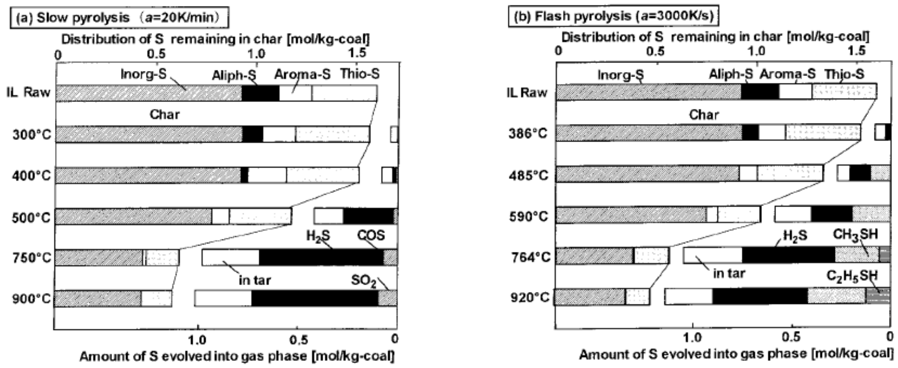

Figure 3.3: Change in the sulphur allotments between the slow pyrolysis and the flash pyrolysis for Illinois No. 6 coal [5]

ure 3.3 displays the results of the comparison. During flash pyrolysis, no SO_2 was formed, but large amounts of thiols (CH_3SH and C_2H_5SH) were formed. Thiophenic sulphurs were known to be able to decompose into C_2H_5SH by the scission of C - S and C - C bonds attached to a benzene ring. As no thiols were detected during the slow pyrolysis, this demonstrated that they are easily decomposed to H_2S or oxidised to SO_2 by H_2O or CO_2 during slow pyrolysis. The amount of SO_2 produced during the slow pyrolysis was greater than the amount of thiols produced in flash pyrolysis, suggesting that SO_2 also comes from components other than the fractured thiols [5].

Mullens et al. (2005) studied sulphur in lignite under pyrolysis in hydrogen and helium. In reductive pyrolysis in H_2, the evolution profile on H_2S revealed the decomposition of dialkyl and alkyl aryl sulphides around a peak at 480°C, the decomposition of diaryl sulphides around a broad peak at 665°C, and the decomposition of thiophenic structures around a peak at 745°C. Pyrite was believed do decompose between 500-600°C, whilst some inorganic sulphates were believed to decompose at temperatures over 900°C [79].

The study demonstrated the fracturing of aliphatic and aromatic compounds to the gaseous phase from the coal matrix. An evolution peak found at 480°C was attributed chiefly to alkanes, whilst a broad peak between 550 and 800°C was attributed to aromatics. Thiophenic structures were shown to only be detectable at high temperatures, it was concluded that these compounds likely make up a significant portion of the tar fraction by partially condensing above the oven. These species were not hydrogenated to H_2S due to the insufficient reduction efficiency of the H_2 atmosphere, especially in the lower temperature regions [79].

Mullens et al. (2003) studied the effect of reductive pyrolysis on sulphur model compounds. The study investigated the decomposition of thiophenic and oxidised model compounds to H_2S. Three main side reactions were identified. The first two side reactions occurred at relatively low temperatures and consisted of the evolution of volatile sulphur species that are not completely reduced to H_2S. The reducing capacity of the hydrogen atmosphere was judged to be insufficient to insure complete reduction to H_2S in the studied temperature range. Depending on the thermal stability and boiling point of the sulphur-containing compound, the compound may be encompassed into either the gas phase or condense in the pyrolysis reactor to form part of the tar fraction. The third side reaction contributing to the low reduction efficiency to H_2S was found to be that some model compounds formed complex and stable aromatic sulphur species in the char during the charring stage of pyrolysis [84].

The reductive pyrolysis of inorganic sulphur compounds was also investigated by Mullens et al. (2003) Calcium sulphate, zinc sulphate, iron (II) sulphate, and iron (III) sulphate were studied. Calcium and zinc sulphate were both found to be only weakly reduced at high temperatures, by 6% with a 855°C maximum and 13% with a 570°C maximum respectively. The reduction of calcium and zinc sulphate are described in Equations 3.5-3.7 [84].

$$CaSO_4 \rightarrow CaO + SO_3 \tag{3.5}$$

$$2ZnSO_4 + 4H_2 \rightarrow ZnS.ZnO + SO_3 + 4H_2O \tag{3.6}$$

$$SO_3 \rightarrow SO_2 + 1/2O_2 \tag{3.7}$$

The reduction efficiency of iron (II) sulphate ($FeSO_4$) and iron (III) sulphate was found to be far greater than that of the calcium and zinc sulphates. Iron (II) sulphate degraded in a two step process, whilst iron (III) sulphate degraded in a three step process. It was concluded that iron (III) sulphate was easily reduced to iron (II) sulphate and that both compounds followed similar reduction reactions. The first step of iron (II) sulphate's degradation corresponds to the thermal decomposition of the compound to iron oxide around a 470°C maximum, resulting in the emission of SO_2. H_2S is produced from the partial reduction of the SO_2. The second step corresponds to the reduction of troilite (FeS) to H_2S around a 750°C maximum. The formation and degradation of troilite is describe in Equations 3.8-3.10 [84].

$$FeSO_4 + 4H_2 \rightarrow FeS + 4H_2O \tag{3.8}$$

$$FeO + H_2S \rightarrow FeS + H_2O \tag{3.9}$$

$$FeS + H_2 \rightarrow Fe + H_2S \tag{3.10}$$

The additional stage of iron (III) sulphate's degradation corresponds to the thermal decomposition of residual iron (III) sulphate around a 535°C maximum. This is described in Equation 3.11 [84].

$$Fe_2(SO_4)_3 \rightarrow Fe_2O_3 + 3SO_3 \tag{3.11}$$

Rocha et al. (1997) studied the hydropyrolysis of coals and biofuels in a hydrogen atmosphere at 15 MPa hydrogen pressure. Low pyrite bituminous and sub-bituminous coals were pyrolysed under slow (5°C/min) and fast (300°C/min) pyrolysis conditions with and without the presence of a molybdenum catalyst. Lowering the heating rate resulted in greater tar and gas yield in both coals. In comparison to pyrolysis in nitrogen, the hydrogen atmosphere increased both tar yield and overall conversion by 10-15% as the heating rate was lowered from 300 to 5°C/min. In the presence of the catalyst, char yield was below 10%, signifying that a significant fraction of the inertinite was converted. The evolution of H_2S and thiophenic compounds from the coals was studied. Under the conditions thiophenes were judged to account for 75% of organic sulphur in the bituminous coal. It was found to reduce to H_2S with an emission peak at 470°C. H_2S evolved below 430°C was attributed to a mixture of aromatic and aliphatic sulphides and simple thiophenes. In comparison to other studies, the proportion of thiophenic sulphur present in the coal was shown to increase with coal rank [85].

Shen et al. (2019) studied the transformation of sulphur forms of coal blends during pyrolysis in argon. The study found that surface sulphur species are more easily removed from the coal when compared to bulk sulphur species. Volatile sulphur-containing species were found to react with nascent coke, leading to higher sulphide and thiophene contents on the coke surface. The blending of high volatile, low sulphur coals with high sulphur coals, were shown to inhibit the the interactions between sulphur radicals and nascent coke. This results in less heterocyclic sulphur forms being formed in inter-coal matrix reactions. Interactions between external volatile matters and coke were shown to only occur on the outer surface of the coke and do not permeate into the coke structure under the conditions of the experiment [81].

Wang et al. (2013) studied the pyrolysis of inertinite rich coals in nitrogen. The importance of the vitrinite/inertinite (V/I) ratio and hydrogen/carbon (H/C) atomic ratio on transformation of sulphur forms was studied. It was shown that with increasing V/I ratio, the amount of sulphur-containing gases released during pyrolysis increases. Generally, inertinite macerals show a higher degree of aromaticity than vitrinite macerals. With increasing temperature, the aliphatic compounds found in vitrinite easily decompose to form hydrocarbon radicals. These radicals were thought to promote the decomposition of residual sulphur in the nascent char, increasing the formation of H_2S. The H/C is an important parameter affecting the aromaticity factor and ring condensation index of a coal. As a result, vitrinite can usually be shown to have a higher H/C ratio than inertinite. It was shown that with increasing H/C ratio, the yield of sulphur-containing gases increased [64]. The inertinite rich coals studied were shown to have higher levels of alkaline metals, alkaline earth metals, and iron content. These minerals can react with sulphur containing gases, preventing their release from the coal char. This was shown by the production of CaS in the chars of the inertinite rich coals. At high temperatures, inorganic sulphurs were shown to react with nascent char or volatiles [64]. The formation of COS was shown to have a linear relationship with the production of H_2S, which suggested that the formation of COS was generally from a secondary reaction of H_2S and oxygen-containing gases. The suggested pathways of formation are described by Equations 3.12 and 3.13 [64].

$$H_2S + CO \rightleftharpoons H_2 + COS \tag{3.12}$$

$$H_2S + CO_2 \rightleftharpoons H_2O + COS \tag{3.13}$$

Wang et al. (2016) compared the pyrolysis of a lignite and sub-anthracite in

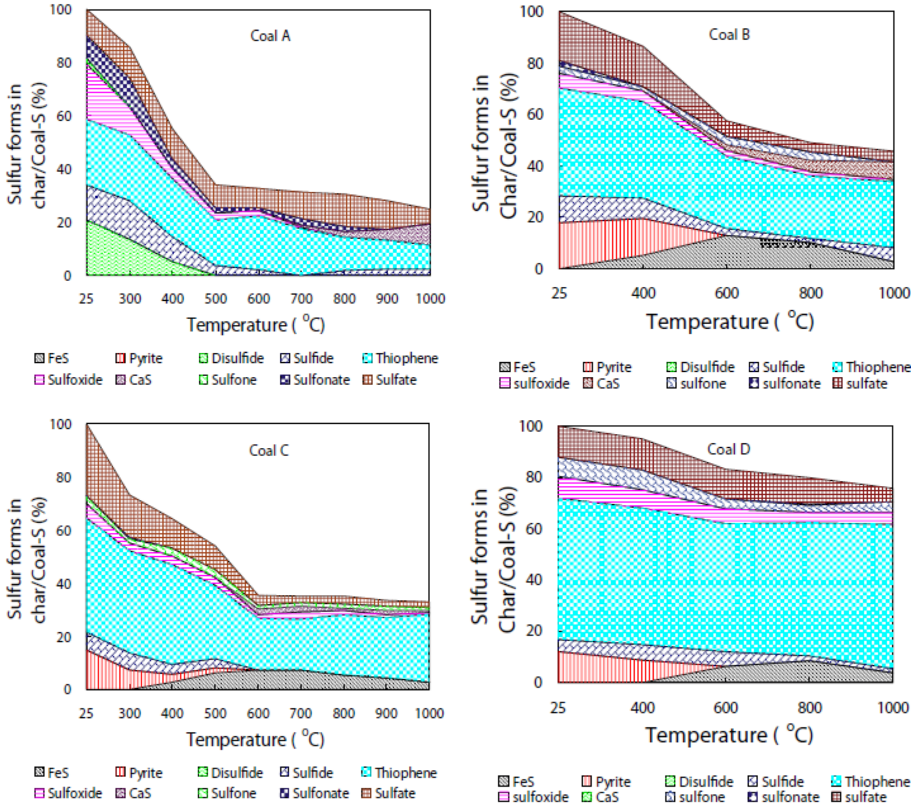

Figure 3.4: Distribution of different sulphur forms in chars compared with total sulphur in coal [6]

an Ar atmosphere. The study chiefly investigated tetrachloroethylene extraction of sulphur forms. However, it also discussed the transformation of sulphur forms within the coal chars. It was shown that the proportion of sulphides and sulphoxides on the surface of the chars was higher than in the bulk of the chars. This was thought to be due to sulphides being more reactive, and therefore more easily migrated from the bulk to the surface of the char during pyrolysis [61].

Wang et al. (2015) investigated the transformation of sulphur forms during the pyrolysis of high sulphur coals in an Ar atmosphere. Figure 3.4 shows the change in the distribution of sulphur forms within the coal chars during pyrolysis. The study shows how large an effect coal rank can have on the changes of sulphur forms during pyrolysis. Included in the study was a lignite (Coal A), sub-bituminous (Coal B), bituminous (Coal C), and sub-anthracite (Coal D) [6].

Coal A, which was rich in Ca and contained no pyrite, showed an increase in CaS and sulphates (likely $CaSO_4$) in the chars above 700°C. These were thought to be formed by the interactions between sulphur radicals, possibly from the decomposition of monocyclic thiophenes, and the Ca based minerals in the coal. The formation of CaS was also seen in the sub-bituminous coal above 800°C. In Coals B and C, the proportion of sulphate decreases in the char after 500°C. This was attributed to the decomposition of $Fe_2(SO_4)$ as the decomposition of $CaSO_4$ is known to occur at temperatures over 1000°C. Sulphoxides, disulphides, and some sulphides, were shown to decompose at temperatures below 500°C [6].

The degradation of pyrite could be seen in Coals B, C, and D. As the proportion of pyrite decreases, the proportion of sulphide (as FeS), increases. The pyrite is completely decomposed in all coals by 600°C. With increasing temperature, FeS also decomposes. In the presence of a plentiful supply of hydrogen-containing or oxygen-containing radicals, H_2S or COS could be produced. Otherwise, the nascent sulphur reacts with the carbon matrix or inorganic compounds to form new sulphur species within the char [6].

Simple, monocyclic thiophenes were shown to readily decompose in Coals A, B, and C at temperatures between 400 and 600°C. Coal D, being a sub-anthracite, contained high quantities of complex thiophenic structures. These were shown not to readily decompose under the conditions of the experiment. In Coals C and D, complex thiophenes were shown to be produced on the decomposition of FeS [6].

Wang et al. (2016) investigated the effect of a CO_2 atmosphere on the pyrolysis of two Chinese coals. In a CO_2 atmosphere, the proportion of sulphur released into the gas phase was shown to increase in comparison to pyrolysis in an Ar atmosphere. As a result, the proportion of sulphur present in the tar decreased. The amount of H_2S, SO_2 and COS produced increased compared to pyrolysis in an Ar atmosphere. The peak evolution temperatures of H_2S and SO_2 were reduced, whilst the peak evolution temperatures of COS increases. At temperatures $>850°C$, the release of COS was shown to be related to CO formation, while it is unrelated to CO at lower temperatures. In a CO_2 atmosphere, parts of the coal mineral matter were thought to catalyse the decomposition of coal structures and organic sulphur structures [86].

Xu et al. (2004) studied the pyrolysis behaviour of organic sulphur model compounds under a coal-like environment in a nitrogen atmosphere. It was shown that the pyrolysis of the model compounds occurred in multiple steps. The breaking of S - $C_{aliphatic}$ bonds occurs more readily than the breaking of S - C_{aryl} bonds, which are usually more stable. The breakage of S - $C_{aliphatic}$ bonds produced sulphur radicals, which reacted with the charcoal to form either volatile or non-volatile sulphur compounds. Radicals containing a S - C_{aryl} bond tended to combine with the charcoal at lower temperatures without evolving volatile compounds [60].

Yang et al. (2019) studied the effects of temperature on the pyrolysis behaviour of a high sulphur coal under Ar and CO_2 atmospheres. The CO_2 atmosphere was shown to promote the breakage of C-S bonds in the organic macro sulphur structure. The CO_2 atmosphere vastly increased the desulphurisation ratio of the coal under pyrolysis compared to the Ar atmosphere. H_2S, COS, and SO_2 release was significantly greater under the CO_2 atmosphere [87].

The CO_2 atmosphere was shown to lower the temperatures at which some sulphur compounds decompose. Disulphides were shown to have completely decomposed by 500°C in Ar compared to 400°C in CO_2. Thiophenes begin to decompose above 700°C in Ar or above 600°C in CO_2. This suggested that the decomposition of thiophenes at high temperatures was aided by the CO_2 atmosphere. Pyrite had completely decomposed to FeS at 600°C in CO_2. The FeS had then almost fully decomposed by 800°C in CO_2, whilst remaining in the char at 800°C in Ar [87].

The CO_2 atmosphere appeared to prevent the formation of CaS as the atmosphere likely promotes the formation of $CaCO_3$, thus preventing the reactions between calcium minerals and H_2S. The CO_2 atmosphere was shown to prevent the decomposition of ferrous sulphate at low temperatures (<500°C) [87].

3.5.2 Combustion

The combustion of coal and coal products is key to many industrial processes and provides the majority of consumable energy to the world. Combustion occurs by the initiation and propagation of a self-supporting exothermic reaction. The key processes in combustion of coal are principally considered to be the oxidation of the coal carbon and hydrogen [9].

Jurado et al. (2014) investigated the co-firing of coal and biomass in an oxy-combustion system. The test system used introduces pulverised coal into the furnace with CO_2, O_2, and recycled flue gases. The oxygen level at the entrance to the burner was between 27-35% v/v. Oxy-combustion showed higher ppmv values of SO_2 in the flue gas, however this was attributed to the circulation of recycled flue gases through the system. SO_3 production during the oxy-combustion of coal/biofuel blends was measured. The SO_3/SO_2 ratio was shown to increase with increasing proportions of biomass in the blends. It was suggested that the conversion of SO_2 to SO_3 may be promoted by the alkali species (K and Na) contained in the fly ashes. The biomass contained significantly higher levels of K and was therefore this was identified as the most likely cause of the increased SO_3/SO_2 ratio [88].

Whilst studying the effect of circulating ash on sulphur conversion characteristics in the coal polygeneration process, Liang et al. (2016) found that sulphur was released from the coal as SO_2 during combustion at temperatures greater than 800°C. Pyrolysis char and circulating ash, which had been used during the pyrolysis experiment to capture sulphur as CaS and FeS, was tested under combustion conditions between 800-900°C. Whilst between 76.39-79.79% of char sulphur was released during the char burnout, only 46.17-55.59% of ash sulphur was released. This was attributed to the char sulphur being mostly organic sulphur, which was oxidised to SO_2, whilst the sulphides in the ash were instead oxidised to sulphates [82].

Zhang et al. (2017) performed a similar study, investigated the effect of foreign minerals on sulphur transformation during coal pyrolysis and combustion. It was found that during pyrolysis, additions of Fe_2O_3 and CaO inhibited the volatilisation of coal sulphur by fixing the sulphur as FeS and CaS, respectively. During combustion conditions, the CaO showed a stronger ability to retain the sulphur in the char by reacting with SO_2 to produce $CaSO_4$, whereas Fe_2O_3 is reported to not react with SO_2 [89] .

Muller et al. (2013) studied the fate of pulverised coal sulphur during conventional and oxy-fuel combustion. Figure 3.5 shows the normalised results of the sulphur modelling produced in the study. The study showed that the combustion of organic sulphur occurred in a two step process, first volatilising and forming H_2S before combusting to form SO_2. The combustion of H_2S is described by Equation 3.14. In parallel, inorganic sulphur was found to release SO_2 directly. Oxy-fuel conditions were shown to produce significantly higher levels of SO_2 and SO_3 than the air-fuel conditions. Staging of the oxidant in both cases delayed the combustion of H_2S to SO_2 [7].

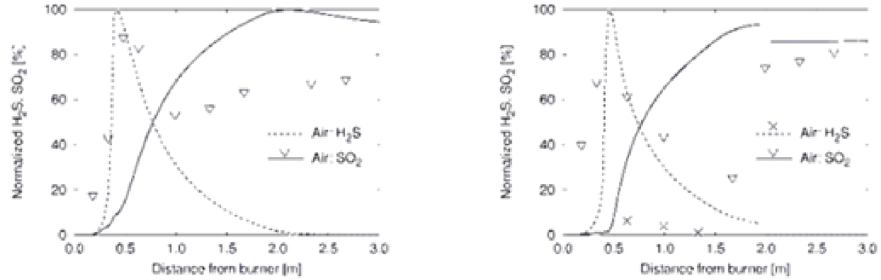

(a) Air, non-staged **(b) Air, staged**

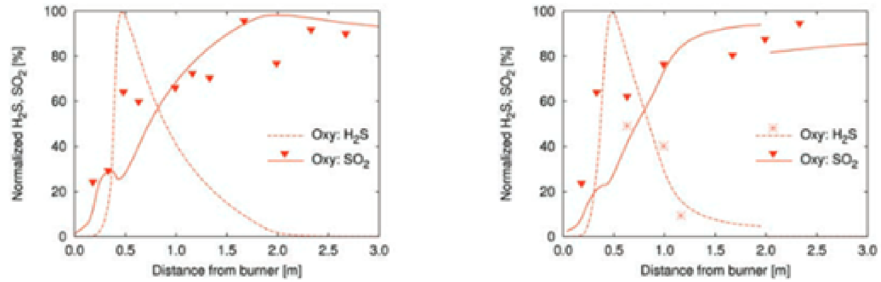

(c) Oxy, non-staged **(d) Oxy, staged**

Figure 3.5: Results of sulphur modelling showing axial profiles along the furnace centerline [7]

$$2H_2S(g) + 3O_2(g) \rightarrow 2SO_2(g) + 2H_2O(g) \qquad \Delta G = -518.9kJ \tag{3.14}$$

Stanger and Wall (2011) showed that oxy-fuel combustion leads to significantly higher levels of SO_2 in the flue gas in comparison to air-fuel combustion [90].

Yan et al. (1999) reported on the affinity of minor elements in coal to SO_x in the flue gas of coal combustion. It was concluded that calcium components are the most favourable for capturing SO_x in the temperature range of 400-800 K when the sulphur content of the coal was between 0.0062-6.2 wt.% [91].

3.6 Chapter conclusions

Coal sulphur is a very well understood topic. Large amounts of research has been conducted on the sulphur forms in coal and their association with coal's formation. Of relevance to this study is the association of organic sulphur in coal with the coal's rank. With large amounts of research having been undertaken on the relative thermal stabilities of different coal sulphur forms, it has been shown that the organic sulphur in higher ranked coals, which are generally aromatic or heterocyclic sulphur compounds, have greater thermal stability than the aliphatic sulphur compounds found in lower ranked coals [4–6, 60, 61, 72, 73, 78, 79, 81, 83, 85]. Coal rank has some indirect effects on the volatilisation of coal sulphur. It was shown that the presence of H_2 increases the rate of volatilisation of coal sulphur and the formation of H_2S during pyrolysis [6, 77, 85]. Lower ranked coals produce greater amounts of H_2 during their pyrolysis, indirectly increasing the rate of sulphur volatilisation. The blending of coals with higher volatile matter content (usually indicative of lower ranked coals) into a coal blend prevented the bonding of newly volatilised sulphur with nascent coke during coal pyrolysis [81].

The presence of CO_2 was shown to increase the rate of volatilisation of coal sulphur during pyrolysis [86,87]. However, it was shown to prevent the formation of CaS and prevent the low temperature decomposition of ferrous sulphate [87]. This indicates that increased CO_2 levels in the blast furnace, possibly as the result of an oxygen enriched blast, could affect the volatilisation and fixation of coal sulphur.

The gaseous sulphur products of pulverised coal injection can be hypothesised by assessing the sulphur forms in the injected coal, the amount of oxygen available, and the rate of the coal's combustion. H_2S was shown to be the primary gaseous of the pyrolysis of organic sulphurs, whilst SO_2 was shown to be released by inorganic sulphurs or via the combustion of H_2S in a secondary reaction [4–7,60,61,72,73,78,79,81,83,85,90]. The amount of H_2S that is oxidised to SO_2 was shown to increase with increased O_2 [90]. As the combustion of H_2S to SO_2 is a secondary reaction, the rate of SO_2 formation would be limited by the rate of H_2S formation. As already discussed, the rate of H_2S formation can be influenced by a coal's rank, this would therefore suggest that the combustion of lower ranked coals may lead to the more rapid production of SO_2. The relative amounts of H_2S and SO_2 leaving the raceway may affect the rate of sulphur fixation as there may be preferential reactions preventing the fixation of one of the gases in comparison to the other. Examples of which are the prevention of the reaction of H_2S with CaO due to the presence of CO_2, or SO_2 not reacting with Fe_2O_3 [87,89]

Part II

Experimental design and analysis

Chapter 4

Materials and experimental rigs

To pursue the answers to questions derived during the study of existing literature, a range of experiments were devised. The aim of these experiments was to replicate conditions found within the blast furnace as closely as feasibly possible with the equipment available within the laboratory. Relevant samples were procured from Tata Steel Europe and a range of third parties.

4.1 Drop tube furnace

A drop tube furnace (DTF) in Cardiff University School of Engineering's Combustion Laboratory was used to replicate conditions similar to the raceway region of a blast furnace coal injection system. This can be seen in Figure 4.1 and is described in Figure 4.2. The key conditions being high temperatures, high heating rates, and a dynamic, dilute particle phase [92]. In this work, coal samples were passed through the DTF at a temperature of 1100°C with residence times of 35 ms, 100 ms, 350 ms, and 700 ms. 1100°C is a typical hot blast temperature and specific to the application being studied [15]. Residence times were controlled by altering the length of a moveable water cooled collector probe up to a maximum length of 1.2 m from a water cooled feeder probe. The coal samples were fed into the top of the furnace via the screw feeder with a feed rate of 30 g/h, entrained into a laminar gas flow of 20 l/min. The partially burnt coal (char) was collected in a cyclone collector at the bottom of the furnace. The exhaust gas was then passed through a cellulose filter, which collected a volatile mixture of tar and fine particulates. The flue gas was sampled post filter for gas analysis by the Testo 350XL. The exhaust lines were also connected to an in-line O_2 analyser and flow could also be diverted to the Emerson gas analyser discussed in Section 5.11. The method expands upon those used by previous users of the furnace [13, 26, 93–96].

4.2 Coal Samples

Samples of four blast furnace injection coals that were of commercial interest were supplied by Tata Steel Europe. For reasons of commercial sensitivity, the coals were not named, but labelled from A to D. The coals were ground to a pulverised size distribution as described in Section 4.4. The proximate analysis (Section 5.1), sulphur forms (Section 5.1), and total sulphur (Section 5.4) can be found in Table 4.1.

Table 4.1: Proximate analyses and distribution of sulphur forms

Coal	Proximate analysis / % mass (dry)			Sulphur forms / % mass (dry)			
	Fixed carbon	Volatile matter	Ash	Pyritic sulphur	Sulphatic sulphur	Organic sulphur	Total Sulphur
A	71.8	20.9	7.2	0.04	0.00	0.24	0.28
B	60.9	34.8	4.3	0.01	0.07	0.35	0.43
C	68.9	21.2	9.9	0.05	0.02	0.32	0.39
D	58.1	38.5	3.4	0.05	0.08	0.26	0.39

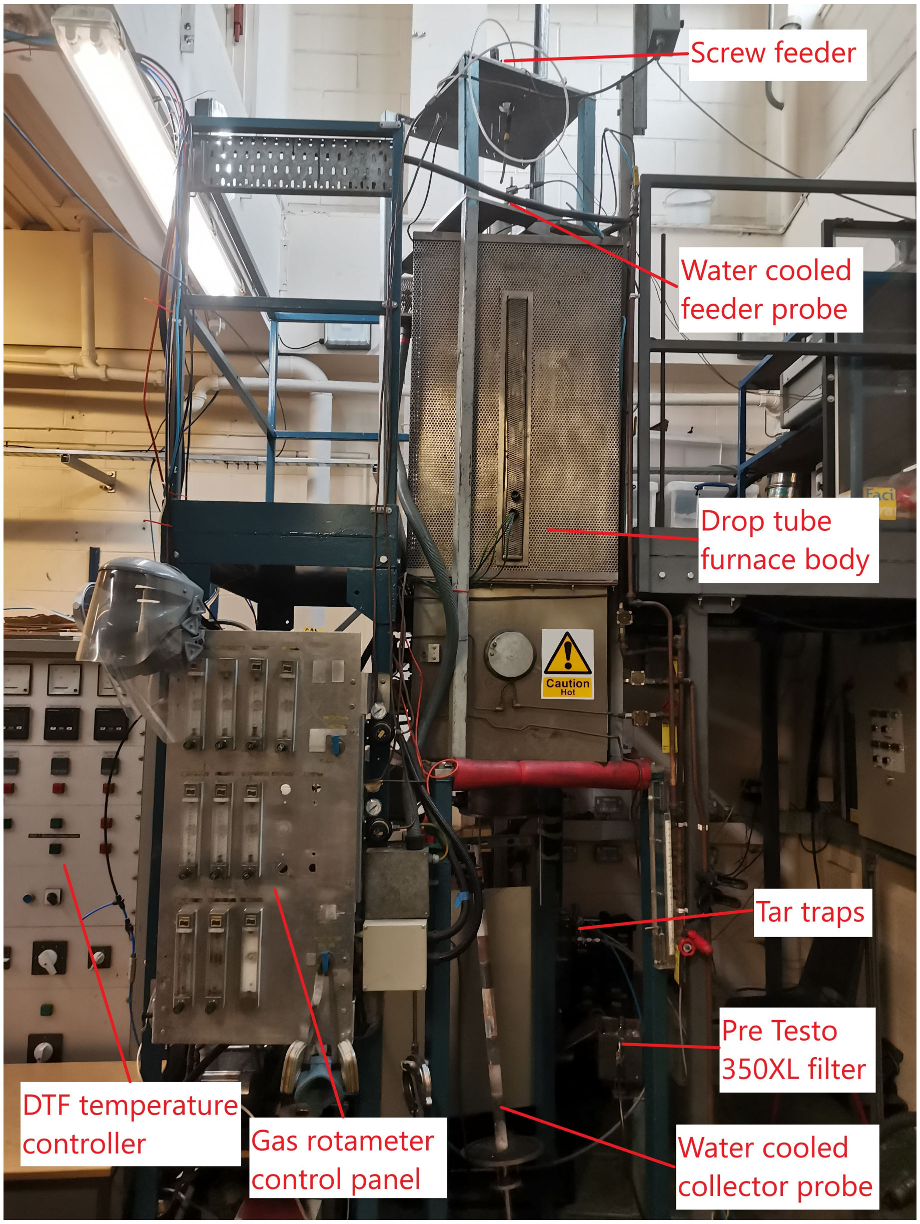

Figure 4.1: DTF in Cardiff University School of Engineering's Combustion Lab

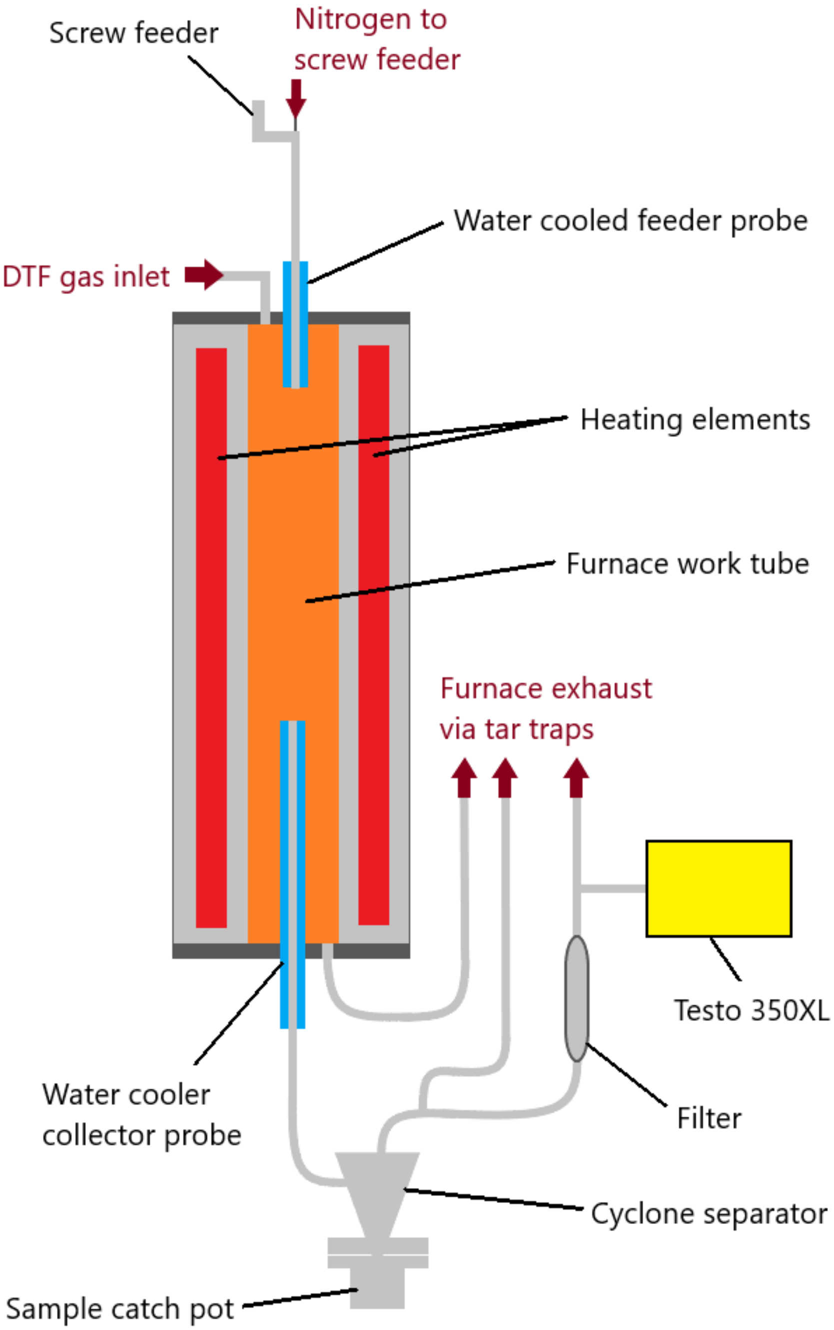

Figure 4.2: Schematic of DTF in Cardiff University School of Engineering's Combustion Lab

4.3 Alternative blast furnace injectants

4.3.1 Solid injectants

A number of alternative solid injectants were selected for use in this study. They represent a range of materials available on the open market, or in the case of one of the samples, an available waste product on-site. The proximate analysis of the materials used can be found in Table 4.2. The blast furnace dust is a waste product filtered from the top gas of the blast furnace. The NCT and Maxibrite biochars are both wood based biochars. The tyre derived fuel is, as the name suggests, produced from waste tyres. The Yorkshire Water biochar is produced from the pyrolysis of sewage sludge.

Table 4.2: Proximate analyses and total sulphur of alternative solid injectants

Injectant	Proximate analysis / % mass (dry)			Total sulphur / % mass (dry)
	Fixed carbon	Volatile matter	Ash	
Blast furnace dust	32.3	6.5	61.2	0.55
NCT biochar	81.0	16.2	2.8	0.75
Maxibrite biochar	70.2	10.8	19.0	0.22
Tyre derived fuel	27.6	64.9	7.5	1.99
Yorkshire Water biochar	57.2	6.8	36.0	0.54

Each of these injectants were ground to a pulverised size distribution, as described in Section 4.4, and blended with Coal C with a ratio of 10 mass% alternative injectant to 90 mass% of coal. The proximate analysis of these blends can be found in Table 4.3. Coal C was selected as the blend coal as it was the easiest coal to handle with regards to the drop tube furnace. By which, it fed easily, showed little agglomeration and therefore did not block either the injection or collector probes, and did not burn out too rapidly and so any variation due to the presence of the alternative injectants should have been measurable.

These blends were tested using the drop tube furnace as described in Section

Table 4.3: Proximate analyses and total sulphur of alternative solid injectants and Coal C 10:90 blends

Coal C blend plus	Proximate analysis / % mass (dry)			Total sulphur / % mass (dry)
	Fixed carbon	Volatile matter	Ash	
Blast furnace dust	63.5	22.0	14.5	0.37
NCT biochar	70.3	20.7	9.0	0.30
Maxibrite biochar	68.3	21.1	10.6	0.34
Tyre derived fuel	63.9	26.9	9.2	0.48
Yorkshire Water biochar	66.8	21.2	12.0	0.35

4.1. The produced chars were analysed by proximate analysis and the burnouts calculated using the ash tracer method, as described in Sections 5.1 respectively 5.2. Carbon and sulphur analysis was conducted by Tata Steel Europe in Port Talbot, as described in Section 5.4. The gasification reactivity of the produced chars was analysed using the method described in Section 5.6.1.

4.3.2 Gaseous injectants

Alternative gaseous atmospheres were used within the drop tube furnace to study the affect of these gases on the burnout of coals and the volatilisation of their sulphur. As described in Section 4.1, in standard operation, the air flow of the drop tube furnace was 20 l/min. During this study, the air flow was reduced to 10 l/min and premixed with 10 l/min of the test gas. The gases used were N_2, a 5 vol% H_2 95 vol% N_2 blend, and CO_2. The N_2 was used to produce a "blank" test with oxygen:carbon ratios that were comparable to the other test gases. This resulted in the gaseous atmospheres described in Table 4.4. The atmospheres were validated using an Emerson gas analyser, as discussed in Section 5.11, and an in-line oxygen analyser downstream of the drop tube furnace. Due to issues with particle swelling and blockages, no 35 ms chars were collected. The chars produced from this experiment were analysed using the Mettler Toledo TGA-DSC 3+ and the LECO SC32DR carbon and sulphur analyser, as described in Sections 5.6.3 and 5.4 respectively.

Table 4.4: Gas compositions of DTF test atmospheres

Gaseous atmosphere label	Gas composition / % vol			
	N_2	O_2	CO_2	H_2
N_2:Air	90	10	<0.1	0
N_2:H_2:Air	87.5	10	<0.1	2.5
CO_2:Air	40	10	50	0

4.4 Sample preparation

The samples used in the drop tube furnace were ground to a pulverised size specification (100% $< 300\mu m$, 50% $< 75\mu m$) using a TEMA disc mill (shown in Figure 4.3) and classified by dry sieving using BS ISO 1953:2015. Blast furnace burden material samples used in the adsorption of sulphur experiment were ground to a granulated size specification (100% $< 1mm$, 50% $< 250\mu m$) using the same method.

The samples were oven dried at 105°C for at least one hour prior to milling. This was done to prevent the adhesion of wet dust to the mill. The dry sample was placed in the fixed disc and the rotating disc was placed upon the sample. The lid was placed on the fixed disc and it was slotted into the rotator. The safety lid was closed and the mill was activated. The sample was left to mill for a couple of seconds before being removed and sieved. Sieves were placed on a vibrating plate and allowed to distribute through the meshes for several minutes. Each size fraction was weighed and any oversized particles were added back into the disc mill. This process was repeated as necessary to produce samples of the desired size specification.

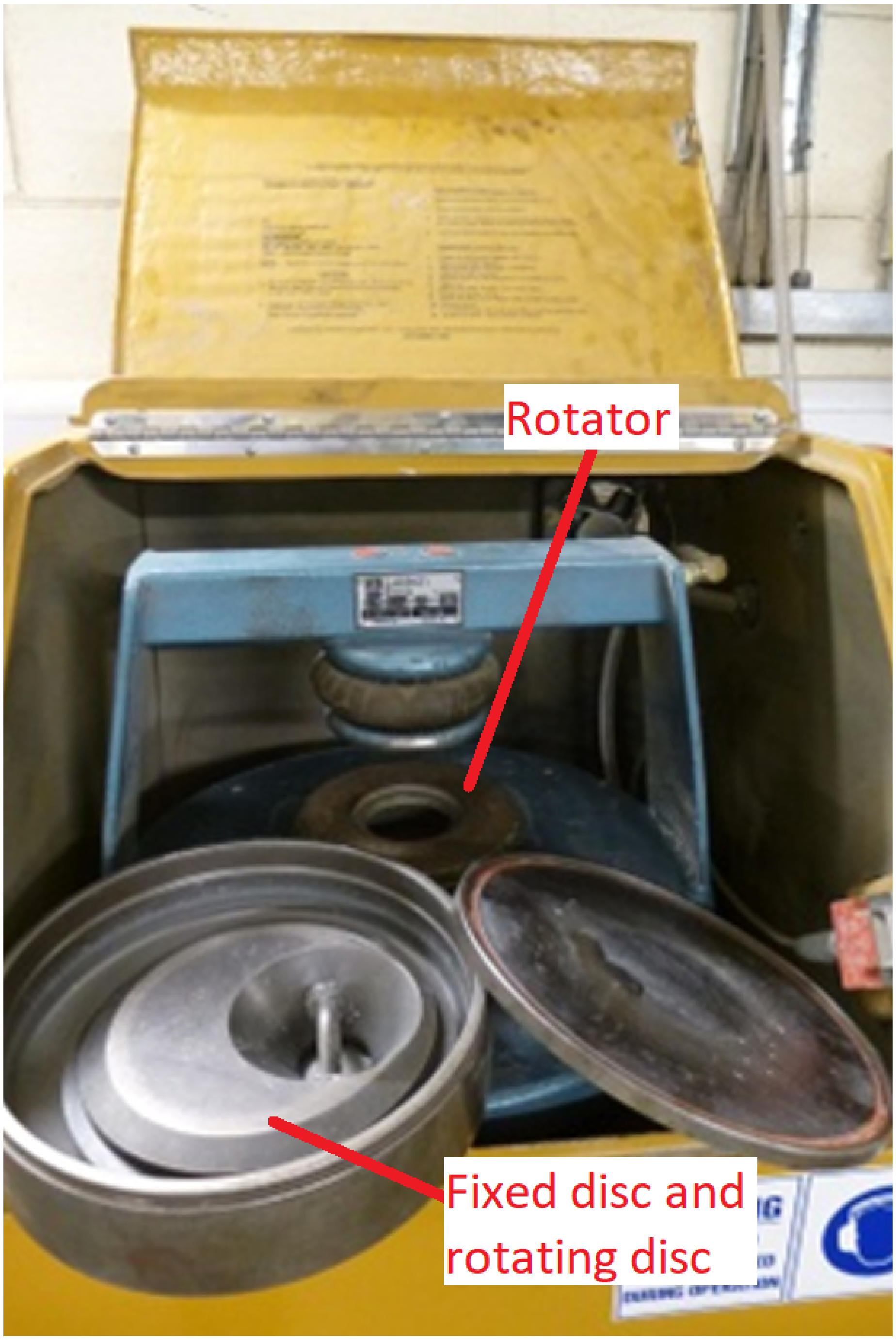

Figure 4.3: TEMA mill used for the grinding of coal samples

4.5 Fixation of gaseous sulphur by blast furnace materials

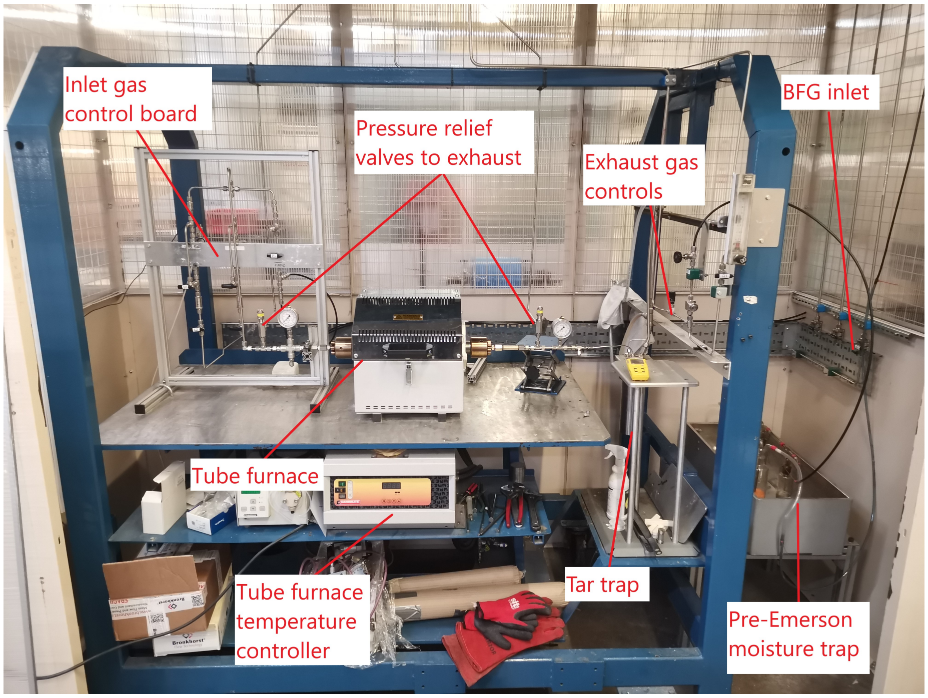

Figure 4.4: Experimental rig for investigating the relative desulphurising capacities of blast furnace gas by blast furnace materials

A horizontal tube furnace was operated under a moderate positive pressure to investigate the relative sulphur fixation of blast furnace gas by blast furnace materials at a range of temperatures. The experimental rig is shown in Figure 4.4, whilst a schematic of the rig can be found in Figure 4.5. In this experiment, 5 g of blast furnace material was placed in a quartz boat and heated to the test temperature in a 2 l/min flow of N_2 within the tube furnace visible in the centre of Figure 4.4. The reaction tube of the furnace had an internal volume of 0.21 l. At the test temperature, the N_2 was switched off and a mass flow controller (MFC) was used to release a flow of 1 l/min of a synthetic blast furnace gas

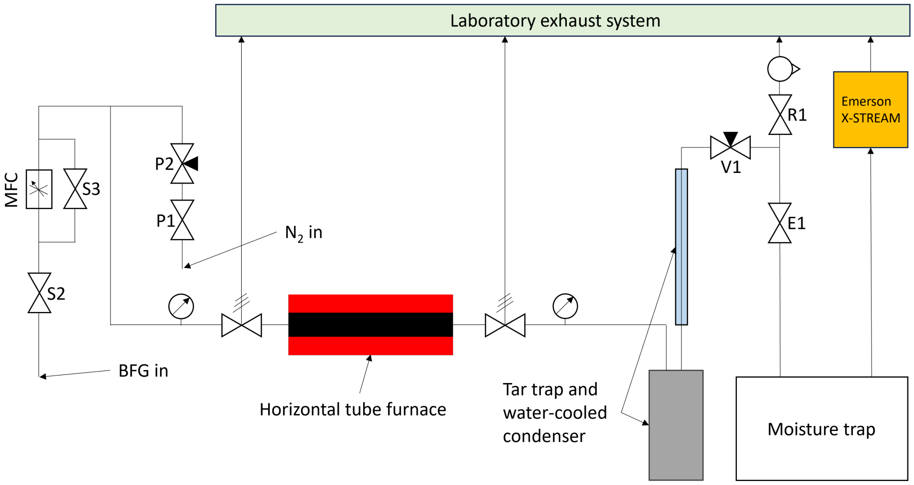

Figure 4.5: Experiment schematic for investigating the relative desulphurising capacities of blast furnace gas by blast furnace materials

(BFG) blend for a period of 1 hour. This allowed accurate measurement of the mass of sulphur entering the furnace. The composition of the BFG blend can be seen in Table 4.5. The gas was a custom blend supplied by Air Liquide and was composed in accordance with blast furnace top gas compositions from plant analysis and literature. The pressure of the experiment was controlled by a needle valve on the downstream of the furnace and was maintained at a target pressure of 1.5 barg, measured on pressure gauges either side of the furnace, replicating the pressure at the top of the blast furnace. At higher temperatures, this was difficult to maintain and sometimes fluctuated up to a maximum of 3 barg. The downstream exhaust was split into two lines, with one going to the extraction system and the other to the Emerson X-STREAM gas analyser discussed in Section 5.11. A more thorough description of the method is given in Section 4.5.1.

The blast furnace materials used in this experiment were supplied by Tata Steel Europe. The ICP elemental analysis can be seen in Table 4.6. The coke sample failed to digest for the ICP analysis, as such, only the sulphur analysis

Table 4.5: Gas composition of synthetic blast furnace gas

Gas composition / % vol				
N_2	CO	CO_2	H_2	H_2S
52.95	25	20	2	0.05

from the LECO SC32DR is given in the table. The methods for these analyses can be found in Sections 5.7 and 5.4 respectively.

Table 4.6: Elemental analysis of blast furnace materials using ICP

Sample	Elemental composition / % mass						
	Fe	Mg	K	Ca	Na	Si	S
Sinter	54.83	0.81	0.19	8.38	1.02	5.36	0.03
Pellet	64.32	0.85	0.17	1.07	0.79	4.79	0.01
Dolomite	0.61	6.57	0.23	17.03	0.76	3.74	0.03
Limestone	0.11	1.55	0.14	18.11	0.71	3.68	0.02
Coke*	-	-	-	-	-	-	0.71

*Sample analysed using LECO SC32DR.

After undergoing the experiment. The sample materials were weighed and analysed using either ICP analysis (sinter, pellets, dolomite, limestone) or via the LECO SC32DR (coke) to measure the change in total sulphur. This allowed the calculation of the percentage of gaseous sulphur removed from the BFG flow by the sample.

4.5.1 Development of the experimental rig and method

Due to the highly toxic nature of the synthetic BFG blend, which contains a significant percentage of toxic CO, as well as toxic H_2S, the development of the experimental rig and operating method was a time consuming and labour intensive process. As the BFG was both toxic and flammable, COSHH and DSEAR assessments were undertaken. A gas cloud model produced by staff at Cardiff University's Gas Turbine Research Centre was used to assess the release of the gas from system, this information was central to justifying the fabrication of control measures. In construction of the model and within the production of risk assessments, the following documents were consulted:

- HSE document L138 (Second Edition) – Dangerous Substances and Explosive Atmospheres Regulations, Approved Code of Practice and guidance.
- The Equipment and Protective Systems Intended for Use in Potentially Explosive Atmospheres Regulations 1996.
- HSE document INDG370 – Controlling fire and explosion risks in the workplace.
- BCGA Code of Practice CP4 – Industrial gas cylinder manifolds and gas distribution pipework (excluding acetylene) Revision 4: 2012.
- BCGA Guidance Note GN13 – DSEAR Risk Assessment 2008.
- BS EN 60079-0:2012 Explosive atmospheres, Part 0 – General Requirements.
- BS EN 60079-10-1:2009 Explosive atmospheres – Part 10-1: Classification of areas - Explosive gas atmospheres.
- BS EN 60079-10-1:2021 Explosive atmospheres – Part 10-1: Classification of areas - Explosive gas atmospheres.
- BS EN 60079-20-1:2010 Explosive atmospheres, Material characteristics for gas and vapour classification. Test methods and data.
- BS EN 60079-32-1:2013 Explosive atmospheres, Electrostatic hazards, guidance.
- OGP 434-14 Vulnerability of humans

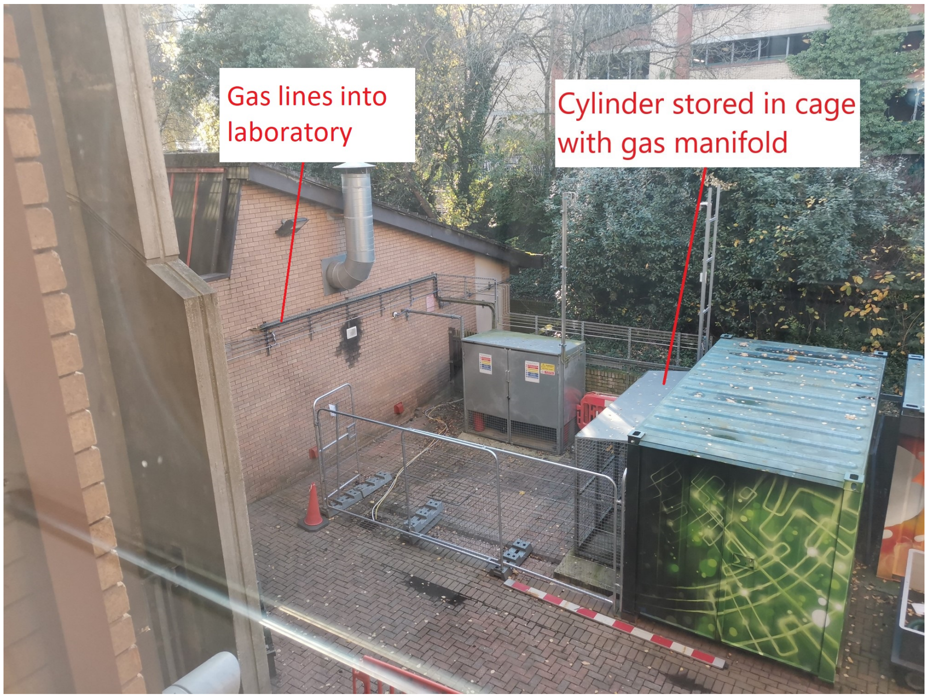

Figure 4.6: Gas bottle storage outside laboratory

Upon completion of the relevant assessments, the first consideration was the storage of the gas cylinder. Calculations of possible gas cloud sizes from accidental release of the gas were used to produce a suitable cordon size for the gas bottle store, which can be seen in Figure 4.6. A new, Chem-Master Gas Arc manifold was installed to accommodate the presence of corrosive H_2S in the gas mix. An e-stop was connected to the manifold to cut off the flow of the BFG cylinder to the manifold in the case of an emergency. A N_2 purge was also connected to the manifold.

The BFG entered the laboratory through a continuously welded stainless-steel pipe. Once within the laboratory, similar considerations had to be made regarding the accidental release of toxic gas clouds. The pipe had two drop points within the lab. The first was blocked off and was a dead leg. As per

Figure 4.7: Fume hood built to house experiment within laboratory

the risk assessment, this was checked with a portable gas monitor prior when the gas was brought into the lab for potential leakage. The second drop point was brought into a fume hood that was constructed to house the experiment. This can be seen in Figure 4.7. This fume hood was connected to the lab air extraction system, which was always on during operation of the experiment. The flow rate of the extraction system was used in the aforementioned gas cloud model to ensure that this was a suitable control to prevent the formation of a toxic/flammable gas cloud within the laboratory. Additional gas monitors were present in several locations around the laboratory.

The experimental rig was constructed so that it could be operated using N_2, CO_2, or the synthetic BFG mix. These gases were brought to the left-hand side of the rig, where they were controlled by a series of valves, and in the case of

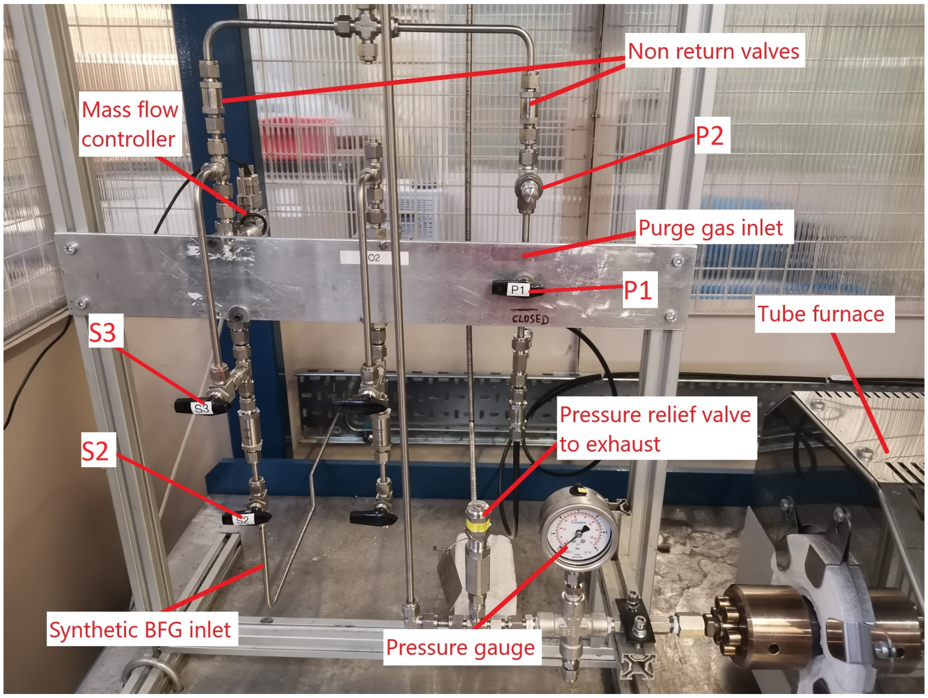

Figure 4.8: Left-hand side of the experimental rig

the BFG, by a MFC. Figure 4.8 shows the left-hand side of the experimental rig. The valve P1 opened the ”purge” line, which was connected to N_2 and CO_2 drop points outside of the fume hood, where their corresponding valves could be found. P2 was a needle valve that was used to control the inlet flow of the purge gas. The valve S2 connected the BFG to the MFC from the point at which the gas enters the fume hood at valve S1, which can be seen in the background of Figure 4.9. S3 was a bypass for the MFC which was used during the priming and purging of the gas line. The central set of valves with the O2 label were left over from a previous configuration of the rig and were not connected to the system. The gas passed through a pressure relief valve (PRV) set at 5 barg (the yellow topped connection to the exhaust) and a pressure gauge before entering the tube furnace.

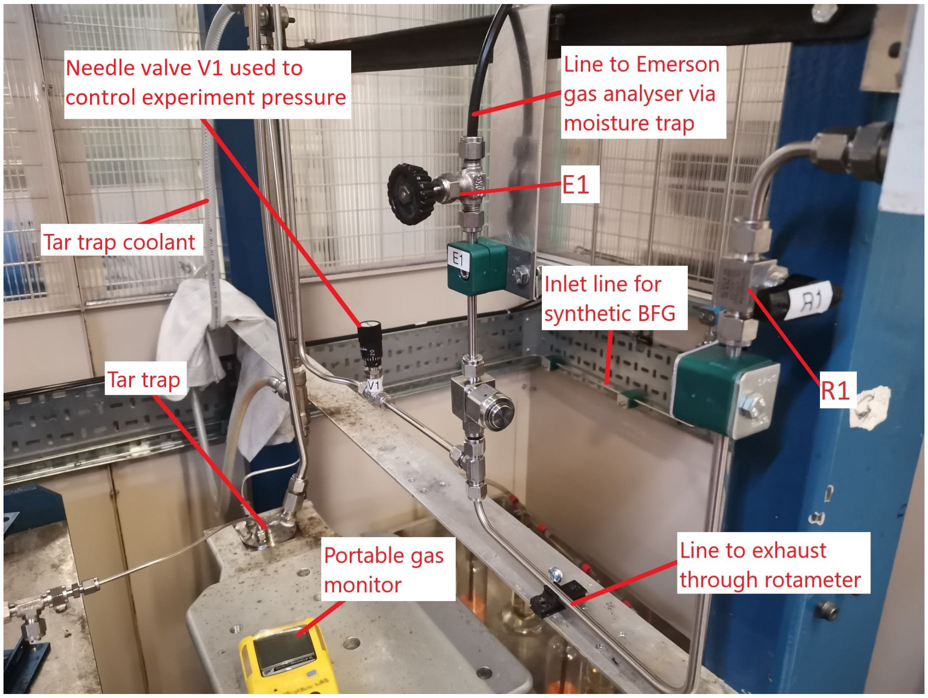

Figure 4.9: Right-hand side of the experimental rig

On the right-hand side of the rig, the gas exits the tube furnace, passes through another PRV set at 5 barg, enters a water-cooled tar trap, passes through the Vernier gauge V1, which was used to control the system pressure, before the line is split leading to valves E1 and R1. E1 controlled the gas flow through the moisture traps, visible at the bottom of Figure 4.9. This line then leaves the fume hood and proceeds to the Emerson gas analyser, discussed in Section 5.11, before entering the lab exhaust. As per the risk assessment, this line was checked with a portable gas monitor for possible leaks. R1 controlled the flow to a rotameter calibrated to CO_2, which was used to roughly validate the flow of the MFC, before heading to the lab exhaust.

The operation of the experiment was subject to a standard operating procedure due to the need to ensure the safety of the user and others, however a condensed description of the method is as below.

1. The lab extraction system was started. Portable gas monitors with CO, H_2, C_XH_Y, and O_2 channels were activated. One was placed on the right-hand side of the rig and one was worn by the operator of the experiment.
2. The experimental rig was sealed and all valves start in the closed position.
3. N_2 was passed through the rig by opening valves P1 and P2, opening the valves in sequence and leak checking each joint. When the system was fully leak checked, the N_2 was switched off by closing valve P1.
4. The BFG cylinder was opened, the e-stop pressurised (allowing the flow of the gas to the manifold), and the manifold exit pressure set to 3 barg.
5. The BFG was brought through to the MFC by opening the valves S1 and S2. S3 was opened and the rig primed with the BFG. S2 and S3 were closed when the BFG was detected by the Emerson gas analyser.
6. The system was purged with N_2 by opening valve P1. The N_2 was switched off when the values measured by the Emerson indicated that it was safe to do so.
7. The right-hand side of the furnace was opened and 5 g of dried sample was entered into the furnace within a quartz boat. The system was resealed and leak checked using N_2.
8. The furnace was turned on and set to the experiment temperature. The furnace was allowed to heat in a 2 l/min flow of N_2.
9. Once the desired temperature was reached, the N_2 was switched off and the system allowed to depressurise. Valve S2 was opened and the MFC was set to allow a flow of 1 l/min (normalised) of the BFG for a period of

one hour. This allowed an accurate knowledge of the amount of sulphur entered into the experiment.

10. The Vernier Gauge V1 was used to control the pressure of the experiment at 1.5 barg.

11. After an hour, the MFC automatically closed and the system was allowed to depressurise. Valve S2 was closed. The N_2 purge was turned on and the furnace set to cool.

12. When both the temperature and gas measurement on the Emerson were suitable, the N_2 was turned off and the right-hand side of the furnace were opened to retrieve the sample. The sample was weighed and placed within a sample container.

13. The experimental rig was then either resealed with a new sample and the process repeated, or sealed without a sample, leak checked with N_2, and then the BFG line is purged with N_2 ready for the shut down procedure.

Chapter 5

Analytical instruments and techniques

5.1 Proximate analysis

Proximate analysis was conducted using BS ISO 17246:2010. In this standard, coal was analysed for moisture, ash, and volatile matter. In this work, the results are reported on a dry basis and so the moisture content was disregarded. Drying was undertaken by heating the samples at 105°C for an hour before being cooled in a desiccator. Fixed carbon (C_{fix}) was calculated using Equation 5.1.

$$C_{fix} = 100 - (A + V) \tag{5.1}$$

Where A was the ash and V was the volatile matter, expressed as percentage mass fractions.

The determination of ash was conducted using BS ISO 1171:2010. The ash was what remained after the coal has been incinerated in air and was derived from inorganic complexes present in the original coal and associated mineral matter. The test portion was heated in air to 500°C and held at that temperature for an hour before being heated to 815°C and held again at that temperature for an hour. The test portion was then removed and cooled in a desiccator. Ash was then calculated using Equation 5.2.

$$A = \frac{m_{A3} - m_{A1}}{m_{A2} - m_{A1}} \times 100 \tag{5.2}$$

Where m_{A1} was the mass of the empty dish, m_{A2} was the mass of the dish plus the test portion, and m_{A3} was the mass of the dish plus the ash.

The determination of volatile matter was conducted using BS ISO 562:2010. The volatile matter of a coal was determined as the mass portion that is lost when the coal was heated in the absence of air at 900°C for 7 minutes. As the samples were dried prior to testing, the moisture content need not be considered in this case. Volatile matter was calculated using Equation 5.3.

$$V = \frac{m_{V2} - m_{V3}}{m_{V2} - m_{V1}} \times 100 \tag{5.3}$$

Where m_{V1} was the mass of the empty crucible and lid, m_{V2} was the mass of the crucible, lid, and test portion prior to heating, and m_{V3} was the mass of the crucible, lid, and test portion after heating.

5.2 Burnout calculations using the ash tracer method

The burnout of the coal samples was used in production of a sulphur mass balance. The burnout (%) was calculated using the ash tracer method, as shown in Equation 5.4, using the ash content of the coal (A_{coal}) and the ash content of the corresponding char (A_{char}).

$$Burnout(\%) = \frac{10^4(A_{char} - A_{coal})}{A_{char}(100 - A_{coal})} \quad (5.4)$$

The ash tracer method is a commonly used method of analysing the mass lost during partial combustion of a sample [26, 94]. The method assumes that the coal ash remains conserved in the char residue under the test conditions and that no ash species are volatilised. This assumption may therefore lead to a small degree of error. However, the ash tracer method is a more reliable way of measuring the combusted portion of the coal in this instance as experimental constraints prevent accurate mass measurements before and after the coal is passed through the DTF. In this work, it has been used as a normalising value in the production of the sulphur mass balances, an adaptation of its use in previously published work [94]. Error values were calculated by propagating the standard deviations of the coal and char ash measurements.

5.3 Determination of sulphur forms

The determination of sulphur forms in the coals and DTF chars were undertaken using the method described in BS 1016-106.5:1996, ISO 157:1996 Methods for analysis and testing of coal and coke. Ultimate analysis of coal and coke. Determination of forms of sulfur in coal.

The method described by the standard allows the identification of pyritic and sulphatic sulphur in a coal sample. This was done by utilising the different solubilities of pyrites and sulphates in dilute hydrochloric and nitric acids under reflux conditions, such that each can be taken into solution successively and determined directly [8]. An overview of the method is shown in Figure 5.1.

The work was performed using laboratory grade reagents supplied by Fischer Scientific. Due to the low sulphur content of the samples being analysed, 8 g of sample was used in each repeat. The pyrite content of the samples was

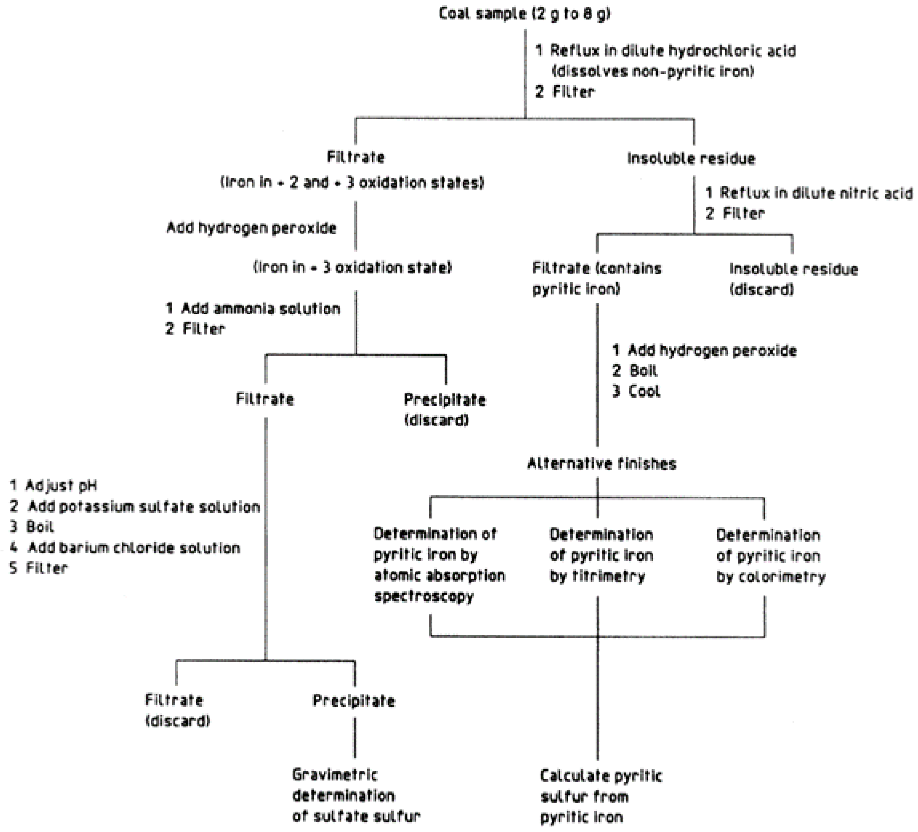

NOTE — Organic sulfur = Total sulfur − (sulfate sulfur + pyritic sulfur)

Figure 5.1: An overview of the method employed by BS 1016-106.5:1996, ISO 157:1996 [8]

determined by the titrimetry finish. The work was completed in duplicate and results did not differ by more than 0.02% absolute.

The data gathered in this experiment was used in conjunction with total sulphur measurements and burnout calculations as described in Sections 5.4 and 5.2 respectively.

5.4 Total carbon and sulphur analysis

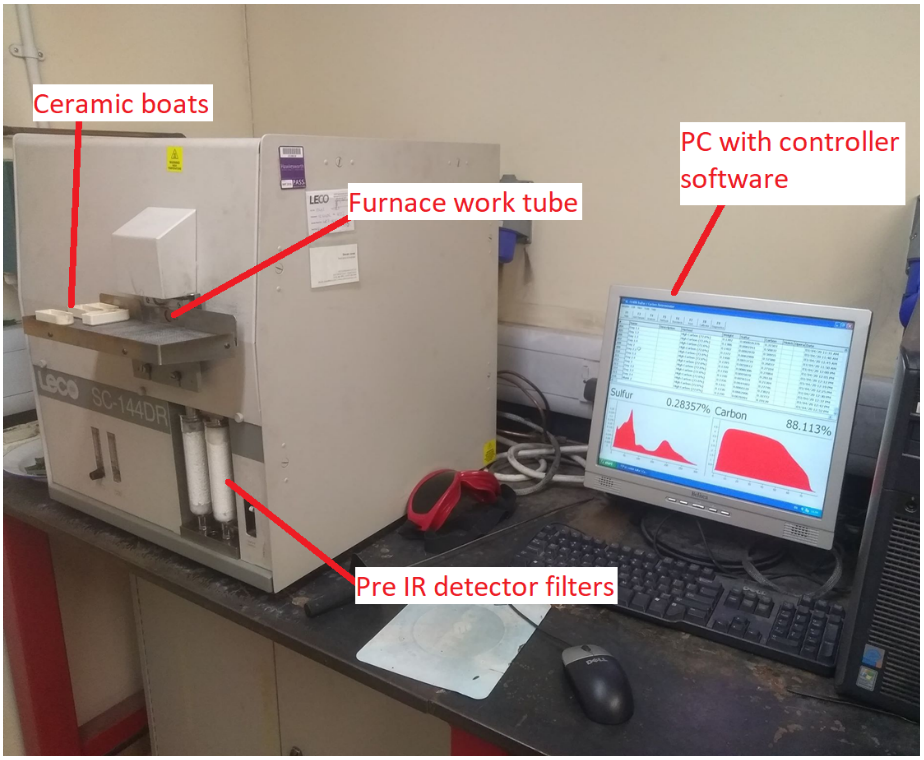

Figure 5.2: The LECO SC-144DR carbon and sulphur analyser in Cardiff University School of Engineering

The total sulphur of sample materials was measured using the LECO SC-144DR carbon and sulphur analyser shown in Figure 5.2. The analyser operates at 1350°C in an oxygen atmosphere, promoting the complete combustion of the samples. The analyser then measures the CO_2 and SO_2 produced by comparing the quantity of measured gas to the inputted sample mass, a total sulphur value can be produced. The instrument was regularly calibrated with standards supplied by LECO and checked prior to the commencing of any work. Results were taken from the mean value of a minimum of three repeats. Error values were calculated by using the standard deviations of these results.

The method used to operate the LECO SC-144DR is described below.

1. Ensure that the oxygen flow to the device was on and that the furnace was operating at desired temperature (1350°C).

2. A nickel boat liner was placed in a ceramic boat. Samples of between 0.1-0.3g were added to the boat, the exact mass was noted on the computer software. The mass used was changed depending on factors such as sample volatility and density.

3. The sample was placed ready to be inserted into the instrument. The instrument was set to run, after initial stabilisation of the readings, a prompt to insert the sample boat was given. The sample was pushed into the instrument and combustion began. The gas analysis detected the the presence of combustion products using an infra-red detector and began logging the data automatically.

4. The experiment was completed when the detection of combustion products was returned to the base levels and remained constant. The sample boat was then removed from the instrument and allowed to cool. The sample's % mass of carbon and sulphur was displayed on the software.

During the study period, the LECO SC-144DR was mothballed due to the development of unrepairable faults. A replacement was not made available with sufficient time left in the project. Instead, later analysis was performed by the Tata Steel UK analytical team in Port Talbot. They performed the analysis initially on an ELTRA CS500 Carbon Sulfur Determinator. This was later replaced by a LECO SC832DR. The analysers operated in a similar fashion to the LECO SC-144DR. 0.25 g of sample was combusted in oxygen at 1350°C, which facilitated the complete combustion of the sample. The produced carbon dioxide and sulphur dioxide was then measured using an infra-red detector.

5.5 TESTO 350XL

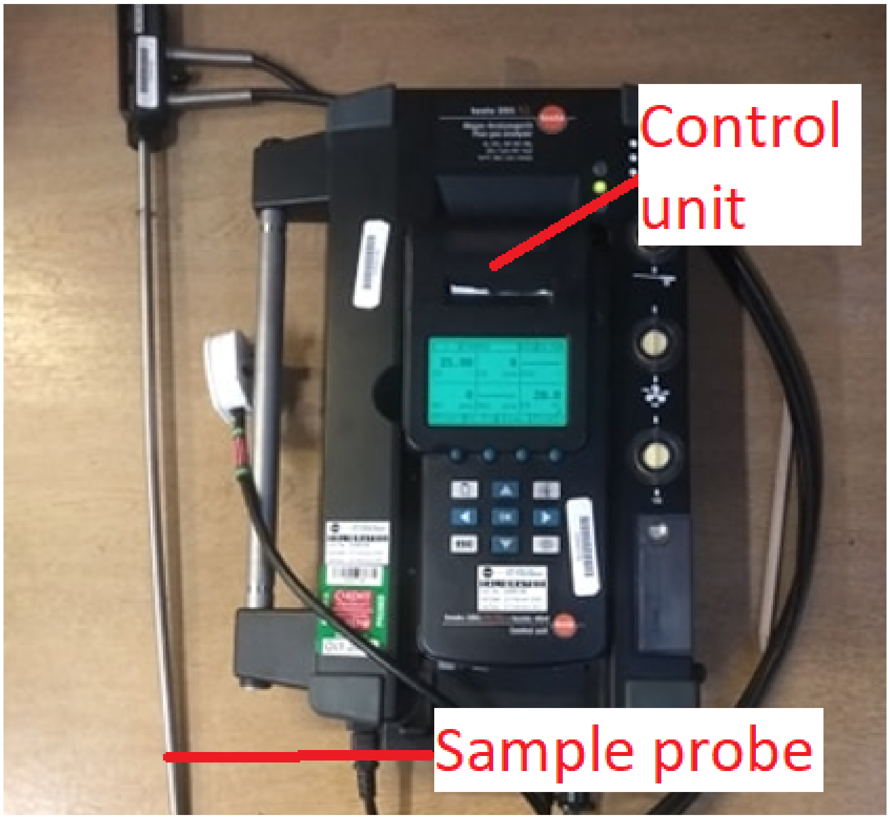

Figure 5.3: The TESTO 350XL gas analyser

Gas analysis of the DTF flue gas was conducted using a Testo 350XL, shown in Figure 5.3. CO, CO_2, O_2, SO_2, and H_2S levels were measured in real time and tracked using Testo's easyEmission software. This allowed the monitoring of the combustion occurring in the DTF whilst also providing information that could be used in the creation of sulphur mass balances. The Testo 350XL sampled the DTF flue gas at a rate of 1 l/min in parallel to the exhaust line. Calibrations were performed by Testo Limited prior to the commencing of the study and checked regularly with calibration gases provided by Rockall Safety Limited.

5.6 Thermogravimetric analysis

Figure 5.4: Mettler Toledo TGA-DSC 3+ in Cardiff University School of Engineering's Combustion Lab

Thermogravimetric Analysis (TGA) is a commonly used analytical technique that measures the mass of a sample over time whilst it is heated. This can be done in a range of gaseous atmospheres and allows, amongst other things, the analysis of combustion, pyrolysis, and gasification. Analysis was undertaken using the Mettler Toledo TGA-DSC 3+ in Cardiff University School of Engineering's Combustion Lab, which can be seen in Figure 5.4.

5.6.1 TGA char gasification reactivity

A heating program was designed to produce conditions representative of conditions found in the blast furnace. Samples were heated in N_2 from 25°C to 900°C at a heating rate of 25°C/min. The sample was then held for 7 minutes at 900°C in N_2 to remove the remaining volatile components present in the chars, allowing the analysis of the solid chars only. The char was then held at 900°C in a 100 ml/min flow of CO_2 for 480 minutes. 900°C was selected as the experimental temperature as this represents a temperature region higher in the blast furnace where unburnt char may accumulate. The reverse Boudouard shown in Equation 5.5 causes the gasification of the remaining solid char.

$$CO_2 + C \rightarrow 2CO \tag{5.5}$$

Mass loss was measured against time and used to calculate char conversion in Equation 5.6 below.

$$x = \frac{m_{initial} - m}{m_{initial} - m_{final}} \tag{5.6}$$

Where x was the char conversion, $m_{initial}$ was the initial sample mass, m was the instantaneous mass, and m_{final} was the mass of the final char ash. The results of this experiment are expressed in the gasification figure $t_{0.5}$, which was the time in minutes taken to reach 50% char conversion. The lower the $t_{0.5}$ number, the more reactive the char [95].

The Mettler Toledo TGA-DSC 3+ was damaged by the human error of another user towards the end of the study period, as such, some planned char gasification reactivity work was unable to be completed.

5.6.2 TGA combustion analysis

The Mettler Toledo TGA-DSC 3+ was used to examine the combustion of alternative solid fuels. In this process, samples were heated in a 100 ml/min flow of air from 25°C to 1000°C at a heating rate of 10°C/min before being held at 1000°C for 60 minutes. Comparisons in ignition points and mass loss were compared to the studied coals.

5.6.3 TGA proximate analysis

In order to conserve samples where only a small amount of char was produced, the TGA was used to perform proximate analysis on a number of chars. This was undertaken by performing the following method on the TGA:

1. The sample was heated from 25°C to 900°C at a heating rate of 50°C/m in a 50 ml/m flow of N_2.
2. The sample was held at 900°C for 7 minutes in a 50 ml/m flow of N_2.
3. The sample was cooled from 900°C to 815°C at a cooling rate of 50°C/m in a 50 ml/m flow of N_2.
4. The sample was held at 815°C for an hour in a 50 ml/m flow of air.

The volatile matter and ash were calculated by measuring the mass losses in steps 2 and 4 and using the values in Equations 5.3 and 5.2 respectively.

5.7 Inductively coupled plasma optical emission spectroscopy

Inductively coupled plasma optical emission spectroscopy (ICP-OES or commonly just ICP) was used to analyse the elemental composition of mineral based powders. The method provides greater accuracy than XRF, but also has some drawbacks in that it is a destructive, wet chemistry method and requires carbonaceous samples to be ashed prior to analysis. This work was conducted by the technician in Cardiff University School of Engineering CLEER labs.

The method used is descried below.

1. 100 mg of sample was weighed to the nearest mg on a 4 figure balance.
2. 2 ml of reagent grade hydrofluoric acid at a concentration of 48-51% was added to the weighed sample, and left to soak overnight for 18 hours.

3. 3 ml of 37% reagent grade hydrochloric acid and 3 ml of 70% reagent grade nitric acid were added and then the sample was microwaved for 30 minutes in an Anton Parr Multiwave 3000.
4. The hydrofluoric acid was neutralised with 12 ml of 4% boric acid H_3BO_3, and then replaced into the microwave for a further 30 minutes.
5. The final volume was made up to 50 ml with deionised water.
6. These digested samples were analysed using a Perkin Elmer Optima 2100 DV ICP-OES machine.
7. The ICP machine was calibrated prior to each test campaign using a 28 element calibration solution with a concentration of 100 mg/l.
8. The solution was diluted down to 10 mg/l and 1 mg/l to perform the calibration, and the calibration curves created during this process were used to determine the concentration of the elements in the tested samples.
9. The given results were expressed as mg/kg, these are divided by 10,000 to be expressed as mass%.

ICP analysis was mostly utilised to measure the change in Total Sulphur in the samples produced by the experiment discussed in Section 4.5.

5.8 X-ray photoelectron spectroscopy

A Kratos Axis Ultra DLD system (shown if Figure 5.5) was used to collect X-ray photoelectron spectroscopy (XPS) spectra using monochromatic Al Kα X-ray source operating at 144 W (12 mA x 12 kV). Data was collected with pass energies of 160 eV for survey spectra, and 20 eV for the high-resolution scans with step sizes of 1 eV and 0.1 eV respectively. Samples were mounted by pressing on to doubled sided Scotch tape (type 665) which was attached to

Figure 5.5: Kratos Axis Ultra DLD system used for X-ray photoelectron spectroscopy

a glass slide to ensure the sample was floated from the spectrometer. Analysis was performed using the Hybrid mode, which utilised a magnetic immersion and electrostatic transfer lenses to enhance electron detection. Data was collected over a rectangular analysis area of approximately 300 x 700 μm^2. A magnetically confined low energy electron charge compensation system was used to minimize charging of the sample surface, and all spectra were taken with a 90° take of angle. A base pressure of ca. 1 x 10^{-9} Torr was maintained during collection of the spectra. Data was analysed using CasaXPS (v2.3.24) after subtraction of a Shirley background and using modified Wagner sensitivity factors as supplied by the manufacturer. The analysis was undertaken in Cardiff University's School of Chemistry by Dr David Morgan, an expert in surface analysis.

5.9 X-ray fluorescence

Figure 5.6: Innov-X Systems X-5000 X-ray fluorescence analyser

An Innov-X Systems X-5000 X-ray fluorescence (XRF) analyser, shown in Figure 5.6, was used to measure the elemental compositions of dry, powdered samples. XRF results were used to quickly identify which elements to analyse for in the more accurate ICP analysis, as discussed in Section 5.7. The benefit of XRF in this instance was that it was a quick, non-destructive method. The instrument did have its limitations with magnesium being the lightest element detectable. The instrument was calibrated with a 316 stainless steel sample prior to use and operated in the "Mining Plus" mode.

5.10 Scanning electron microscopy

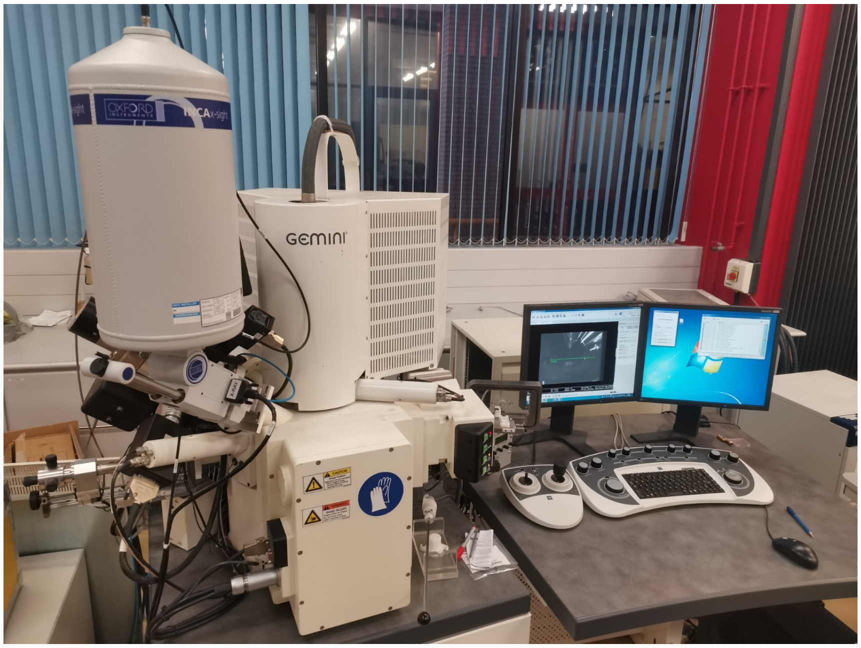

Figure 5.7: ZEISS CrossBeam 1540 XB

Scanning electron microscope (SEM) images were taken using a ZEISS CrossBeam 1540 XB, which is shown in Figure 5.7. SEM images were used to examine the surface morphology of test materials. Energy-dispersive X-ray spectroscopy is a technique utilising SEM and can be used to determine the elemental composition of selected points of a sample.

5.11 Emerson X-STREAM gas analyser

An Emerson X-STREAM gas analyser was used to monitor the CO, CO_2, CH_4, and H_2 in the flue gases of the DTF and from the horizontal tube furnace experiment described in Section 4.5. It was calibrated by Emerson technicians and checked against gas mixes of known concentrations when in use. Flue gas was fed into the instrument at a flow rate of 50 ml/min. The analyser vented

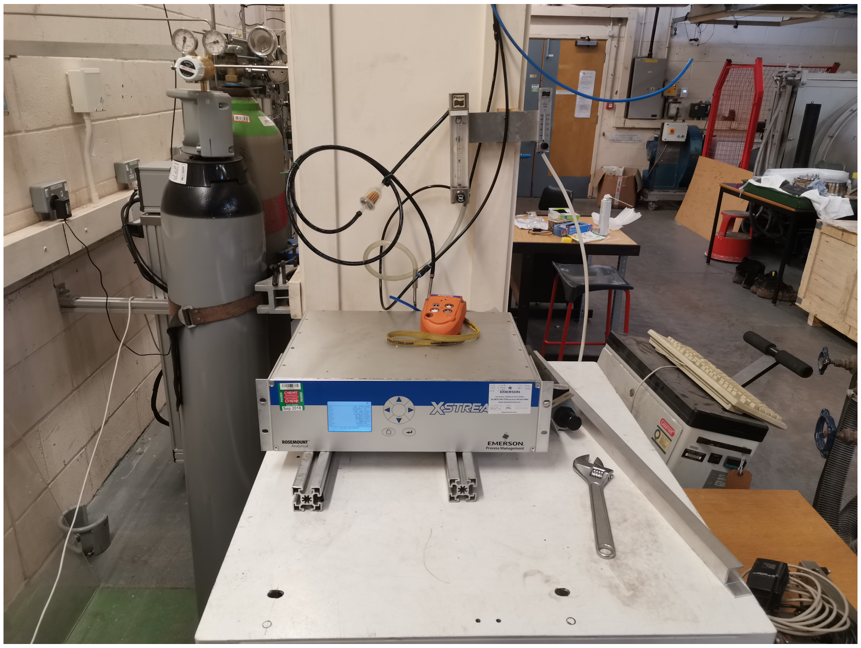

Figure 5.8: Emerson X-STREAM gas analyser

to the laboratory extraction system.

5.12 Analysis of standard deviation

The standard deviation measures how dispersed a data set is in relation to the mean. It was used in this study in the estimation of experimental error. The standard deviation (σ) was calculated via Equation 5.7.

$$\sigma = \sqrt{\frac{\Sigma(x - \bar{x})^2}{(n-1)}} \tag{5.7}$$

Where x was the observed value of the samples, $\bar{x}$ was the sample mean, and n was the sample size.

On multiple occasions, results that are presented in this thesis were produced from the accumulation of several analyses. On these occasions, it was possible for errors to accumulate and produce a greater range of error than each individual analysis or experiment. To quantify the accumulation of error, the propagated error was calculated by using Equation 5.8.

$$\sigma_x = \sqrt{\left(\frac{\sigma_a}{\bar{a}}\right)^2 + \left(\frac{\sigma_b}{\bar{b}}\right)^2} \tag{5.8}$$

Where σ_x was the propagated error, σ_a was the standard deviation of variable a, of which $\bar{a}$ was the mean value, and σ_b was the standard deviation of variable b, of which $\bar{b}$ was the mean value.

Part III

Results

Chapter 6

The volatilisation of coal sulphur in the DTF

6.1 Introduction

By analysing the volatility of coal sulphur in the DTF, it may be possible to predict the effect that each of the component sulphur forms may have on the sulphur chemistry of a blast furnace. This could prove to be crucial information when considering coal selection or blending as it could minimise the need for costly desulphurisation processes or improve blast furnace efficiency by allowing changes to slag chemistry. By manipulation of coal blends, it may be possible to mitigate against the formation of undesirable sulphur compounds within the blast furnace by removing certain sulphur sources or by exploiting specific coal properties that affect sulphur transformation within the furnace.

6.2 Char burnout, 35 ms char gasification reactivity, and total sulphur volatilisation

The relative burnouts of the coal chars generated in the DTF can be seen along with the relative volatilisation of the coal sulphur to H_2S or SO_2 in Figure 6.1, whilst Figure 6.2 shows the distribution of sulphur between the solid and gaseous phases, measured by the TESTO 350XL, at each of the studied residence times. The char reactivity of the produced 35 ms chars was measured on the Mettler Toledo TGA-DSC 3+ and can be found in Table 6.1.

Coal A has the lowest total sulphur of the four tested coals. After 35 ms, the majority of the original sulphur remains in the char with only 29.3% of the sulphur being liberated to H_2S. The burnout of Coal A's 35 ms char was quite low, only 11.1%. This was much lower than the burnouts of all the other coals at 35 ms. After 100 ms, 50.2% of sulphur was liberated to H_2S with a burnout of 35.6%. After 700 ms, 98.3% of sulphur was liberated to H_2S with a burnout of 95.0%.

Coal B had the highest total sulphur of the four tested coals. After 35 ms, 66.6% of the sulphur had been liberated to H_2S with a 48.8% burnout. The result after 100 ms is comparable to the 35 ms residence time, with 65.1% of sulphur liberated with a burnout of 55.8%. The similarity between the two residence times is likely explained by the large volatile matter content in the coal (34.8%) being quickly liberated in the first 35 ms. In the same sense, the similarity in the amount of sulphur liberated can likely be attributed in part to the liberation of less thermally stable sulphur compounds, such as aliphatic organic sulphurs or pyrite, and the survival of more thermally stable sulphur compounds in the char, such as thiophenes and sulphates, which has previously been shown to occur by several authors [4, 5, 73, 77, 82, 84, 97]. After 700 ms,

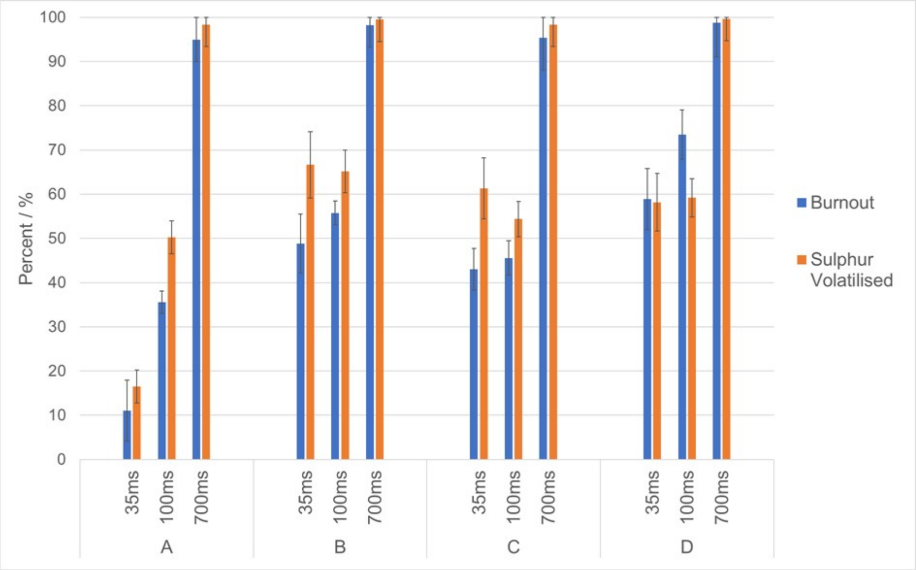

Figure 6.1: Relative burnouts and coal sulphur volatilisation to H_2S or SO_2 of DTF 35 ms, 100 ms, and 700 ms chars.

99.5% of the sulphur has been liberated with a 98.2% burnout. In this instance, SO_2 is the major gaseous product. This is thought to be primarily produced by the oxidation of H_2S as opposed to being directly released from the coal.

Coal C liberated 61.3% of its sulphur at 35 ms with a burnout of 43.0%. At 100 ms, the sulphur liberated was 54.4% with a burnout of 45.6%. At 700 ms, 98.3% of sulphur was liberated at 95.4% burnout. H_2S remains the major gaseous product at 700 ms with a smaller fraction of SO_2 being produced. Coal C showed a larger initial volatilisation of sulphur than the other medium volatile coal, Coal A, and was more closely following the trend of the high volatile coals, Coals B and D. Coal C's initial rate of burnout is also higher than Coal A's, but not quite as great as the highly volatile coals, Coals B and D. Why Coal C does not continue to behave like Coals B and D may be explained by the reactivity of the produced char. Table 6.1 shows that Coal C produced the least reactive 35 ms char. Reactivity of a char has been linked to the presence of pores in the char,

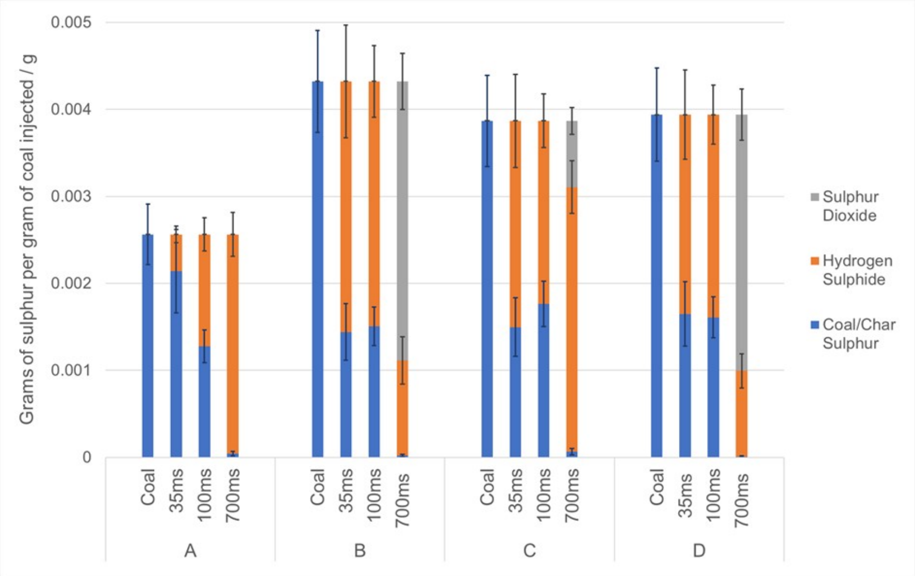

Figure 6.2: Distribution of sulphur in sampled coals, DTF exhaust gases, and 35 ms, 100 ms, and 700 ms chars.

which would allow for the increased flow of gases into the char particle [95]. This would likely accelerate the decomposition and volatilisation of the remaining, non-volatile char particle.

Coal D liberated 58.2% of its sulphur at 35 ms with a burnout of 58.9%. At 100 ms, 59.2% of sulphur was liberated with a burnout of 73.5%. This is the largest change in burnout between 35 ms and 100 ms, whilst maintaining only a small change in the amount of sulphur liberated, supporting the idea that most of the less thermally stable sulphur compounds are liberated in the first 35 ms. After 700 ms, 99.7% of sulphur is liberated with a burnout of 98.8%. SO_2 is the major gaseous product.

Comparing the results of each coal, the emission of coal sulphur in the DTF appears to be occurring in a two-step process, with the decomposition of less thermally stable sulphur compound occurring at lower residence times, with the decomposition of more stable sulphur compounds occurring at some point between 100 ms and 700 ms upon combustion of the remaining, non-volatile component of the coal molecule.

The heterogeneous nature of coal, along with the dynamic interactions in the DTF are likely responsible for the measured increase in sulphur retained in the chars between the 35 ms and 100 ms residence times of Coals B and C. The differences are within the scope of experimental error and assumed not to be as a result of any one influencing factor. SO_2 is primarily produced by the oxidation of the newly produced H_2S [7]. Whilst the DTF is an environment where oxygen is in excess for the complete combustion of the coal and any intermediary compounds released upon the decomposition of the coal, other factors likely limit the rate at which the combustion of H_2S occurs. The coals with the greater volatile matter content, which volatilise their sulphur more quickly, have produced the greatest quantities of SO_2 at 700 ms, whilst the coal with lowest volatile matter content has not produced any SO_2 at 700 ms. Coals with higher volatile matter contents often produce chars with large pores, which can be identified by their increased char reactivity as shown in Table 6.1 [95]. This could possibly accelerate the decomposition of the remaining char, volatilising any sulphur within. By volatilising at an earlier residence time, sulphur compounds will have longer to oxidise to SO_2 before leaving the DTF.

Table 6.1: Char reactivity of DTF 35ms coal chars

Coal	35 ms char reactivity $t_{0.5}$ / min
A	140.6
B	123.9
C	178.3
D	86.4

6.3 Distribution of sulphur forms between coals and 35 ms chars

The determination of sulphur forms experiment allowed the identification of the sulphur forms in the coals and 35 ms chars. From this, it is possible to show which sulphur forms were volatilised to H_2S in the DTF. The results are shown in Figure 6.3. The sulphur in Coal A was shown to be primarily organic, with a small portion of pyrite and no detected sulphates. In the 35 ms char, the portions of pyrite and organic sulphur decreased by 54.2% and 39.7% respectively, whilst sulphates were also detected. This could be because of the oxidation of portion of the coal pyrite to iron (III) sulphate by a mechanism such as the one reported by Schwab and Philinis, or by the reaction of gaseous sulphur forms with calcium or iron oxides [98].

$$FeS_2 + \frac{11}{4}O_2 \rightarrow \frac{1}{2}Fe_2O_3 + 2SO_2 \tag{6.1}$$

$$FeS_2 + \frac{7}{2}O_2 \rightarrow \frac{1}{2}Fe_2(SO_4)_3 + \frac{1}{2}SO_2 \tag{6.2}$$

With equation 6.2 possibly being a sum of the equations below.

$$\frac{3}{2}SO_2 + \frac{3}{4}O_2 \rightarrow \frac{3}{2}SO_3 \tag{6.3}$$

$$\frac{1}{2}FeS_2O_3 + \frac{3}{2}SO_3 \rightarrow \frac{1}{2}Fe_2(SO_4)_3 \tag{6.4}$$

Schwab and Philinis reported that within the range of 400-500°C, the oxidation of pyrite proceeds chiefly via Equation 6.1. The oxidation of pyrite by Equation 6.2 was found to only contribute a minor proportion of sulphate formation with the rate of reaction decreasing with increasing temperature, however that experiment was conducted at a lower temperature, over a much longer

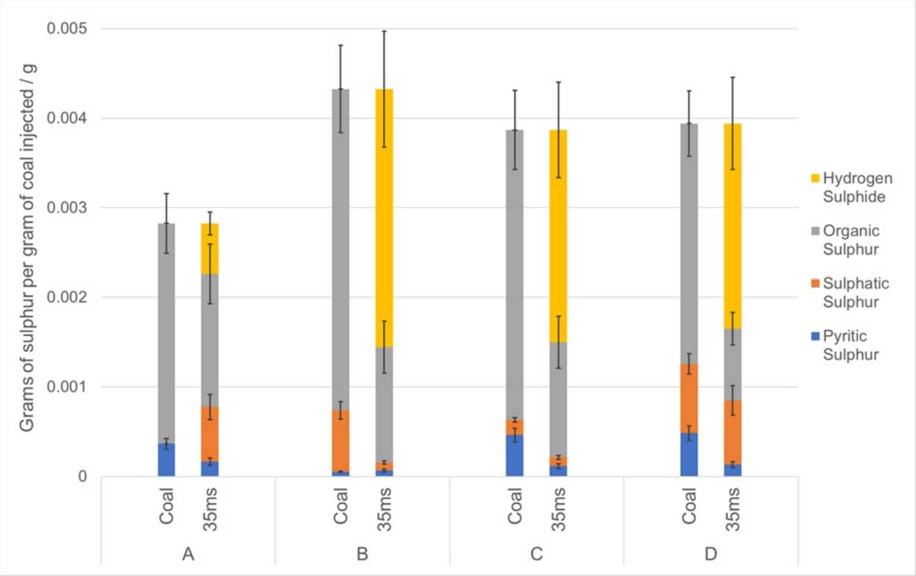

Figure 6.3: Distribution of sulphur species in sampled coals, DTF exhaust gases, and 35ms chars.

duration, and without the presence of combustible coal which could limit the amount of oxygen available for these reactions to occur [98]. The low burnout of Coal A's 35ms char may produce conditions where the excess oxygen in the DTF is able to react with solid sulphur forms to produce sulphates, as opposed to being consumed by reacting with any volatilised hydrocarbons. No SO_2 was detected by the Testo 350XL, suggesting that any produced SO_2 was either subsequently trapped within the char, or that the amount released was under the limit of detection.

Coal B was shown to contain primarily organic sulphur. A small sulphate content and a very small pyrite content was measured. After 35 ms, the char had a burnout of 48.8% whilst 66.6% of the sulphur had been liberated. 64.1% of the organic sulphur was volatilised, whilst 87.2% of the sulphate content was volatilised. Pyrite content measured a slight increased, however was within range of experimental error.

In contrast to Coal A, Coal B demonstrated a high burnout at 35 ms, likely due to its increased volatile matter content. Not only would this likely raise the temperature of the coal particles whilst passing through the DTF due to the increased amount of combustion, but also consume a greater amount of oxygen, possibly producing an area of localised oxygen deficiency around the coal particles and becoming comparable to flash pyrolysis conditions. The increased volatile matter content of Coal B would also produce a larger amount of H_2 upon thermal decomposition. Gu et al. showed that a H_2 atmosphere would increase the volatilisation of coal sulphur during pyrolysis, encouraging the formation of H_2S [77]. The combination of these conditions may be produce enough of a difference between the two coals to explain why sulphates are formed in Coal A, but removed from Coal B.

Sulphates in coal are primarily calcium or iron sulphates [23, 67, 68]. Calcium sulphate is a very thermally stable compound, not readily decomposing at temperatures under 1000°C. Iron sulphates, however, are known to decompose at much lower temperatures and therefore, this suggests that sulphates in Coal B are primarily iron sulphates [84]. The thermal decomposition of sulphates usually leads to the emission of SO_2, however, none was detected in this case. It is theoretically possible to draw a series of reactions in which H_2S can be produced from iron sulphates without the release of comparable amounts of SO_2. Mullens et al. investigated the reductive pyrolysis behaviour of iron (II) sulphate ($FeSO_4$) and iron (III) sulphate ($Fe_2(SO_4)_3$). It was shown that iron (II) sulphate could be reduced to troilite (FeS) in the reaction below [84].

$$FeSO_4 + 4H_2 \rightarrow FeS + 4H_2O \tag{6.5}$$

$$FeS + H_2 \rightleftharpoons Fe + H_2S \tag{6.6}$$

If conditions in the DTF could be compared to flash pyrolysis, then via this reaction pathway, it is possible that iron sulphates could thermally decompose without producing enough SO_2 to be above the limit of detection of the Testo 350XL.

The majority of sulphur in Coal C was found to be organic, with a small pyrite portion and a smaller sulphate portion. After 35 ms, the char had a burnout of 43.0% and had liberated 61.3% of the sulphur present in the coal. The changes in sulphur forms were unsurprising with 75.1% of pyrite, 60.3% of organic sulphur, and 43.0% of sulphates being volatilised. As mentioned in Section 6.2, Coal C has an unexpectedly high burnout and volatilisation of sulphur. With large portions of all sulphur forms being volatilised.

The sulphur in Coal D, like the other three coals, was primarily composed of organic sulphur compounds. It did have the highest proportion of inorganic sulphur, however, with pyrite and sulphates both being measured. After 35 ms, the char had a burnout of 58.9% with 58.2% of the original sulphur being liberated. Of this, 72.9% of the pyrite and 70.1% of the organic sulphur was volatilised. Only 7.5% of the sulphates were lost. This is indicative of the presence of calcium sulphates in Coal D that are not easily thermally decomposed.

It can be seen from the results of the four coals that the volatilisation of most sulphur forms occurs at a greater rate than the burnout of the coals. In terms of which sulphur forms may be exiting the raceway region in a blast furnace environment, considering the burnout of a coal may allow some ability to predict the sulphur containing products. Coals with high burnouts will likely behave predictably in terms of the sulphurous products of their partial combustion, volatilising the majority of the sulphur present, leaving mainly the more thermally stable sulphur compounds in the char. Coals with lower burnouts may behave differently, seeing portions of the sulphur content oxidised in the solid phase as opposed to volatilised. However, this conclusion cannot be made with the current amount of low burnout coals analysed and additional investigation would need to be completed.

By looking at the work of previous authors, it could be hypothesised that pyrite would decompose readily under the conditions in the DTF and likewise therefore be thought to also decompose readily within the blast furnace raceway, however small amounts of pyrite have been detected in all of the 35 ms chars [4, 98–100]. This may be explained by Maes et al., who studied the desulphurisation of pyrite. The decomposition of pyrite to H_2S and elemental iron was shown to occur in a two-step process. The conversion of pyrite to troilite is described by the equation below, whilst the conversion of troilite to iron is already described above in Equation 6.6 [99].

$$FeS_2 + H_2 \rightleftharpoons FeS + H_2S \tag{6.7}$$

Maes et al. showed that the presence of a small amount of H_2S in the atmosphere could reverse the reduction of troilite in Equation 6.6, therefore inhibiting the desulphurisation process [99]. The reversible nature of pyrite desulphurisation may therefore explain why pyrite is still detected in all of the 35 ms chars, despite being one of the more thermally unstable sulphur forms found in coal. Considering this, it may be possible for small portions of an injected coal's pyrite content to survive the blast furnace raceway region within any unburnt char.

6.4 XPS analysis of coals and 35 ms chars

XPS was used to show the differences in the sulphur chemistry on the surface of the coal before and after passing through the DTF with a residence time of 35 ms. Where the analysed portion of sample is representative of the whole

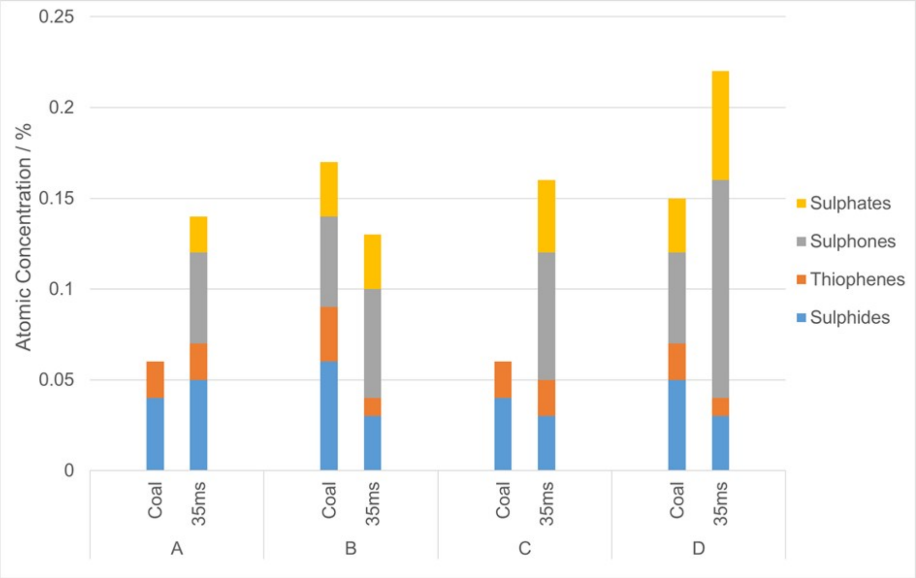

Figure 6.4: XPS measurements of surface sulphur species on sampled coals and 35 ms chars.

sample surface, atomic concentration is comparable to an element's percentage concentration [101]. It is assumed in this instance that by having the scanning area being large enough to encompass several coal/char particles that this is achieved, however this is a potential source of error.

Examining Figure 6.4, it's interesting to see that none of the coals or chars reach the same sulphur contents as the bulk values obtained from the LECO in Figure 6.2. The differences are quite large, with the surface measurements being between 20-65% of the bulk sulphur measurements. Whilst this could be indicative of systematic error, each instrument was carefully calibrated prior to use and so confidence in the measured values is high. The data could therefore be indicating a variation between the surface and bulk sulphur values. This could be explained somewhat by the presence of inorganic sulphur compounds, which tend to exist as larger inclusions within the coal as opposed to being distributed more evenly within the coal macromolecule.

It can be seen for three of the four coals, that the relative atomic concentrations of sulphur compounds increase on the surface of the chars in comparison to the coals. The reduction in carbon content in the chars after their partial burnouts could possibly be identified as the reason for these changes, however as the rate of bulk sulphur volatilisation was greater than the rate of char burnout for three of the four coals, it would be expected that the relative sulphur content on the char surfaces would decrease as opposed to increase for those chars. This could therefore suggest that sulphur is migrating from the bulk of the coal to the surface, in which sulphur is liberated within the core of coal particle but then bonds to nascent char on the surface of the particle. The phenomenon of released sulphur bonding to nascent char has been identified by several authors [6, 60, 81, 97, 102, 103]. It is possible to see increases in the proportion of oxidised sulphur forms on the surfaces of the chars in comparison with the coals. This is not surprising to see in a post combustion sample. Generally, across the samples there is a reduction in less thermally stable sulphides, the maintenance or slight loss of more thermally stable thiophenes, and the maintenance or increase in oxidised sulphones and sulphates. This correlates well with the changes to the bulk sulphur forms shown in Section 6.3. By comparing the results of the XPS with the sulphur distributions discussed in the bulk samples in Section 6.3, the most notable changes are with the organic sulphur forms. Where in some coals, large decreases in bulk organic sulphur are seen, there are also large increases in the quantity of sulphones present on the surface. Sulphone can be produced by the oxidation of a sulphide or by the reaction of SO_2 with a hydrocarbon. The large increase in sulphones seen on the char surfaces and the lack of SO_2 measured by the Testo 350XL could be an indication of the reaction of produced SO_2 with nascent char.

6.5 Determination of error

During the DTF work described in this chapter, error was calculated using the standard deviations of the measured values. Runs were repeated on multiple occasions, with a minimum of two runs undergone for each coal at each residence time. Each of these runs was tested via proximate analysis, as described in Section 5.1. The standard deviation between the results of the ash analysis was calculated using Equation 5.7. Two standard deviations is usually representative of about 95% of values around the mean, as such, this was selected as the error in the ash value of each coal and char. Where sufficient samples were not tested to establish a standard deviation, an error of 3% was applied, as per the maximum reproducibility limit in the BSI, discussed in Section 5.1.

The error in the burnout, calculated via the ash tracer method in Section 5.2, was calculated by propagating the error in the ash values of the coal and the corresponding char using Equation 5.8. Where this value was calculated to be less than 5%, the value of the error was adjusted to 5%.

The error in the sulphur value was calculated by using the standard deviations of the measurements made by the LECO SC-144DR using Equation 5.7. To calculate the error value of the sulphur volatilisation, the standard deviation of the sulphur measurements were propagated with the standard deviation of the burnout using Equation 5.8.

The error in the sulphur forms was calculated using the maximum acceptable reproducibility of the analytical method described in Section 5.3 and propagating this with the standard deviation of the burnout measurements by using Equation 5.8.

6.6 Chapter conclusions

Four blast furnace injection coals have been studied via use of a drop tube furnace. The presence of sulphur in iron produced in a blast furnace is costly and time consuming to remove, this work is a necessary part of understanding the fate of the sulphur from injection coals with a view to influencing the selection and blending of injected coals.

- The biggest contributing factor to the volatilisation of coal sulphur appears to be the burnout of the coal particle. The rate of coal burnout is often increased with increased volatile matter content, as was the case with the studied coals.
- Coals with lower volatile matter contents showed the largest increase in the presence of oxidised sulphur forms in the char. The formation of H_2S is known to be dependent on the availability of volatilised hydrogen, which itself is linked to volatile matter content. Where insufficient hydrogen is available, the bonding of volatilised sulphur to nascent char appears to occur.
- Coals with higher volatile matter contents not only produce higher char burnouts and more H_2S, but generally also produce more reactive chars. This could lead to the accelerated decomposition of the remaining, non-volatile component of the char, volatilising any sulphur within.
- The volatile matter content of a coal could therefore be considered a key indicator to the rate of sulphur volatilisation during pulverised coal injection.
- The volatilisation of sulphur from a coal appears to occur in a two stage process. During the combustion of the volatile matter content of a coal,

less thermally stable sulphur compounds in the coal decompose, volatilising the sulphur. More thermally stable compounds do not decompose until the combustion of the remaining non-volatile coal macromolecule.

- The sulphur forms existing in the initial coal samples can therefore give an indication of the sulphur forms that could be found in any unburnt char.

Chapter 7

The effect of alternative injectants on the volatilisation of coal sulphur in the DTF

7.1 Introduction

As discussed in Chapter 2, the use of alternative injectants as a partial replacement for coal injection has been investigated as a method of reducing the reliance of the blast furnace on fossil fuels. The use of biofuels, recycled materials, or hydrogen rich fuels has the potential to bridge a gap in the steel industry's transition to fossil fuel free steelmaking. This chapter will study the effect of these alternative injectants on the burnout, sulphur volatilisation, and char reactivity of DTF chars. This information could be used in the consideration of alternative fuels or the adaptation of blast furnace process conditions to facilitate their use.

7.2 Alternative solid fuel injectants

7.2.1 TGA combustion

To produce an idea of how the alternative solid fuel injectants may affect the combustion of a coal blend, a combustion test was performed on the TGA, as described in Section 5.6.2. Figure 7.1 shows the results of this test.

As referred to in Section 4.3.1, Coal C was selected as the reference coal during the study of alternative solid fuel injectants as it was the easiest coal to handle with regards to the drop tube furnace. By which, it fed easily, showed little agglomeration and therefore did not block either the injection or collector probes, and did not burn out too rapidly and so any variation due to the presence of the alternative injectants should have been measurable.

It can be seen that the combustion of the alternative solid fuels varies from that of Coal C. Coal C initially shows a mass gain, expected to be due to surface oxidation, before beginning to combust around 350°C. Coal C does not finish combusting until around 710°C. In comparison, the Tyre derived fuel begins combusting at the lowest temperature, around 250°C. The NCT biochar and Maxibrite biochar both show evidence of drying below 100°C. It is possible that samples were left too long between drying and analysis and that water was reabsorbed by the materials. Both the NCT and Maxibrite biochars show evidence of slow devolatilisation before combustion begins. The NCT curve shows a shoulder between 250°C and 375°C, it is unclear whether this is due to devolatilisation or the beginning of combustion. Combustion is clearly occurring by 400°C and continues until around 640°C. The Maxibrite biochar begins combustion around 400°C, finishing around 640°C. The Yorkshire water

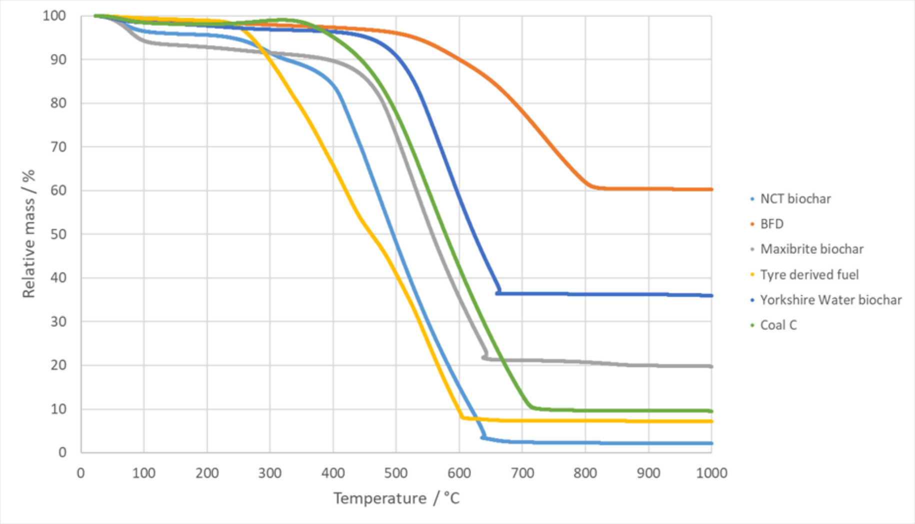

Figure 7.1: TGA combustion temperature profile of alternative solid fuel injectants

biochar begins combusting around 430°C, finishing around 660°C. The BFD does not begin combusting until around 500°C and finishes around 820°C. Out of all the materials, only the BFD fails to finish combusting before Coal C.

Considering this with application to the DTF, one would expect that only the BFD would reduce the burnout of the pulverised coal at longer residence times, whilst at lower residence times, the presence of fuels such as the Tyre derived fuel might raise the burnout.

Some considerations of this test are whether the amount of ash is relevant to the temperature at which combustion is completed and whether the test is limited by the rate of combustion of the sample in the crucible. The rate of combustion appears similar for most of the samples, which may mean it is limited by the rate at which the sample can be oxidised.

7.2.2 Char burnout and total sulphur volatilisation

Figure 7.2 shows the burnout and sulphur volatilised of the alternative solid fuel injectant - Coal C blends discussed in Section 4.3.1 and described in Table 4.3 alongside the burnout and sulphur volatilisation of Coal C, as previously discussed in Chapter 6. It is noted that the majority of these results are within the scope of experimental error of each other and therefore whilst explanations of trends or differences are suggested, it should be understood that this is a comparatively small dataset and further work would be required to confirm them.

The BFD blend showed a slight increase in burnout at 35 ms compared to Coal C, increasing to 43.8% from 43.0%. The amount of sulphur volatilised was reduced, decreasing to 51.4% from 61.3%. However, as discussed in Chapter 6, the sulphur volatilisation of Coal C at 35 ms was unexpectedly high and may not be accurately representative of a larger quantity of 35 ms char. The BFD blend burnout at 100 ms was greater than Coal C, at 59.5% compared to 45.6%. The BFD blend had a higher sulphur volatilisation at 100 ms than Coal C, 67.2% compared to 54.4%. This is mostly likely as a result of the increased burnout. The final burnout at 700 ms is slightly lower for the blend than Coal C, 94.9% compared to 95.4%, however the sulphur volatilised is greater in the blend, 99.7% compared to 98.3%. This may be as the sulphur present in the BFD is fully volatilisable, reducing the relative proportions of more thermally stable compounds such as $CaSO_4$ in the blend compared to the coal.

The NCT biochar blend showed an increase in burnout at 35 ms compared to Coal C, 45.2% compared to 43.0%. Sulphur volatilisation at 35 ms was lower for the NCT biochar blend than Coal C, 43.4% compared to 61.3%. At 100 ms the burnout of the NCT biochar blend was higher than Coal C, 59.4% compared to 45.6%. Sulphur volatilised was also larger for the NCT biochar blend than

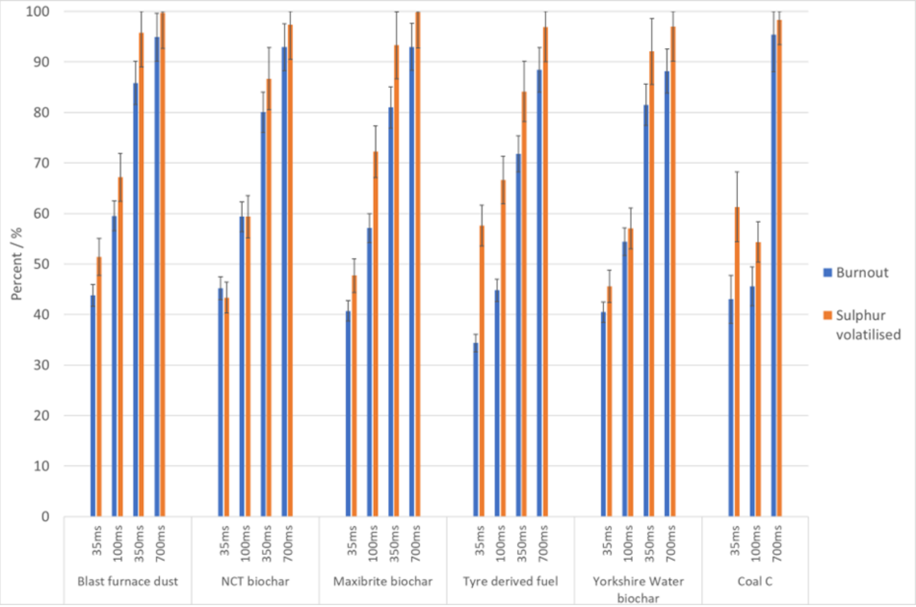

Figure 7.2: DTF burnout and sulphur volatilisation of alternative solid fuel injectant - Coal C blends

Coal C at 100 ms, 59.4% compared to 54.4%, likely as a result of the increased burnout. At 700 ms, the burnout of the NCT biochar blend was lower than that of Coal C, 92.9% compared to 95.4%. The sulpuhr volatilisation of the NCT biochar blend was also lower than that of Coal C, 97.4% and 98.3% respectively.

The Maxibrite biochar blend showed a decreased 35 ms burnout in comparison to Coal C, 40.7% reduced from 43.0%. The sulphur volatilisation was also decreased, 47.7% compared to 61.3%. At 100 ms, the burnout and sulphur volatilisation of the Maxibrite blend are both greater than Coal C, the burnout increasing to 57.1% from 45.6% and the sulphur volatilisation increasing to 72.3% from 54.4%. At 700 ms, the burnout of the Maxibrite blend is lower than that of Coal C, 93.0% compared to 95.4%, however the sulphur volatilisation has increased to 99.8% compared to 98.3%. This could be due to the reduction in relative proportions of more thermally stable compounds such as $CaSO_4$ in the blend compared to the coal.

The Tyre derived fuel blend showed a decreased burnout at 35 ms in comparison to Coal C. This was surprising as increased volatile matter content usually results in increased burnout, as discussed in Chapter 6, however this isn't the case for this blend. Comparing the results with Section 7.2.1, it is evident that the Tyre derived fuel certainly volatilises in this temperature range, but it may be possible that the halogen fire retardant used in tyres either retards the combustion of the volatilised material or the char, preventing the accelerated combustion of the char particle due to the increased volatile matter content, however this has not been confirmed in this work. At 35 ms, 57.6% of the sulphur is volatilised in the Tyre derived fuel blend compared to 61.3% in Coal C. Relative to the other samples, this is a large amount volatilised when considering the reduced burnout. This is likely as a result of the Tyre derived fuel containing the most sulphur out of all the alternative fuels whilst also having the largest volatile matter, which increased the proportion of thermally unstable sulphur in the blend in comparison to the coal. At 100 ms, the burnout of the Tyre derived fuel blend is less than Coal C, 44.8% compared to 45.6%. The sulphur volatilisation of the Tyre derived fuel is greater than Coal C, 66.6% compared to 54.4%. This is once again likely due to the higher proportion of less thermally stable sulphur in the blend in comparison to the coal. At 700 ms, the burnout of the Tyre derived fuel blend is less than Coal C. 88.4% compared to 95.4%. This is possibly due to the effect of fire retardants in the Tyre derived fuel. The sulphur volatilisation of the Tyre derived fuel blend is less than Coal C at 700 ms. This is possibly as a result of the reduced burnout of the char preventing the liberation of the sulphur from the remaining carbon matrix.

The Yorkshire Water biochar blend showed a decreased burnout and sulphur volatilisation at 35 ms compared to Coal C, the burnout decreasing to 40.5%

from 43.0% and the sulphur volatilisation decreasing to 45.6% from 61.3%. At 100 ms, the burnout and sulphur volatilisation of the Yorkshire Water biochar blend was greater than Coal C, the burnout increasing to 54.5% from 45.6% and the sulphur volatilisation increasing to 57.1% from 54.4%. At 700 ms, the burnout of the Yorkshire Water biochar blend is less than Coal C, decreasing to 88.2% from 95.4%. The sulphur volatilisation is also reduces, decreasing to 97.0% from 98.3%.

Comparing the blends at 35 ms, the Tyre derived fuel blend had the lowest burnout, whilst the NCT biochar blend had the highest. However, the Tyre derived fuel blend volatilised the most sulphur whilst the NCT biochar volatilised the least. As already discussed, the Tyre derived fuel blend has a higher volatile matter and sulphur content, whilst tyres are treated with halogens to retard combustion. This may have resulted in a large amount of volatile sulphur leaving the Tyre derived fuel blend whilst retarding the actual combustion of the coal. The biochars are pyrolysed in their production, which would have volatilised the less thermally stable sulphur present. This may have impacted the rate of sulphur volatilisation in the biochar - Coal C blends as it would have increased the relative proportions of more thermally stable sulphur compounds in comparison to Coal C.

At 100 ms, only the Tyre derived fuel blend showed a reduced burnout in comparison to Coal C. The burnout of the BFD blend was the highest at 59.5% but was closely followed by the NCT biochar at 59.4%. All the blends showed increased sulphur volatilisation in comparison to Coal C, likely as a result of the increased burnout for most of the blends.

At 700 ms, none of the blends had as high a burnout as Coal C. This may be as, with the exception of the Tyre derived fuel, the alternative reductants had a lower volatile matter content than Coal C. This may have reduced the overall burnout of the char particle within the DTF. The Tyre derived fuel blend's reduced burnout is possibly explained by the fuel containing fire retardants, however this has not been confirmed in this work. The BFD and Maxibrite biochar blends volatilised more sulphur than Coal C at 700 ms. Whilst the reduction of sulphur volatilisation in the other blends can likely be explained by the reduction in burnout, it is unclear as to why these blends volatilise more sulphur. As previously suggested, it may be that the sulphurs introduced in these materials are less thermally stable and therefore reduce the relative proportion of stable sulphur compounds, such as $CaSO_4$ which would remain in the char.

7.2.3 Char reactivity

As discussed in Section 6.2, char reactivity can be used as an indicator to the rate of decomposition of a char under blast furnace conditions [95]. Figure 7.3 shows the changing char reactivity of the alternative injectant - Coal C blends. As $t_{0.5}$ represents the time taken to achieve 50% gasification, a larger number indicated a less reactive char. Recalling the $t_{0.5}$ of the 35 ms Coal C char being 178.3 min, as can be seen in Table 6.1 in Chapter 6. It can be seen that each of the blends produces a less reactive 35 ms char. This could be as a result of most of the blends having lower volatile matter contents, which could reduce the porosity of the formed chars, reducing the reactivity. The reactivity of the Tyre derived fuel blend, which has a higher volatile matter content than Coal C, may be influenced by fire retardants, as previously discussed. The 35 ms $t_{0.5}$s range from 201.7 min for the BFD blend to 223.0 min for the Tyre derived fuel blend.

At 100 ms, the Maxibrite biochar blend and Yorkshire Water biochar blend each show decreases in $t_{0.5}$, equating to increased char reactivity. If comparing with Figure 7.2, it can be seen that the Maxibrite biochar and Yorkshire Water

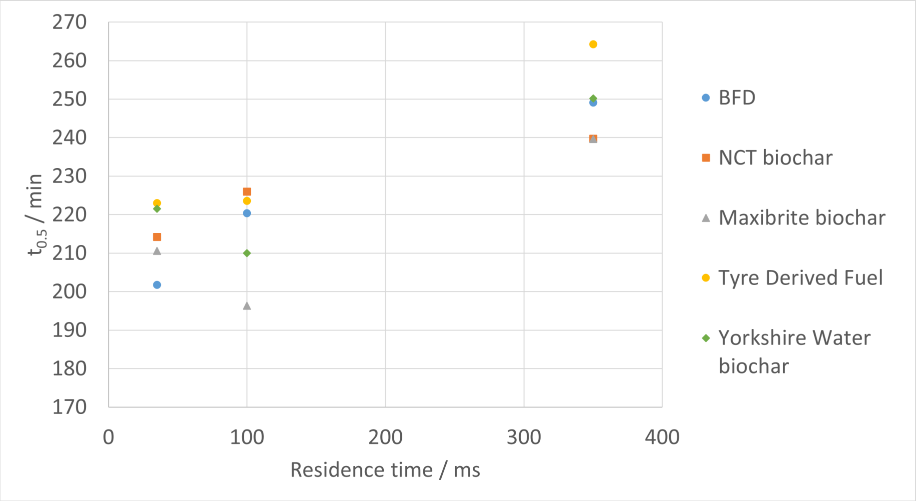

Figure 7.3: DTF char gasification reactivity of alternative solid fuel injectant - Coal C blends

biochar each have a lower 35 ms burnout than the BFD and NCT biochar blends. The relationship between burnout and gasification reactivity has been shown by previous authors [26, 104]. When comparing the relationship between $t_{0.5}$ and burnout of 35 ms and 700 ms chars, they found that coals that produce chars with higher 35 ms burnouts will produce more reactive chars at both 35 ms and 700 ms. As the initial stage of char combustion is responsible for the formation of pores, it may be that a small delay or retardation of the initial combustion may delay the production of the char with the highest reactivity.

At 350 ms, the chars have all become less reactive, producing $t_{0.5}$ values of between 239.6 min and 264.3 min. This occurs as the more reactive components of the coal are consumed and the char's properties change [26].

In terms of blast furnace application, it has been suggested that the use of coals that produce chars with lower char gasification reactivities is preferable, as the partially burnt chars ascending the blast furnace have a lower heat requirement for the endothermic reverse Boudouard reaction, see Equation 5.5

in Section 5.6.1, than chars with higher gasification reactivities. This in turn will result in less localised cooling and allow better heat distribution in the furnace [26]. The blending of alternative reductants with Coal C resulted in a decrease in gasification reactivity of 35 ms chars of all blends. This may suggest that the blending of alternative reductants such as those studied into the pulverised coal injection of a blast furnace may lead to improved heat distribution.

7.3 Alternative gaseous atmospheres

7.3.1 Char burnout and total sulphur volatilisation

The injection coals supplied by TATA steel were tested under three atmospheres in order to analyse the effect of H_2 and CO_2 on the burnout and sulphur volatilisation of chars in the DTF, as described in Section 4.3.2. The compositions of the three test atmospheres can be found in Table 7.1, which is revisited below. The N_2:Air atmosphere represents conditions most similar to a current blast furnace raceway but with carbon:oxygen ratios comparable with the other atmosphere conditions. The trends of this atmosphere roughly follow the same trends discussed in Chapter The volatilisation of coal sulphur in the DTF, this section will focus on how the presence of H_2 and CO_2 in the gas mix effects these trends.

Table 7.1: Gas compositions of DTF test atmospheres

Gaseous atmosphere label	Gas composition / % vol			
	N_2	O_2	CO_2	H_2
N_2:Air	90	10	<0.1	0
N_2:H_2:Air	87.5	10	<0.1	2.5
CO_2:Air	40	10	50	0

Figure 7.4 shows the DTF burnout and sulphur volatilisation of Coal A under alternative gaseous atmospheres. The burnout at 100 ms for the N_2:Air

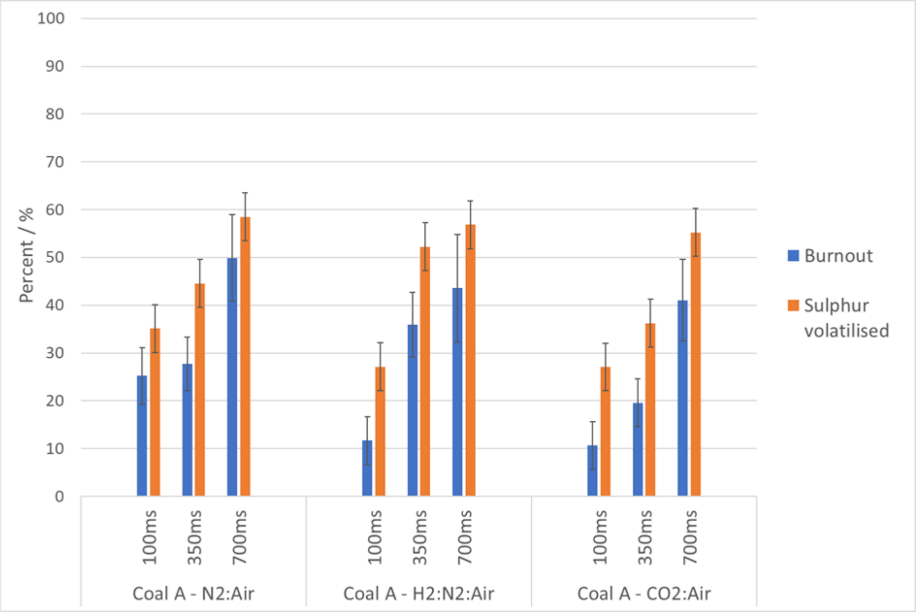

Figure 7.4: DTF burnout and sulphur volatilisation of Coal A under alternative gaseous atmospheres

atmosphere was 25.2%. The 100 ms burnouts for the N_2:H_2:Air and CO_2:Air atmospheres were 11.7% and 10.6%, respectively. The sulphur volatilisation of the 100 ms N_2:Air atmosphere was 35.1%. The 100 ms sulphur volatilisation for the N_2:H_2:Air and CO_2:Air atmospheres were 27.1% and 27.1%, respectively. The burnout at 350 ms for the N_2:Air atmosphere was 27.7%. The 350 ms burnouts for the N_2:H_2:Air and CO_2:Air atmospheres were 36.0% and 19.6%, respectively. The sulphur volatilisation of the 350 ms N_2:Air atmosphere was 44.6%. The 350 ms sulphur volatilisation for the N_2:H_2:Air and CO_2:Air atmospheres were 52.3% and 36.2%, respectively. The burnout at 700 ms for the N_2:Air atmosphere was 49.9%. The 700 ms burnouts for the N_2:H_2:Air and CO_2:Air atmospheres were 43.6% and 41.1%, respectively. The sulphur volatilisation of the 700 ms N_2:Air atmosphere was 58.5%. The 700 ms sulphur volatilisation for the N_2:H_2:Air and CO_2:Air atmospheres were 56.8% and 55.2%, respectively.

It is evident that the introduction of alternative gases to the combustion atmosphere has reduced the burnouts of the 100 ms chars of Coal A. In the case of the N_2:H_2:Air mix, this could be considered unexpected as several authors have reported increased low residence time burnout as a result of hydrogen injection [37, 38, 40]. The trend of the sulphur volatilisation follows that of the burnout, as would be expected from the findings of Chapter 6. However, the slight increase in sulphur volatilisation relative to the burnout could suggest the presence of more readily hydrolysed sulphurs present in Coal A. The increased relative burnout and sulphur volatilisation of the 350 ms N_2:H_2:Air char may be explained by Coal A producing chars with relatively low burnout at lower residence times. If this coal takes longer to complete the first stage of combustion, i.e. devolatilisation, the accelerating effect of the H_2 on the combustion of the volatile matter may be delayed until a later residence time. The reduced burnout of the 700 ms N_2:H_2:Air char is concurrent with the findings of previous authors that showed a decreased high residence time burnout after the injection of H_2.

Gasification of unburnt char by CO_2 during the char combustion stage of coal combustion is important to the burnout of the char particle [38]. However, as shown by previous authors, the gasification reactivity of a char can be correlated to its low residence time burnout [26]. This would suggest that the CO_2:Air atmosphere would accelerate the burnout of coals that already produce low residence time chars with high burnout. As can also be seen in Chapter 6, Coal A produces the lowest burnout chars out of the tested coals. It is therefore more likely that gasification by CO_2 does not play a large role in the burnout of chars produced from Coal A.

Figure 7.5 shows the DTF burnout and sulphur volatilisation of Coal B under alternative gaseous atmospheres. The burnout at 100 ms for the N_2:Air atmosphere was 26.8%. The 100 ms burnouts for the N_2:H_2:Air and CO_2:Air atmospheres were 45.7% and 44.4%, respectively. The sulphur volatilisation of the 100 ms N_2:Air atmosphere was 39.4%. The 100 ms sulphur volatilisation for the N_2:H_2:Air and CO_2:Air atmospheres were 52.3% and 54.5%, respectively. The burnout at 350 ms for the N_2:Air atmosphere was 69.2%. The 350 ms burnouts for the N_2:H_2:Air and CO_2:Air atmospheres were 60.7% and 60.5%, respectively. The sulphur volatilisation of the 350 ms N_2:Air atmosphere was 75.7%. The 350 ms sulphur volatilisation for the N_2:H_2:Air and CO_2:Air atmospheres were 67.8% and 69.4%, respectively. The burnout at 700 ms for the N_2:Air atmosphere was 82.7%. The 700 ms burnouts for the N_2:H_2:Air and CO_2:Air atmospheres were 75.9% and 81.3%, respectively. The sulphur volatilisation of the 700 ms N_2:Air atmosphere was 87.3%. The 700 ms sulphur volatilisation for the N_2:H_2:Air and CO_2:Air atmospheres were 79.8% and 86.0%, respectively.

The addition of alternative gases to the DTF atmosphere have obviously affected the burnouts of the chars produced from Coal B. At 100 ms, the burnout of the chars from the N_2:H_2:Air and CO_2:Air atmospheres were significantly higher than the char produced in the N_2:Air atmosphere. The sulphur volatilisation also increases in these atmospheres, however whilst displaying similar burnouts, the CO_2:Air atmosphere volatilised relatively more sulphur. At 350 ms and 700 ms, the burnout and sulphur volatilisation of the N_2:H_2:Air and CO_2:Air atmosphere chars were lower than their comparative N_2:Air atmosphere chars. The changes in burnout and sulphur volatilisation can possibly be explained by the findings of other authors.

The effect of H_2 on the burnout of co-injected pulverised coal has been studied by several authors. A general consensus appears to be that hydrogen co-injection encourages the initial volatile matter release from the char and ini-

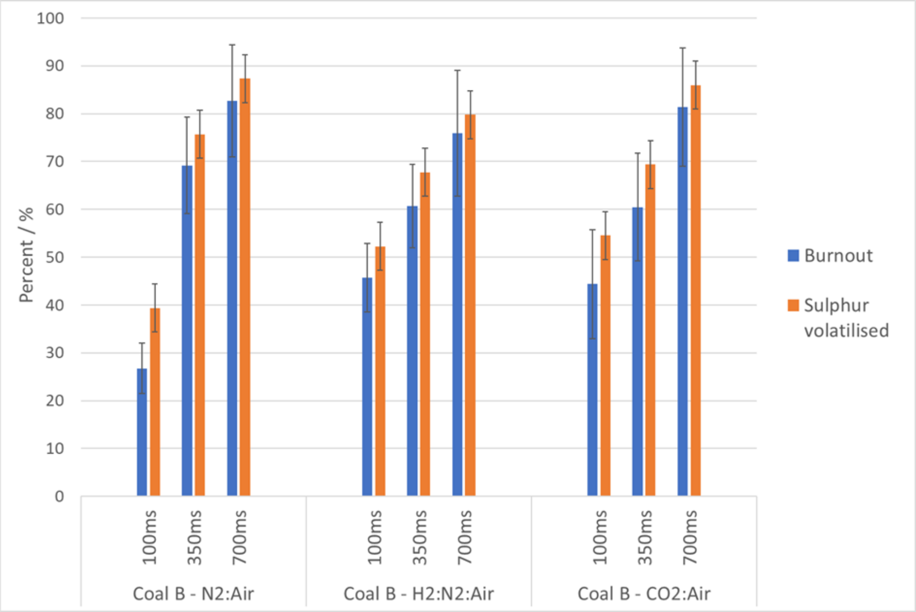

Figure 7.5: DTF burnout and sulphur volatilisation of Coal B under alternative gaseous atmospheres

tially enhances combustion due to the particle temperature increasing from the combustion of H_2 and the volatile matter. However, the excessive combustion of H_2 reduces the O_2 around the char particle, retarding further combustion and reducing overall burnout [37, 38, 40].

CO_2 is a reactive gas and has been shown to increase the rate of coal volatilisation and increases the rate of volatilisation of coal sulphur in comparison to an inert atmosphere [73, 77, 86]. CO_2 promotes the scission of C-S bonds and lowers the temperature at which sulphur is volatilised. It prevents the formation of CaS by promoting the formation of $CaCO_3$, which would prevent sulphur fixation in the char by calcium [87].

In the case of the Coal B 100 ms chars, this may explain both the increased burnout of the N_2:H_2:Air and CO_2:Air atmospheres in comparison to the N_2:Air atmosphere and the increased sulphur volatilisation of the CO_2:Air atmosphere compared to the N_2:H_2:Air atmosphere, despite the similar burnouts. The changes in sulphur volatilisation of the chars produced in the N_2:H_2:Air in comparison to the N_2:Air atmosphere are likely best explain by the relative changes to the burnouts. The reduction in 350 ms and 700 ms burnout under the N_2:H_2:Air atmosphere is then likely explained by a reduction in O_2 around the char particle, but the reduction in burnout in CO_2 at 350 ms is unexplained. In contrast to Coal A, Coal B produces chars with relatively high burnouts at lower residence times, which suggests that the gasification of char by CO_2 may play a greater role. The final burnout of the CO_2:Air atmosphere is comparable to the N_2:Air atmosphere, which may indicate an intermediate stage which may temporarily retard the combustion. It could be possible that the gasification of the char by CO_2 via the endothermic reverse Boudouard reaction, shown in Equation 2.2, lowered the particle temperature and retarded the combustion, before the gasified material is combusted and raises the particle temperature, accelerating the combustion. Further work will be required to investigate this phenomenon further.

Figure 7.6 shows the DTF burnout and sulphur volatilisation of Coal C under alternative gaseous atmospheres. The burnout at 100 ms for the N_2:Air atmosphere was 29.9%. The 100 ms burnouts for the N_2:H_2:Air and CO_2:Air atmospheres were 36.0% and 29.3%, respectively. The sulphur volatilisation of the 100 ms N_2:Air atmosphere was 41.7%. The 100 ms sulphur volatilisation for the N_2:H_2:Air and CO_2:Air atmospheres were 50.9% and 41.4%, respectively. The burnout at 350 ms for the N_2:Air atmosphere was 53.9%. The 350 ms burnouts for the N_2:H_2:Air and CO_2:Air atmospheres were 47.6% and 45.5%, respectively. The sulphur volatilisation of the 350 ms N_2:Air atmosphere was 65.4%. The 350 ms sulphur volatilisation for the N_2:H_2:Air and CO_2:Air atmospheres were 61.5% and 59.5%, respectively. The burnout at 700 ms for

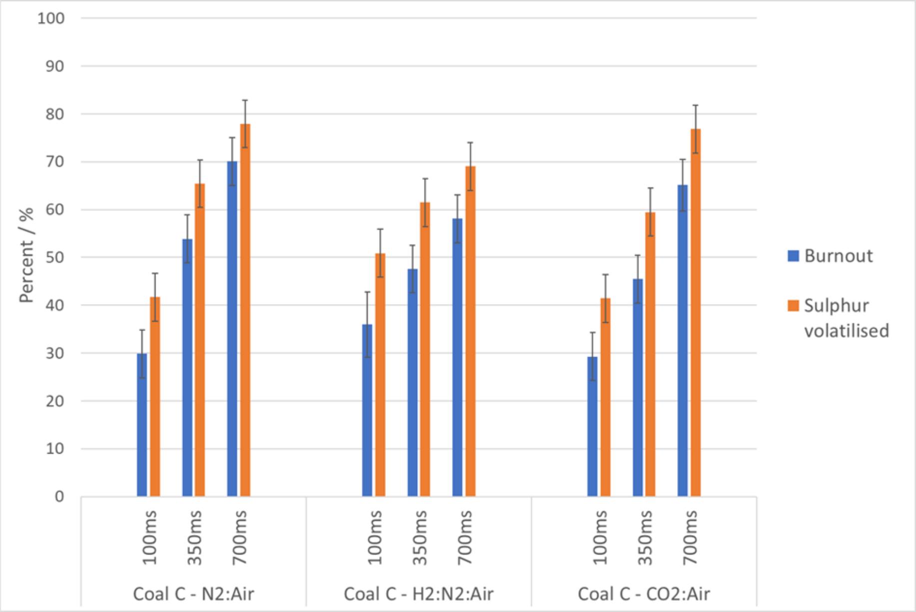

Figure 7.6: DTF burnout and sulphur volatilisation of Coal C under alternative gaseous atmospheres

the N_2:Air atmosphere was 70.1%. The 700 ms burnouts for the N_2:H_2:Air and CO_2:Air atmospheres were 58.1% and 65.1%, respectively. The sulphur volatilisation of the 700 ms N_2:Air atmosphere was 77.9%. The 700 ms sulphur volatilisation for the N_2:H_2:Air and CO_2:Air atmospheres were 69.0% and 76.9%, respectively.

As with Coal B, the N_2:H_2:Air atmosphere produced an initial increase in char burnout at 100 ms, before then reducing lower comparative burnouts at 350 ms and 700 ms. The comparative sulphur volatilisation is mostly explainable by the change in burnout, however there is a slight increase in sulphur volatilisation relative to the burnout, possibly suggesting the presence of more readily hydrolysed sulphurs present in Coal C.

The CO_2:Air atmosphere yielded lower burnout chars in comparison to the N_2:Air atmosphere, however the sulphur volatilisation remains similar for chars

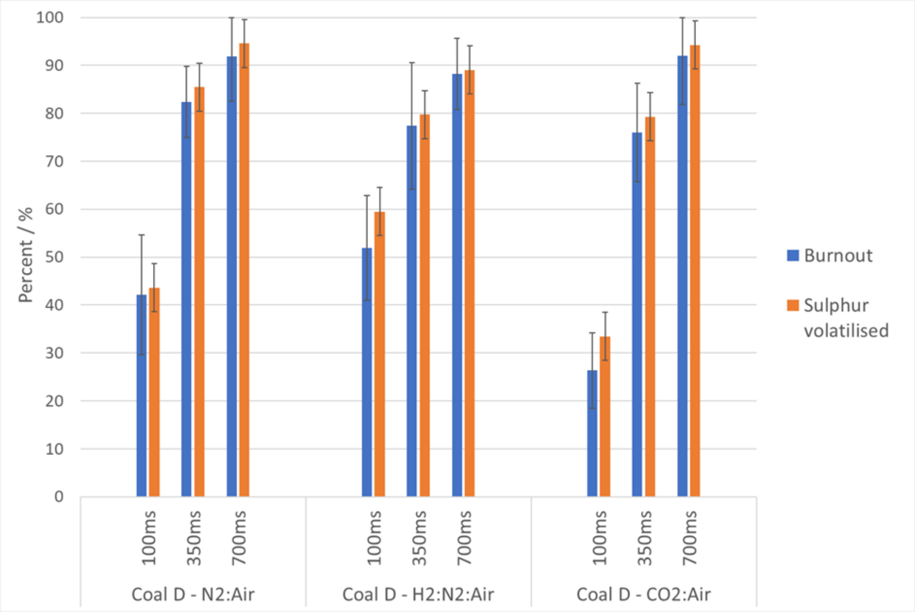

Figure 7.7: DTF burnout and sulphur volatilisation of Coal D under alternative gaseous atmospheres

produced at 100 ms and 700 ms, despite a reduction in burnout. This supports the findings of previous authors that the CO_2 may promote the increased volatilisation of coal sulphur [73, 77, 86, 87] Unlike Coal B, the final 700 ms burnout does not reach the same level as the N_2:Air atmosphere.

Figure 7.7 shows the DTF burnout and sulphur volatilisation of Coal D under alternative gaseous atmospheres. The burnout at 100 ms for the N_2:Air atmosphere was 42.1%. The 100 ms burnouts for the N_2:H_2:Air and CO_2:Air atmospheres were 51.9% and 26.3%, respectively. The sulphur volatilisation of the 100 ms N_2:Air atmosphere was 43.6%. The 100 ms sulphur volatilisation for the N_2:H_2:Air and CO_2:Air atmospheres were 59.5% and 33.5%, respectively. The burnout at 350 ms for the N_2:Air atmosphere was 82.4%. The 350 ms burnouts for the N_2:H_2:Air and CO_2:Air atmospheres were 77.4% and 76.0%, respectively. The sulphur volatilisation of the 350 ms N_2:Air atmosphere was 85.4%.

The 350 ms sulphur volatilisation for the N_2:H_2:Air and CO_2:Air atmospheres were 79.7% and 79.3%, respectively. The burnout at 700 ms for the N_2:Air atmosphere was 91.9%. The 700 ms burnouts for the N_2:H_2:Air and CO_2:Air atmospheres were 88.2% and 92.0%, respectively. The sulphur volatilisation of the 700 ms N_2:Air atmosphere was 94.6%. The 700 ms sulphur volatilisation for the N_2:H_2:Air and CO_2:Air atmospheres were 89.0% and 94.2%, respectively.

As with Coals B and C, the N_2:H_2:Air atmosphere produced an initial increase in char burnout at 100 ms, before then reducing lower comparative burnouts at 350 ms and 700 ms. The comparative sulphur volatilisation is explainable by the change in burnout.

The char produced at 100 ms in the CO_2:Air atmosphere produced an unexpectedly low burnout and therefore sulphur volatilisation. However, the burnout rapidly increases and at 700 ms, the char burnout produced is comparable to that produced in the N_2:Air atmosphere. This is comparable to Coal B, the other high volatile matter coal. This may suggest a link between CO_2:Air atmosphere 700 ms burnout and coal volatile matter content. Both of these coals produced chars with higher gasification reactivity in Chapter 6, it is possible that the gasification of the higher reactivity chars at higher residence times is responsible for the increased 700 ms burnout.

7.3.2 SEM analysis of 100 ms char and filtered material

During the course of the DTF experiments, it was noticed that during the 100 ms runs, a fine particulate matter was being caught in the pre-Testo 350XL filter. This was particularly prominent in Coal B and D. This substance did not appear in the filter at higher residence times and only made up a minute portion of the entered sample, no more that 100 mg per 15 g of coal. As this material appeared finer than the char gathered in the collection pot, it asked the question whether this was a condensing material accumulating in the filter or whether

Table 7.2: Proximate analysis of 100 ms CO_2 chars and filtrate

Sample	Proximate analysis / % mass (dry)		
	Fixed carbon	Volatile matter	Ash
Char A	83.4	8.2	8.4
Filtrate A	72.0	12.4	15.6
Char B	85.3	6.4	8.3
Filtrate B	69.2	10.5	20.3
Char C	82.5	5.6	11.9
Filtrate C	70.8	10.3	18.9
Char D	86.5	9.1	4.4
Filtrate D	73.8	9.4	16.8

it was a finer, less dense portion of the char. This was particularly of interest due to a correlation of increased coal fines being identified in the sponsor's blast furnace dust when these particular coals were in the coal injection blend.

The chars and filtrate from the 100 ms CO_2 were analysed by proximate analysis using the TGA, as described in Section 5.6.3. The results are displayed in Table 7.2. Due to constraints on resources, it was assumed that the composition of the filtrate material was not significantly altered by the gaseous atmosphere and so that the analysis of one set of samples would sufficiently explain the material. The proximate analysis showed that this material had an increased volatile matter and ash compared to the collected char.

The proximate analyses suggests that the filtered material is part of a lighter, finer portion of the char carried through the cyclone separator. The higher ash content indicates that the material wasn't simply hydrocarbons condensing in the filter, as that would result in a minimal amount of ash. To confirm this, Char B and Filtrate B were analysed using a SEM, as described in Section 5.7.

Figure 7.8 shows the char at 700 X magnification. The particles are very porous or swollen, which is indicative of the high volatile matter content being liberated from the coal particle. Figure 7.9 shows the filtrate at 700 X magnification. It can be clearly seen in these images that there is a massive change in

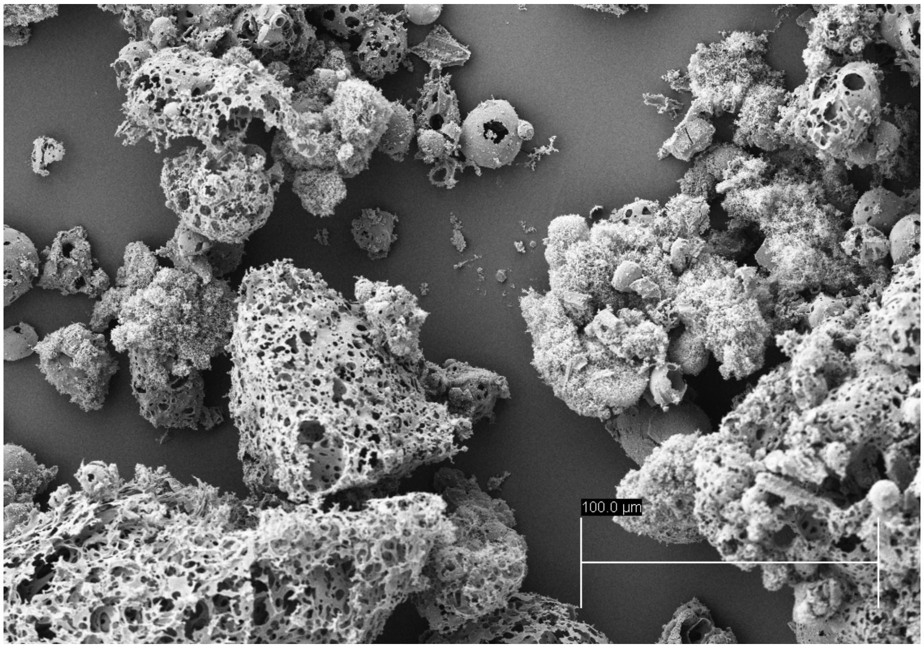

Figure 7.8: SEM image of 100 ms CO_2 Char B at 700× magnification.

the size distribution of the particles, with the particles in Figure 7.9 being far smaller than those in Figure 7.8. Many particles show signs of swelling, with also some particles having become porous following the release of the particle's volatile matter. It could be that the filtrate has partially been produced by the fracturing of larger char particles. As previously mentioned, Coals B and D produced far larger amounts of filtrate. The release of a large amount of volatile matter in Coals B and D, which causes the char to have a low relative density, may have caused the smallest particles in the coal to have been carried through the cyclone separator.

Whilst subjective and not easily quantifiable, it appears from the images that a higher proportion of the char in Figure 7.8 has devolatilised, leaving the porous, sponge like structures, whilst the filtrate has a greater proportion of the balloon like swelling, indicating that the devolatilisation has yet to fully

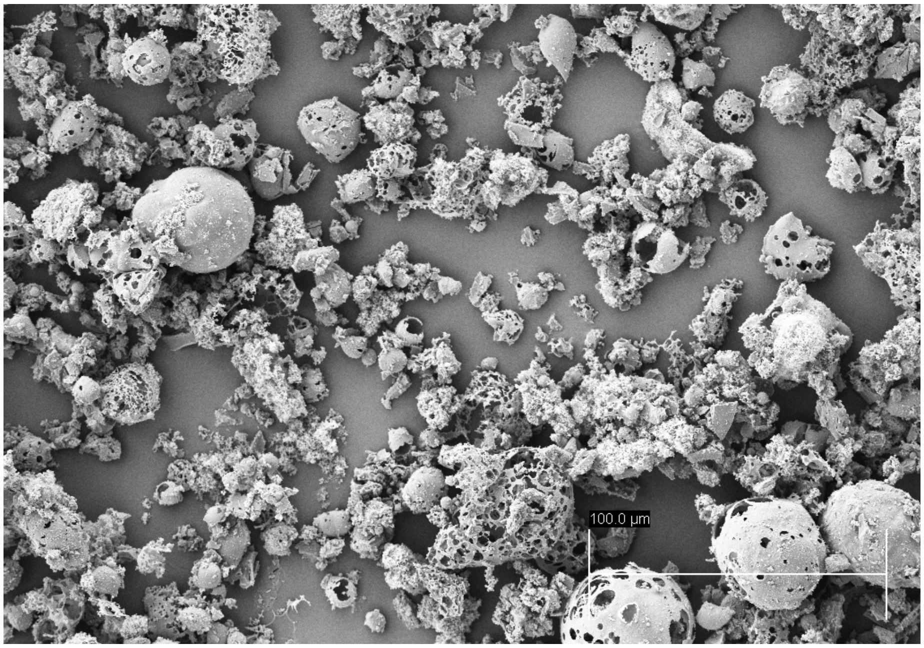

Figure 7.9: SEM image of 100 ms CO_2 Filtrate B at 700× magnification.

complete. This may explain why the filtrates in Table 7.2 have shown a greater retention of volatile matter in comparison to their respective chars.

The SEM images help to confirm that the filtrate material is not a condensate and is instead made up of a finer portion of the char. Theoretically, this could happen within the blast furnace, with a smaller, lighter portion of the char leaving the raceway and either accumulating in the stack or being blown out of the furnace into the blast furnace dust.

7.4 Determination of error

The error calculated for the measurements in this chapter was done so in a similar way to that in Chapter 6. The standard deviation of ash measurements were calculated and used to calculate the error in the burnout via propagating the error of the coal and char ash measurements using Equations 5.7 and 5.8, respectively. Where sufficient samples were not tested to establish a standard deviation of the ash test, an error of 3% was applied, as per the maximum reproducibility limit in the BSI, discussed in Section 5.1. Where the burnout error value was calculated to be less than 5%, the value of the error was adjusted to 5%. The sulphur measurements were conducted externally and therefore sufficient repeats to establish an accurate standard deviation could not be achieved. However they were completed in duplicate. It was calculated that the average variance between the duplicate samples was 3.12% of the measured value. By comparing the repeatability of the sulphur measurements, it has been assumed that a maximum error of 5% of the measured value would be a suitable estimation for the quantification of error. This value has then been used in the propagation of error to determine the error in the volatilisation of sulphur.

A thorough study of the error of the TGA char gasification reactivity was not undertaken due to damage to the analytical instrument, as mentioned in Section 5.6.1. It is unclear therefore, whether any trends or conclusions produced from this work are genuine or the result of error. The only consideration is a study from a previous user of the equipment and method. They showed that there was a good level of repeatability in this experiment, with a calculated error of ±2 min on a $t_{0.5}$ of 72 min, which equates to a percentage error of less than 3% [104].

7.5 Chapter conclusions

The suitability of alternative solid fuel injectants for blast furnace co-injection with reference to the effects on burnout and sulphur volatilisation were studied using blends of the alternative solid fuel and Coal C in a mass ratio of 1:9.

- The blending of 10% mass of alternative solid fuel injectant was shown to affect the burnout and sulphur volatilisation of the produced chars.

Burnout remains the major factor in sulphur volatilisation, with the sulphur volatilisation of each material following the same trend as the char burnout, however differences likely arise from the introduction of different sulphur forms in differing quantities to Coal C. When considering that with some of the alternative fuels, the 10% total mass will contain over a third of the total sulphur (in the case of the Tyre derived fuel blend), the relative thermal stability of those sulphur compounds will play a large role in the volatilisation of sulphur from the blend. It would therefore be a requirement of fuel selection to not only consider total sulphur, but the form of sulphur present in the fuel.

- The reduction of char gasification reactivity by the addition of alternative solid fuel injectants to a coal blend is an interesting finding, which could be positive in blast furnace application. The lower char gasification reactivity could result in better heat distribution within the blast furnace by reducing the effect of localised cooling.
- It should be noted that the use of waste or recycled materials can lead to the introduction of undesirable elements or compounds into the injectant blend. The presence of these materials could inadvertently lead to increased coke rates, offsetting any potential savings introduced by the use of the alternative solid fuels.
- It is evident that the blending of alternative solid fuel injectants into a coal blend can produce chars of similar characteristics to those of pure coal injection when considering only the burnout and sulphur volatilisation. Other factors, such as the introduction of undesirable elements and compounds into the blast furnace, cost, or security of supply will therefore more likely dictate the suitability of these materials for blast furnace co-injection.

The effects of H_2 and CO_2 addition on the burnout and sulphur volatilisation of four injection coals was studied by the manipulation of the gaseous atmosphere of the DTF.

- It was shown that the addition of H_2 produced results concurrent with recent literature. The burnout of the chars initially increased, which has been attributed in literature to the increased volatilisation and combustion of the coal's volatile matter. The final burnouts were decreased in comparison to the reference atmosphere, which in literature has been attributed to the localised depletion of O_2 around the char particle due to the preferential combustion of the H_2. The sulphur volatilisation may have been slightly affected by the addition of hydrogen, with the relative sulphur volatilisation in comparison to the burnout increasing for Coals A and C, which may be due to the presence of sulphur forms in the coals that are more readily hydrolysed.

- It was shown that the addition of CO_2 affected both the burnout and sulphur volatilisation of the studied coals. In Coal A and Coal C, the introduction of CO_2 led to a reduction in burnout. This could be as a result of the low gasification reactivity of these chars or possibly as a result of the cooling effect of the reverse Boudouard reaction. However, whilst burnout fell, sulphur volatilisation did not fall as greatly. This could be due to the effect of CO_2 on promoting the scission of C-S bonds and lowering the temperature at which sulphur is volatilised. In Coals B and D, the burnouts were also affected by the addition of CO_2. Whilst Coal B initially showed a higher burnout in the CO_2:Air atmosphere at 100 ms, both coals produced 350 ms chars with reduced burnouts before producing 700 ms chars with burnouts equivalent to the reference atmosphere. This may suggest a relationship with the higher volatile matter contents or possibly the higher char gasification reactivities, which were discerned in Chapter 6. The relative sulphur volatilisation in the CO_2:Air atmosphere was also slightly higher in Coals B and D, once again supporting the literature findings.

- The analysis of a filtered material was investigated using SEM. The analysis showed that the conditions under which this material was formed likely encouraged the fracturing of larger char particles, which was carried through the DTF cyclone separator and into the pre-Testo 350XL filter. The production of this fine char could have negative effects within the blast furnace, as such, higher char burnout should be encouraged to lower the amount of fine char leaving the raceway.

This work has shown that there may be additional benefits in the use of alternative injectants that have not been previously considered, such as increased sulphur volatilisation in the raceway and reduced char reactivity. This could allow for fuel rate savings resulting from increased furnace stability or changes to slag chemistry.

Chapter 8

The fixation of sulphur from synthetic blast furnace top gas by blast furnace charge materials

8.1 Introduction

The fate of raceway sulphur in the combustion of coal and alternative fuels has been studied in Chapters 6 and 7. The fate of any solid sulphur remaining in the unburnt char can be predicted, with a good understanding of the interactions between coke sulphur and slag already existing. However, as shown in the previous chapters, under high burnouts, the majority of sulphur introduced from pulverised coal injection is transformed to the gaseous phase. It has been shown that at lower levels of burnout, H_2S is the major gaseous sulphur species produced. The production of SO_2 was observed with some coals at high burnout levels in the DTF. The formation of SO_2 primarily occurs due to the combustion of H_2S, as such, the oxygen rich conditions of the DTF may have facilitated its production in levels that may not be seen within the blast furnace. As the blast furnace is a largely reducing atmosphere, it would not be unreasonable to consider that any SO_2 exiting the raceway could be reduced in a reaction such as in Equation 8.1 below.

$$SO_2 + 2C \rightarrow 0.5S_2 + 2CO \tag{8.1}$$

It is estimated that 2-5% of the sulphur balance leaves the blast furnace through the top gas as H_2S or SO_2 [15]. Whether this can be influenced by the volatilisation of sulphur in the raceway is unknown. Is the raceway the source of this gaseous sulphur, or is it also formed by the thermal decomposition of materials in the stack and belly of the furnace? How much of the gaseous sulphur released from the raceway reaches the top gas? How much of it reacts with with the blast furnace materials on its journey through the furnace? Answering these questions could provide an indication of whether manipulating the volatilisation of sulphur in the raceway could lead to reductions in emissions or costs. The aim of this chapter was to establish the sulphur fixation capacities of blast furnace charge materials by using a synthetic blast furnace top gas containing 500 ppm of H_2S. As H_2S and SO_2 readily react with each other, as in the key reaction of the Claus process, producing an experiment with both gases present was not viable. As such, H_2S was selected as the sulphur containing gas in the test gas blend.

8.2 The fixation of H_2S from the synthetic blast furnace gas by the blast furnace charge materials

Figure 8.1 shows the percentage fixation of gaseous sulphur from the synthetic BFG using the experiment and analysis described in Section 4.5. This percentage was calculated by comparing the measured sulphur value of the test material with the total sulphur passed through the furnace during the experiment. Six data points were selected for each material tested across the temperature range expected in the "dry" section of the blast furnace above the cohesive zone where gas-solid interactions are prevalent.

The sinter showed an almost linear increase in sulphur fixed as temperature increased. Whilst a marginal amount of sulphur was fixed by the sinter at 150°C, at 300°C 5.7% was fixed. This increased to the maximum value of 46.4% at 900°C.

The pellet showed a relatively similar trend to the sinter, however a greater amount of sulphur was fixed from the gas above 300°C. The sulphur fixed at 150°C was negligible before increasing to 12.9% at 300°C. This increased in a linear fashion until the maximum value of 58.6% at 750°C, before decreasing to 51.9% at 900°C.

It was expected that the sinter and pellet would show similar trends as they contain similar chemical compositions. The pellet contains a greater portion of iron, 64.3%, as opposed to the 54.8% iron in the sinter. Sulphur is readily reactive with iron, it is therefore possible that this greater portion of iron facilitated a greater level of sulphur fixed from the BFG. The decrease in sulphur fixation for the pellet at 900°C was unexpected and prompted the XPS investigation discussed in Section 8.3, where a reason for this phenomena is suggested.

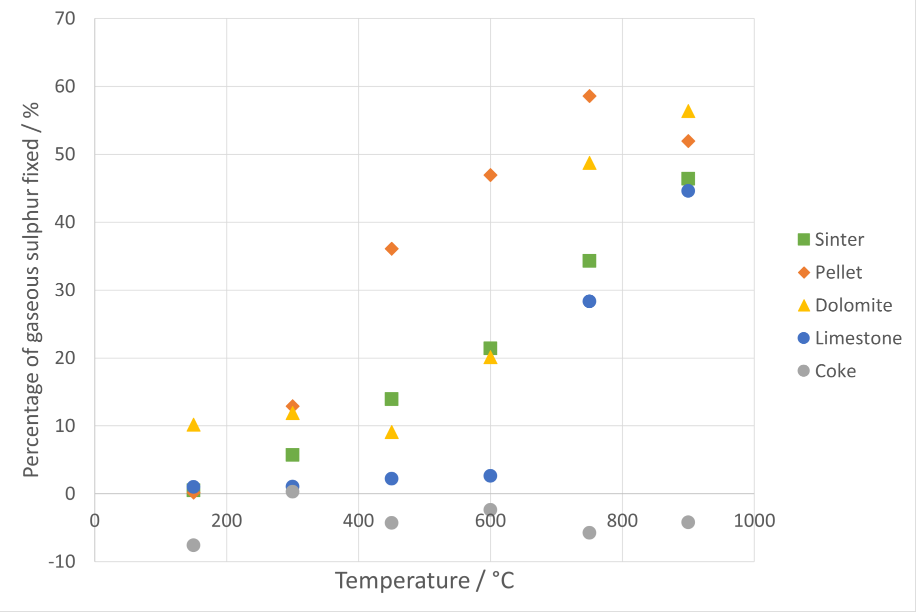

Figure 8.1: Relative sulphur fixation capacities of materials charged into the blast furnace

However, there was particular difficulty in maintaining a constant pressure in this experimental run, which may have introduced a degree of error. This was therefore selected as a data point to repeat during the quantification of error testing described in Section 8.4.1, however this proved inconclusive.

The dolomite showed a sulphur fixation capacity from 150°C, with 10.2% of the BFG sulphur fixed from the gas flow. This remained relatively constant to 450°C, where 9.1% of sulphur was fixed from the BFG flow. The amount of sulphur fixed then increased in a relatively linear fashion to a maxima of 56.4% at 900°C.

The limestone showed little sulphur fixation capacity up to 600°C, where 2.6% of the sulphur was fixed from the BFG flow. The sulphur fixation capacity then increased sharply to 28.3% at 750°C and then to 44.6% at 900°C.

During the course of the experiment, the dolomite and limestone samples thermally decompose. Dolomite decomposes to calcium carbonate (also referred to as calcite), magnesium oxide (also called periclase), and carbon dioxide via Equation 8.2 at around 600-750°C. Limestone is primarily composed of calcite, which decomposes via Equation 8.3 at around 700-900°C. The thermal decomposition of dolomite and calcite is strongly affected by the partial pressure of CO_2, which can reduce the temperature at which these compounds decompose. At the level of CO_2 present in the experiment, it can be expected that the decomposition of dolomite occurs at a temperature about 140°C lower than the decomposition of calcite [105–107].

$$CaMg(CO_3)_2 \rightarrow CaCO_3 + MgO + CO_2 \tag{8.2}$$

$$CaCO_3 \rightarrow CaO + CO_2 \tag{8.3}$$

This would strongly support that the difference between the trends of the dolomite and limestone samples is due to the presence of a greater quantity of magnesium in the dolomite. The formation of magnesium sulphide/sulphate from magnesium oxide could therefore occur in greater quantities at temperatures more than 100°C below the formation of calcium sulphide/sulphate from calcium oxide.

The coke showed no sulphur fixation capacity across the temperature range of the test points, instead displaying a fluctuation of total sulphur values that suggested small changes due to do sample heterogeneity. The minimal change in total sulphur of the coke throughout the experimental conditions suggests that sulphur may not be volatilised from the coke under the conditions in the stack of the blast furnace. This would be a strong indication that the majority of sulphur leaving the blast furnace through the top gas is produced in the raceway upon the combustion of coke and injected coal.

Direct comparison of the results of this experiment with blast furnace interactions would not be accurate due to several factors. The change of blast furnace gas composition through the temperature range is not replicated in this experiment. The particle size of the samples used in this experiment are orders of magnitude smaller than would be found in the blast furnace. However this experiment does show the relative sulphur fixation capacity of blast furnace materials at the tested temperatures, which can be used to theorise the route of sulphur through the blast furnace.

8.3 Analysis of surface sulphur

Table 8.1 shows the results of XPS analysis undertaken at Cardiff University School of Chemistry, as discussed in Section 6.4. The samples were selected to investigate the surface and bulk distributions of sulphur in the raw samples and at the selected temperatures, whilst also attempting to identify the forms of sulphur present.

The temperatures selected for the pellet were the 450°C, the 750°C, and the 900°C as the trend shown in Figure 8.1 warranted further investigation. The decrease in amount of sulphur fixed from the synthetic BFG at 900°C poised the question whether different sulphur forms were being produced during the temperature ranges, which was the reason for including the 450°C sample. The temperatures selected for the sinter were the 750°C and 900°C. The sinter did not show the decrease at 900°C that the pellet did, therefore these samples were selected to see if there was a difference in sulphur forms produced in the pellet and in the sinter. For the dolomite and limestone, only the 900°C samples were analysed as it was believed that these samples would give the clearest data with regards to sulphur forms present in the material.

Table 8.1: Surface elemental analysis of test materials using XPS

Sample	Surface elemental composition / % mass							
	Fe	Ca	C	K	S	Si	Mg	O
Sinter	25.7	3.5	22.5	-	3.2	8.6	1.1	35.3
Sinter 750°C	43.1	2.7	17.5	-	-	4.3	-	32.5
Sinter 900°C	-	14.2	41.6	-	-	6.4	-	37.8
Pellet	29.4	10.6	15.5	1.0	-	7.8	-	35.7
Pellet 450°C	15.8	10.0	33.4	-	3.8	4.2	-	32.8
Pellet 750°C	29.2	10.4	20.5	-	2.7	3.8	-	33.4
Pellet 900°C	31.3	4.0	20.1	-	-	8.4	1.3	34.9
Dolomite	3.9	6.2	35.9	0.9	-	10.0	2.7	40.3
Dolomite 900°C	5.2	19.1	19.0	-	0.5	1.6	16.7	37.9
Limestone	-	34.1	25.0	-	2.8	1.8	-	36.2
Limestone 900°C	4.8	18.5	20.4	-	0.4	1.9	16.0	38.1

It can be seen in Table 8.1 that a substantial amount of carbon was measured on each sample. The dolomite and limestone can expect to contain a larger proportion of carbon as carbonates are the main constituent material, however the sinter and pellet are known to contain less than 1% mass carbon in the bulk, so this was unexpected. This was probably caused by contamination in sample handling. It is possible that some degree of carbonisation of the sample surface occurred during the experiment, however that doesn't explain the high carbon levels in the raw sinter and pellet. The high carbon values do make direct comparisons with bulk composition difficult as it is unclear whether large reductions in an element's composition on the surface is as a result of a change caused by the experiment or whether it is due to the contamination of the sample.

It can be seen in Table 8.1 that sulphur was only detected on the surface of some of the materials, this may be due to the limitations of using a point specific technique, or it could truly indicate that the sulphur is not found on the surface of the material. Where sulphur has been identified, the binding energy of the peak can be used to indicate the form of sulphur present. Table 8.2 displays the

Table 8.2: XPS 2p binding energies of detected sulphur

Sample	Binding energy / eV	Sulphur form
Sinter	162.27	Sulphide
Sinter 750°C	-	-
Sinter 900°C	-	-
Pellet	-	-
Pellet 450°C	168.83	Sulphate
Pellet 750°C	169.07	Sulphate
Pellet 900°C	-	-
Dolomite	-	-
Dolomite 900°C	169.38	Sulphate
Limestone	162.41	Sulphide
Limestone 900°C	169.96	Sulphate

sulphur 2p binding energies of the measured peaks maxima. A binding energy of around 162 eV identifies sulphides, whilst a binding energy of around 169 eV identifies sulphates [108].

Table 8.3 compares the iron, calcium, and sulphur composition of the surface and the bulk of the raw sinter and the sinter after the 750°C and 900°C runs. The bulk iron measurement shows a gradual increase as the temperature increases and the iron oxides present are partially reduced. The surface measurement shows a lower iron composition than the bulk. Considering the lack of an iron measurement on the 900°C Sinter, this has been chiefly attributed to the high carbon content measured on every sample.

The calcium content on the surface of the sinter is initially lower than the bulk measurement, however the sinter 900°C sample displayed a large increase in surface calcium. This would suggest that calcium compounds may have migrated from the bulk of the sample to the surface under the test conditions.

The surface sulphur measurements vary from the bulk sulphur measurements. The raw sinter displayed 3.23% mass sulphur on the surface whilst containing 0.03% mass sulphur in the bulk. This suggests that the XPS may have measured an inorganic sulphur inclusion on the sample surface. Examin-

Table 8.3: Comparison of surface and bulk data for sinter

Sample		Elemental composition / % mass		
		Fe	Ca	S
Sinter	Surface	25.74	3.50	3.23
	Bulk	54.83	8.38	0.03
Sinter 750°C	Surface	43.08	2.66	-
	Bulk	58.66	8.71	0.33
Sinter 900°C	Surface	-	14.25	-
	Bulk	61.03	8.32	0.67

ing Table 8.2, it can be seen that sulphide was identified on the sinter surface. Small quantities of sulphides are known to exist in the sinter in the form of FeS, FeS_2, or CaS [15]. As no sulphur was detected by the XPS analysis for the 750°C and 900°C samples, identification of the sulphur forms by considering the peak position isn't possible, however when comparing with the sulphur forms identified in the pellet, dolomite, and limestone samples, it would be a logical assumption to identify the sulphur in the sinter 750°C and 900°C samples as sulphates. As the S 2p maxima of 169 eV can be representative of the sulphur in both $FeSO_4$ and $CaSO_4$, further identification cannot be achieved with this technique [109, 110].

Table 8.4 compares the iron, calcium, and sulphur composition of the surface and the bulk of the raw pellet and the pellet after the 450°C, 750°C, and 900°C runs. As with the sinter samples, the surface iron contents of the pellet samples are lower than would be expected when considering the bulk quantity. The calcium composition is much higher on the surface of the pellet samples than the bulk, suggesting the production of the pellets may result in greater distribution of the calcium on the surface in comparison to the bulk.

The XPS did not detect any surface sulphur on the raw pellet, which considering the bulk sulphur quantity, is not unsurprising. Where it has been detected on the 450°C and 750°C samples, the sulphur content is greater on the surface

Table 8.4: Comparison of surface and bulk data for pellet

Sample		Elemental composition / % mass		
		Fe	Ca	S
Pellet	Surface	29.41	10.58	-
	Bulk	64.33	1.07	0.01
Pellet 450°C	Surface	15.84	10.04	3.77
	Bulk	60.66	0.65	0.33
Pellet 750°C	Surface	29.18	10.40	2.66
	Bulk	68.64	0.57	0.53
Pellet 900°C	Surface	31.33	3.98	-
	Bulk	71.95	0.43	0.49

than in the bulk. Assuming that the sample is homogeneous, this would suggest that the sulphur bonds more readily to the surface of the sample during the experimental run as opposed to permeating into the bulk of the sample. Table 8.2 shows that these identified sulphur peaks correspond to sulphates. At 900°C, no surface sulphur is detected, whilst a small decrease in sulphur has been measured in the bulk. Whilst there is a degree of uncertainty around sample contamination and sample homogeneity, if this result is a true reflection of the sample surface, this could indicate the greater permeation of the H_2S into the sample's bulk. As the surface sulphur on the pellet decreased between the 450°C and the 750°C sample, as well as the sinter 750°C and 900°C sample also contained no detection of surface sulphur, it is also possible that newly formed ferrous sulphate on the sample surface undergoes thermal decomposition either during the experiment or during cooling of the furnace in a N_2 flow prior to sample withdrawal. The latter should be considered more likely as the presence of CO_2 has been found to inhibit the decomposition of ferrous sulphate, which would have inhibited decomposition during the experiment [87]. It could be extrapolated that this thermal decomposition could have been the cause of the decrease in bulk sulphur measured in the pellet 900°C sample compared to the pellet 750°C, as highlighted in Figure 8.1. Cooling a sample from 900°C results

Table 8.5: Comparison of surface and bulk data for dolomite and limestone

Sample		Elemental composition / % mass		
		Ca	Mg	S
Dolomite	Surface	6.22	2.72	-
	Bulk	17.03	3.74	0.03
Dolomite 900°C	Surface	19.13	16.69	0.49
	Bulk	31.96	14.93	0.90
Limestone	Surface	34.14	-	2.83
	Bulk	18.11	1.55	0.02
Limestone 900°C	Surface	18.55	15.95	0.40
	Bulk	59.90	ND*	0.64

*No data available for sample.

in a greater amount of time at high temperatures in the absence of a sulphur gas when compared to the 750°C sample. A greater proportion of ferrous sulphate may therefore decompose in this time. Why this does not appear in the sinter may be due to the presence of a significantly larger amount of calcium, which may fix any volatilising sulphur in the sample.

Table 8.5 compares the calcium, magnesium, and sulphur composition of the surface and the bulk of the raw dolomite and limestone, and the dolomite and limestone 900°C runs. As described in Equations 8.3 and 8.2 in Section 8.2, the limestone and dolomite samples thermally decompose during the course of the experiment, increasing the mass proportions of calcium and magnesium in the 900°C samples. This is reflected in the increase in calcium and magnesium on the surface from the raw dolomite to the dolomite 900°C sample. The limestone samples also show an increase in surface magnesium from the raw limestone to the limestone 900°C sample, however the calcium content decreases. The surface magnesium is greater than the bulk for the dolomite 900°C sample. No data was gathered for the bulk magnesium of the limestone 900°C sample due to the depletion of financial resources. However it was expected to produce a lower value than the surface measurement. The increasing surface magnesium contents suggest that it more readily travels to the surface of the sample during the course of the experiment. The surface calcium of the raw limestone is almost twice as much as the bulk, suggesting that the sample may not be completely homogeneous. The surface measurement of the limestone 900°C sample is far lower than expected, possibly as a result of contamination.

No sulphur peak was identified on the surface of the raw dolomite, which was not unexpected due to the low bulk value. However a relatively large sulphur measurement, when comparing to the bulk value, was made for the raw limestone surface which, as shown in Table 8.2, was identified as a sulphide. As no iron was identified on the surface of the sample, it would be logical to identify this as an inclusion of CaS. In the dolomite 900°C and limestone 900°C, surface sulphur was identified as sulphates. These values are lower than the bulk measurements, but are within the same order of magnitude to possibly suggest that this is due to sample heterogeneity. The likely sulphate being produced in these samples during the experiment is $CaSO_4$, however $MgSO_4$ could also be formed. Both $CaSO_4$ and $MgSO_4$ are thermally stable compounds, not decomposing under the test conditions. The measurement of surface sulphur on the dolomite 900°C and limestone 900°C whilst the absence of any on the sinter 900°C and pellet 900°C samples supports the idea that the sulphates formed on the sinter and pellets are $FeSO_4$, which can thermally decompose above temperatures of 470°C [84].

8.4 Determination of error

An attempt to quantify the error of the experiments undertaken in this chapter was undertaken. Error could be introduced in the undertaking of the designed experiment or in the analysis of the produced materials.

8.4.1 Determination of error introduced in the experimental rig

To determine the error introduced during the undertaking of the experiment, four additional repeat runs were undertaken using the pellet at 450°C and at 900°C to give a total of five repeats at each temperature. Due to the time and resource restrains of the study, repeats of each material and each data point were not feasible. The pellet was selected as the first 900°C run produced an unexpected total sulphur value which encouraged a repeat test. The 900°C data point was troublesome for all the materials as it proved very difficult to keep the rig within a suitable pressure range to allow the mass flow controller to operate as intended. The 450°C data point was selected to evaluate the effect of temperature on the error and to evaluate the error at a data point where the pressure was easily maintained at a constant value.

The sulphur content of these repeats were analysed using ICP-OES, as in the study. The repeatability of the experiment was evaluated by calculating the standard deviation (see Equation 5.7) of the total sulphur values of the repeats, with two standard deviations being used as the calculated error. Figure 8.2 shows the results of this analysis. As can be seen, there is an exceptionally large range of error in these results. This level of error is unacceptably high and would normally invalidate the findings of the study. However, whilst attempting to avoid confirmation bias, an error range of this magnitude would have certainly affected the results of the main study, during which clear trends were identified. The conducting of this repeatability test was undertaken over three days approximately two months after the main research. The main research took place over approximately five weeks, in comparison. It is believed that a major error may have occurred during the repeatability testing which affected the repeatability of the experiment. This could have occurred for any number

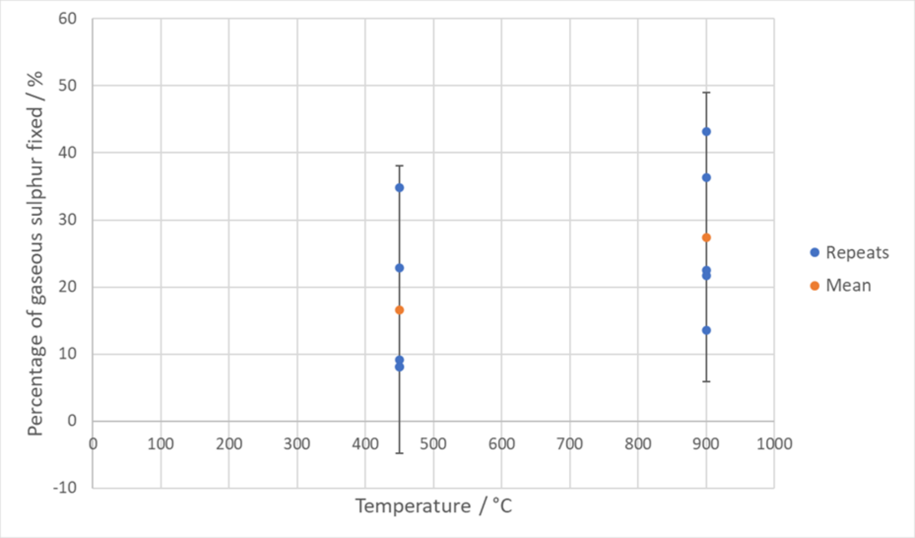

Figure 8.2: Percentage of gaseous sulphur removed from the synthetic blast furnace gas by the pellet - repeatability of experimental rig

of reasons, however the most likely cause is though to be the reaction of the material with air due to insufficient cooling prior to the furnace being opened. This human error occurred as time pressures led to the furnace being opened at higher temperatures.

Due to the failure of this test to establish an appropriate level of error, no error range is reported in the main study. This is an undesired result and if more time was available, this test would be repeated in a more stringent fashion.

8.4.2 Determination of error introduced in the analysis

Due to the issues discovered in the repeatability test, an identification of the source of error was required. To determine whether the error was introduced in the analysis of sulphur using ICP-OES, the analysis of the pellet used in the main study was repeated. The results of this are shown in Figure 8.3. As can be seen, the measurements follow the same trend with a slight decrease in the percentage mass of total sulphur in the second set of repeats. This analysis

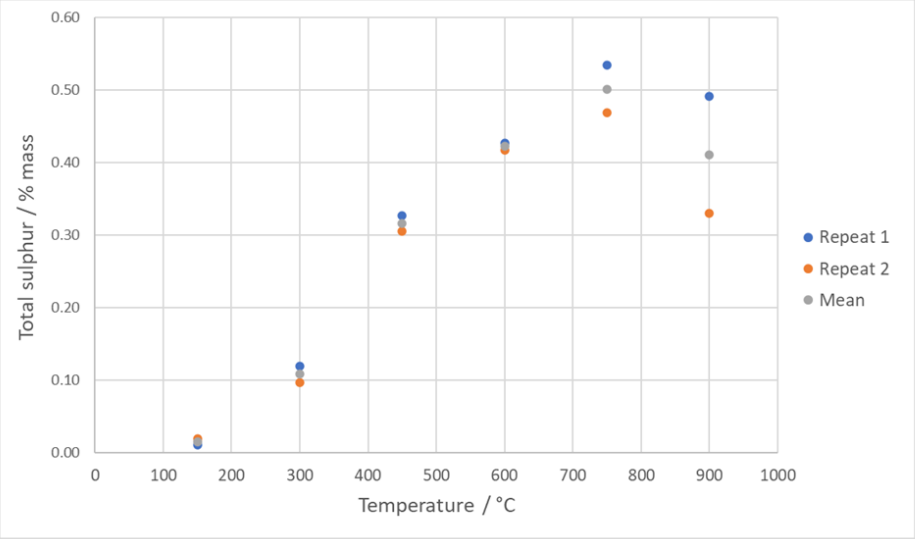

Figure 8.3: Percentage of gaseous sulphur removed from the synthetic blast furnace gas by the pellet - repeatability of ICP-OES analysis

was conducted two months after the initial analysis. It is therefore probable that the samples had partially re-oxidised, which would have reduced the total sulphur percentage mass as the mass of the material is increased. This would have occurred more on the 750°C and 900°C tests, where the pellet would have been more greatly reduced during the experiment, which explains why these repeats are particularly divergent.

As a second check of the ICP-OES analysis, the sulphur results of the repeatability test were compared with total sulphur analysis conducted on a newly replaced LECO SC-144DR, the operation of which is discussed in Section 5.4. The results were concurrent and validated the ICP-OES analysis. This therefore identified that the error in the repeatability test was introduced during the experimental stage and not the analytical stage.

The error in the XPS analysis is difficult to quantify as the technique is a semi-quantitative analysis open to the interpretation of the analyser. The work was conducted by an expert in the use of XPS and it is therefore assumed that any error in the repeatability of their analysis is marginal in comparison to the error introduced by the sample being heterogeneous or from the accuracy of the analytical instrument. XPS is a high precision technique and therefore the analysis of ratios gathered from XPS can be undertaken with a smaller error than the analysis of atomic concentrations. An accuracy of 10% is often quoted for the analysis of atomic concentrations [111].

8.5 Chapter conclusions

The relative sulphur fixation capacities of blast furnace materials have been investigated.

- The iron bearing materials showed a strong sulphur fixation capacity, with the pellet fixing more than double the amount of sulphur at 450°C and 600°C than the other blast furnace materials. The XPS analysis identified the presence of sulphates in the pellet, which would most likely be in the form of ferrous sulphate. The lack of identification of sulphates on the pellet 900°C sample suggests the possible thermal decomposition of the ferrous sulphates upon cooling in N_2, which would be inhibited by the CO_2 during the experimental run. The differences between the pellet and sinter trends have been attributed to the higher iron content in the pellet and the higher calcium content in the sinter. The strong sulphur fixation by the iron bearing materials at 900°C suggests that any gaseous sulphur fixed by the iron bearing burden in the blast furnace would remain in the burden throughout the dry portion of the furnace. This would likely result in this sulphur making its way into the hot metal and consequently being removed from the blast furnace by the slag.
- The fluxing materials begin to show greater sulphur fixation capacity upon their thermal decomposition. As fluxing materials are rarely charged di-

rectly into the blast furnace during modern ironmaking processes, these results are more relevant in the production of fluxed iron burden materials. The presence of magnesium in the dolomite samples likely increased sulphur fixation at lower temperatures compared to the limestone samples. The XPS identified the presence of sulphates in the 900°C samples.

- Coke was shown to have a negligible effect on the sulphur fixation of blast furnace gas. The minimal change in total sulphur of the coke throughout the experimental conditions suggests that sulphur may not be volatilised from the coke under the conditions in the stack of the blast furnace. This would be a strong indication that the majority of sulphur leaving the blast furnace through the top gas is produced in the raceway.
- The XPS identification of only sulphates in the experimental samples suggests that the conditions of the experiment did not favour the production of sulphides on the surface of the samples. Further analysis would be required to confirm whether this is a surface phenomenon or whether this is true for the bulk of the sample.

This work has helped to create an understanding of the interactions of gaseous sulphur with the blast furnace charge materials in the stack of the blast furnace. It has identified that a portion of sulphur volatilised in the raceway would be fixed by the burden and carried back down to the bottom of the furnace. It has also shown that sulphur is not volatilised from the charged materials over this temperature range, strongly suggesting that the main source of sulphur in the blast furnace top gas is from the combustion of coke and injected coal in the raceway region. This suggests that efforts to increase volatilisation of sulphur in the raceway would result in a larger amount of sulphur leaving the blast furnace through the top gas.

Part IV

Discussion and Conclusions

Chapter 9

Application of study to current industrial practice

9.1 The emission and distribution of sulphur in the blast furnace raceway

It has been possible to describe the likely emission mechanics and distribution of sulphur in the blast furnace raceway using the findings of this study and comparison with literature.

9.1.1 Emission of sulphur from the raceway combustion of coal

Figure 9.1 shows the release of sulphur from the injected coal particle as it progresses through the blast furnace raceway.

Upon injection, the coal particle enters the devolatilisation zone of the raceway. Here, the coal particle swells as the volatile component of the coal is released [2]. During the pyrolysis of the coal particle, the major gases released

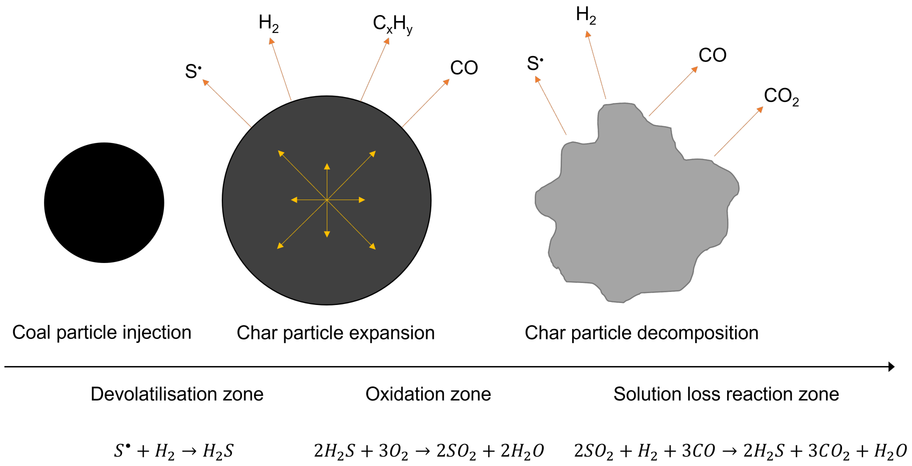

Figure 9.1: Emission of sulphur from injected coal through the blast furnace raceway

from the coal are carbon monoxide, hydrogen, and hydrogen rich hydrocarbons [112]. Sulphur is released from less thermally stable compounds which are found in the coal, such as pyrite or aliphatic organic sulphurs, as sulphur free radicals (either as a sulphur free radical, $S^{\bullet}$, or a sulphur compound free radical, such as sulphanyl, $HS^{\bullet}$). These sulphur free radicals react with the released hydrogen to form hydrogen sulphide, as in Equation 9.1 [77].

$$S^{\bullet} + H_2 \rightarrow H_2S \tag{9.1}$$

During the oxidation zone, sulphur radicals continue to be released from the char as the coal macromolecule decomposes. Oxidation of the nascent hydrogen sulphide occurs, forming sulphur dioxide, as in Equation 9.2 [7].

$$2H_2S + 3O_2 \rightarrow 2SO_2 + 2H_2O \tag{9.2}$$

In the solution loss reaction zone, upon gasification of the char macromolecule by carbon dioxide, sulphur may be emitted from more thermally stable organic sulphur compounds. The reduction of sulphur dioxide produced in the oxidation zone is likely to occur from reaction with carbon monoxide and hydrogen, resulting in the production of hydrogen sulphide via Equation 9.3 [113].

$$2SO_2 + H_2 + 3CO \rightarrow 2H_2S + 3CO_2 + H_2O \tag{9.3}$$

9.1.2 Mass distribution of sulphur forms in the raceway

Figure 9.2 expands upon the release of coal sulphur in the raceway discussed in Section 9.1.1 and displays a proposed mass distribution of injection coal sulphur as the coal passes through the raceway. This distribution was produced based upon a coal containing 25% mass of the total sulphur as pyrite, 10% as sulphates, and the remaining 65% as organic sulphurs. The distribution was produced assuming burnouts comparative with those achieved by the coals studied in Chapter 6. The distribution has been produced to provide an example of how coal sulphur will likely be distributed relatively across the raceway, but actual quantities will vary slightly depending on the coal properties and upon process conditions.

In the devolatilisation zone, the less thermally stable compounds present in the injected coal, such as pyrite and aliphatic organic sulphurs, are decomposed and react with volatilised hydrogen to form hydrogen sulphide. More thermally stable compounds, such as calcium sulphate or complex heterocyclic organic compounds, remain within the coal.

In the oxidation zone, the reaction of the coal's carbon matrix with oxygen increases the coal particle's temperature, facilitating the decomposition of sulphur compounds with greater thermal stability, such as aromatic organic sulphurs. Sulphur continues to be released and reacts with volatilised hydrogen to form hydrogen sulphide. Sulphur dioxide is produced by the oxidation of hydrogen sulphide. At the end of the oxidation zone, the majority of the coal

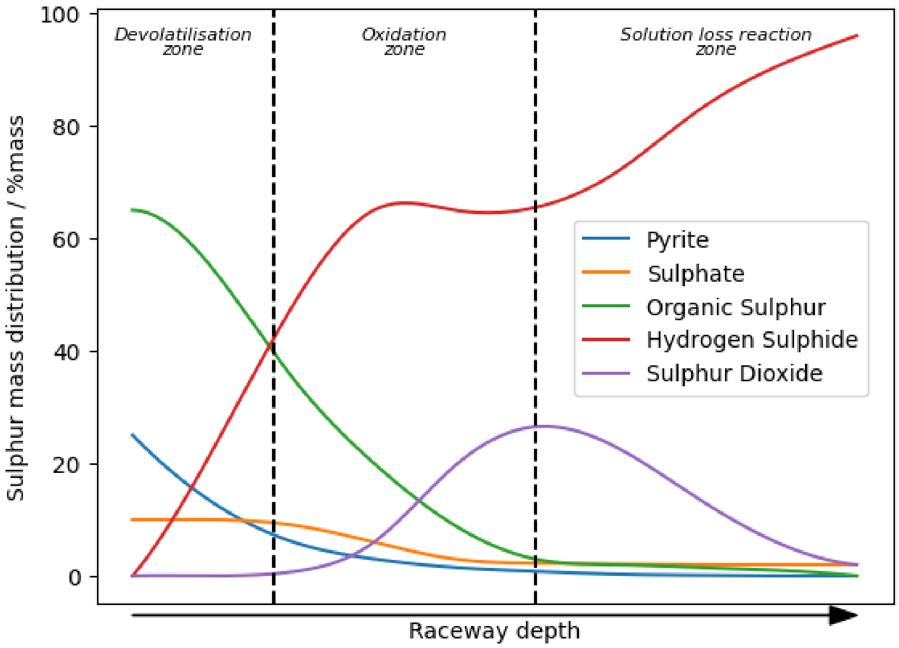

Figure 9.2: Mass distribution of sulphur forms from injected coal through the blast furnace raceway

will have combusted and char burnout will be high. At this point, only the most thermally stable sulphur compounds, such as calcium sulphate or complex heterocyclic organic sulphur will remain in any unburnt char.

The solution loss reaction zone could not be reproduced using the DTF as the DTF remains an oxygen rich environment, even at the highest possible residence times. However, as discussed in Section 9.1.1, it is possible to theorise the remaining distribution using the findings of other authors. As this is an oxygen lean zone, the major sulphur interaction in this zone is likely to be the reduction of sulphur dioxide by carbon monoxide, with the nascent sulphur radicals reacting with hydrogen to form hydrogen sulphide, as in Equation 9.3 [113]. The gasification of the unburnt char by carbon dioxide will lead to the decomposition of any remaining complex heterocyclic organic sulphurs. Whether this happens to completion in the solution loss reaction zone may depend on the coal's properties and the process conditions. Calcium sulphate will remain in the ash of the coal. If a coal has a high calcium content, some volatilised sulphur may also be fixed within the ash as calcium sulphate.

9.2 The fate of sulphur in the blast furnace

Using the findings of this study alongside the knowledge of blast furnace sulphur already present in literature, it is possible to produce a pathway that describes how sulphur enters the furnace, interacts with the materials inside the furnace, and how it leaves the furnace. Figure 9.3 allows visualisation of the pathway of sulphur as it travels through the blast furnace.

Sulphur enters the furnace from two locations, via the charge and via the coal injection. In the charged materials, most of the sulphur is found in the coke. Coke contains thermally stable sulphur compounds that were not volatilised from the coal during the coke making process. Small quantities of inorganic sulphur can be found in the iron bearing materials. Sulphur introduced from the coal injection can be in the form of pyrites, sulphates, and organic sulphurs. About 80-90% of the sulphur is introduced via the coke and coal. The amount of sulphur introduced into the blast furnace by the coke is approximately three times the amount introduced by the coal injection [15].

The majority of sulphur introduced via the charge is thermally stable and does not decompose during the descent through the dry portion of the furnace (the region above the cohesive zone). Below the cohesive zone, the sulphur in the charge is transferred to the hot metal and the slag upon decomposition of the coke. Some of the coke is combusted in the raceway region, volatilising the sulphur to form H_2S or SO_2 if sufficient quantities of oxygen are present.

The sulphur introduced via the coal injection is mostly volatilised to form H_2S or SO_2 in the raceway, as shown in Chapter 6. The production of SO_2 is

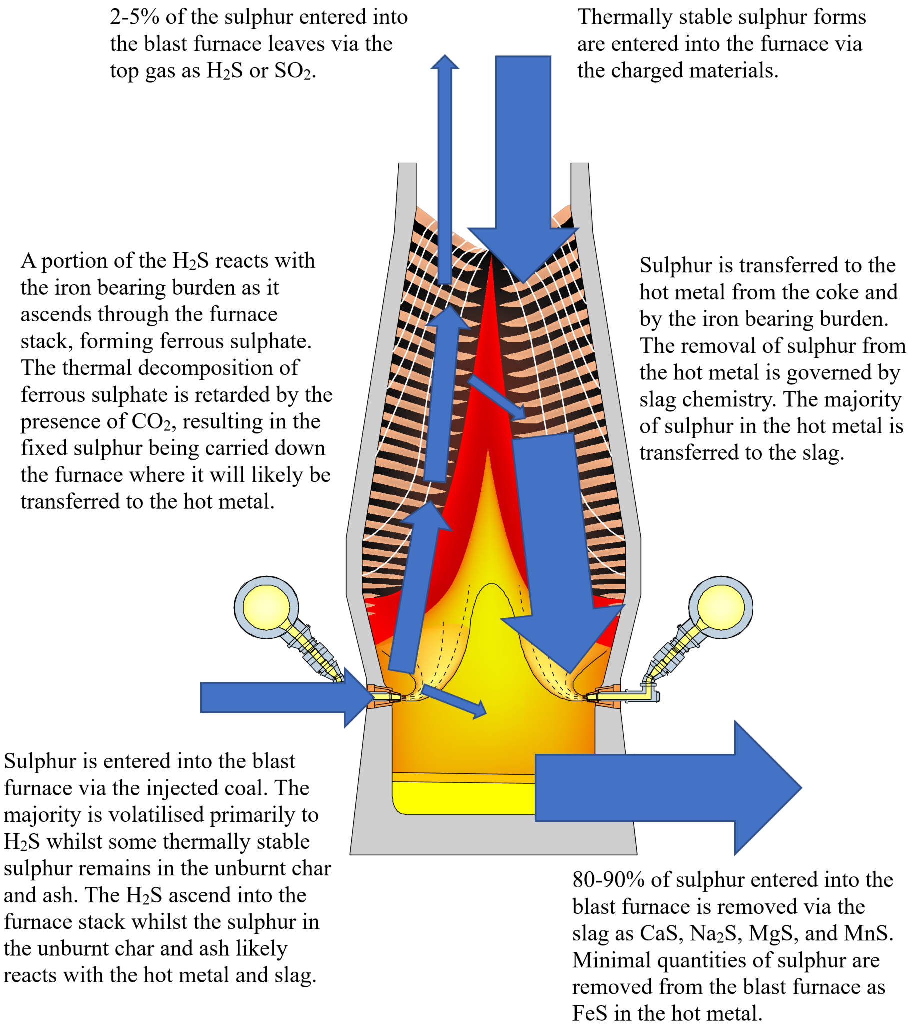

2-5% of the sulphur entered into the blast furnace leaves via the top gas as H_2S or SO_2.

Thermally stable sulphur forms are entered into the furnace via the charged materials.

A portion of the H_2S reacts with the iron bearing burden as it ascends through the furnace stack, forming ferrous sulphate. The thermal decomposition of ferrous sulphate is retarded by the presence of CO_2, resulting in the fixed sulphur being carried down the furnace where it will likely be transferred to the hot metal.

Sulphur is transferred to the hot metal from the coke and by the iron bearing burden. The removal of sulphur from the hot metal is governed by slag chemistry. The majority of sulphur in the hot metal is transferred to the slag.

Sulphur is entered into the blast furnace via the injected coal. The majority is volatilised primarily to H_2S whilst some thermally stable sulphur remains in the unburnt char and ash. The H_2S ascend into the furnace stack whilst the sulphur in the unburnt char and ash likely reacts with the hot metal and slag.

80-90% of sulphur entered into the blast furnace is removed via the slag as CaS, Na_2S, MgS, and MnS. Minimal quantities of sulphur are removed from the blast furnace as FeS in the hot metal.

Figure 9.3: Pathway of sulphur through the blast furnace

primarily as a result of the oxidation of H_2S. Comparing the literature discussed in Chapter 3, the effect of burnout on the production of SO_2 in Chapter 6, and the reduced burnout when coal was combusted in the DTF under lower oxygen-carbon ratios in Chapter 7, H_2S could be expected to be the primary gaseous sulphur form leaving the raceway within the blast furnace as complete combustion of the coal is not expected to occur. The H_2S travels into the stack of the blast furnace, where a portion of the gas reacts with the iron bearing burden. Chapter 8 showed that H_2S reacts with the iron bearing materials most readily at the higher temperatures at the bottom of the dry region. Ferrous sulphate was shown to be produced by the reaction of H_2S with the iron bearing materials in Chapter 8. The presence of CO_2 has been shown to retard the thermal decomposition of ferrous sulphate, which would allow it to descend through the furnace to react with the hot metal and slag below the cohesive zone [87]. Blast furnace operation tells us that between 2-5% of the sulphur entered into the furnace leaves the furnace through the top gas [15]. However, as coal injection is the source of approximately 20% of the sulphur entering the blast furnace, and that the majority of this is volatilised, it can be concluded that a significant portion of H_2S is fixed by the burden in its ascent through the stack. H_2S not fixed by the burden leaves the furnace through the top gas. The coal sulphur not volatilised during combustion leaves the raceway as thermally stable sulphur forms in the unburnt char or coal ash, where it is likely transferred to the hot metal or the slag.

Sulphur is transferred to the hot metal from the coke, the iron bearing burden, and likely also from the unburnt char and ash produced in the raceway. The removal of sulphur from the hot metal is governed by slag chemistry. The majority of sulphur in the hot metal is transferred to the slag. This sulphur is then removed from the blast furnace during tapping.

9.3 The lowering of blast furnace coke rate by the increased volatilisation of coal sulphur in the raceway

The addition of sulphur to the blast furnace increases the cost of producing hot metal. This is as increased sulphur levels raises the required coke rate to compensate for the endothermic desulphurisation of hot metal by the slag, which occurs via Equation 9.4, where denotes [] that the compound is concentrated in the hot metal and () in the slag. An increase of 1% mass in the coke sulphur has been shown to result in an increase in the coke rate of 5 kg/tHM [15].

$$[FeS] + (CaO) + C \rightarrow [Fe] + (CaS) + CO \qquad \Delta G = 158.42MJ \tag{9.4}$$

Assuming that the majority of the coke sulphur passes to the hot metal or slag when it decomposes below the cohesive zone, it is possible to estimate the decrease in required coke rate resulting from the increased volatilisation of coal sulphur in the raceway. Table 9.1 shows the quantities of coal and coke sulphur entered into the blast furnace during a 500 kg reductant charge by using the materials tested in this study in a simplified usage ratio.

Table 9.1: Coal and coke blast furnace sulphur

Material	S / % mass	Usage / kg/tHM	S entered into BF / kg/tHM
Coke	0.71	300	2.13
Coal C	0.39	200	0.78

The sulphur load is the amount of sulphur entering the blast furnace minus the sulphur leaving the furnace in the top gas [15]. Assuming that 100% of the coke sulphur is transferred to the hot metal or slag, therefore contributing to the sulphur load, and by using the information that a 1% mass increase of sulphur requires a 5 kg/tHM increase to the coke rate, the amount of sulphur required to increase the coke rate by 1 kg/tHM can be calculated. As shown in Table 9.2, an increase to the sulphur load of around 0.62 kg/tHM would result in an increase in coke rate requirement of 1 kg/tHM. This value can then be used with the effect of the coal volatilisation to estimate the reduction in required coke rate due to increased sulphur volatilisation.

Table 9.2: Effect of coke sulphur on hot metal sulphur

Material	S / % mass	Usage / kg/tHM	S load / kg/tHM
Coke	0.71	300	2.13
	0.91	301	2.74
	1.11	302	3.35
	1.31	303	3.97
	1.51	304	4.59
	1.71	305	5.22

As was seen in Chapter 6, the volatilisation of sulphur from the coal can vary greatly depending on the burnout of the coal particle. Whilst by comparing the results of Chapter 8.2 with literature, it could be estimated that around two thirds of this volatilised sulphur is fixed by the iron bearing burden through its journey through the dry portion of the furnace [15]. Assuming that the sulphur fixed in the dry portion of the furnace and any sulphur remaining in the unburnt char is transferred to the hot metal or slag, the effect of raceway sulphur volatilisation on hot metal sulphur can be estimated. This is shown in Table 9.3. As can be seen, a 20% increase in coal sulphur volatilisation leads to a 0.052 kg/tHM reduction in the sulphur load. This would equate to a lowering of the required coke rate by 0.084 kg/tHM. In a blast furnace that could produce 10,000 tonnes of hot metal per day, this results in a saving of 840 kg of coke per day.

Table 9.3: Effect of coal sulphur volatilisation on sulphur load

Material	S volatilisation / %	S fixed by burden / kg/tHM	S in top gas / kg/tHM	S load / kg/tHM
Coal C	20	0.104	0.052	0.728
	40	0.208	0.104	0.676
	60	0.312	0.156	0.624
	80	0.418	0.208	0.572
	100	0.520	0.260	0.520

Whilst these calculations are approximations based on some assumptions, they do produce an idea of the order of magnitude of coke rate savings that could be found by increasing the volatilisation of sulphur during coal injection. As already discussed, the primary method of doing so would be by increasing the burnout of the coal. Increased coal injection burnout would also likely have an effect on the coke rate, producing further coke rate savings. The reduction in sulphur load gives a blast furnace operator the opportunity to modify the slag chemistry or volume, which can additionally lead to further coke rate savings, which is explored in Section 9.3.1.

9.3.1 The effect of increasing the volatilisation of coal sulphur in the raceway on slag requirements

Slag is crucial to the desulphurisation of hot metal in the blast furnace. Sulphur enters the hot metal through a range of reactions, as discussed in Section 2.2.7, whilst it is removed from the hot metal by the formation of MnS, MgS, and CaS, which are absorbed by the slag [15]. The chemical affinity of elements to sulphur increases in the sequence: FeS, MnS, MgS, Na_2S, CaS. As such, calcium and magnesium are used as the two main desulphurisation agents in the blast furnace. The desulphurisation of the hot metal by calcium can be seen seen in Equation 9.4 in Section 9.3. The desulphurisation of hot metal is characterised by the sulphur distribution ratio L_S.

$$L_S = \frac{(S)}{[S]} \tag{9.5}$$

Where (S) is the sulphur in the slag and $[S]$ is the sulphur in the hot metal, in kg/tHM.

The sulphur in the hot metal is dependent on the sulphur distribution ratio, sulphur load, and slag volume. This is shown in Equation 9.6.

$$[S] = \frac{0.1 \cdot S}{1 + 0.001 \cdot L_S \cdot n}\% \tag{9.6}$$

Where the sulphur load, S, is the sulphur entering the furnace minus the sulphur leaving the furnace through the top gas, and n is the slag volume, both in kg/tHM.

The blast furnace operates at a sulphur distribution ratios lower than the theoretical equilibrium, ${L_S}^0$. The desulphurisating potential of the slag, σ , is characterised by the degree of approach to the theoretical equilibrium. It is shown in Equation 9.7.

$$\sigma = \frac{L_S}{{L_S}^0} \cdot 100\% \tag{9.7}$$

The theoretical equilibrium is calculated using Equation 9.8.

$$\log {L_S}^0 = 8.45 \log B + \frac{2000}{T} - 0.68 + \frac{f_S}{P_{CO}} \tag{9.8}$$

Where B is the slag basicity index, shown in Equation 9.9; T is the temperature of the metal-slag system, in Kelvin; f_S is the activity of sulphur in hot metal; and P_{CO} is the partial pressure of CO.

$$B = \frac{(CaO) + (MgO) + 0.5(MgO) - 1.75(S)}{(SiO_2) + 0.6(Al_2O_3)\left(\frac{(CaO)+(MgO)+0.5(MgO)-1.75(S)}{(SiO_2)}\right)} \tag{9.9}$$

Considering these equations, a reduction in the sulphur load would have the following results:

1. From Equation 9.6, a lowering of the sulphur load will decrease the sulphur in the hot metal.

2. From Equation 9.9, reducing the sulphur in the slag increases its basicity. Per Equation 9.8, an increase in basicity increases the sulphur distribution theoretical equilibrium.

If hot metal sulphur is reduced below its usual target value, it produces opportunities to either reduce hot metal desulphurising operations outside of the blast furnace, or to lower the basicity or volume of the blast furnace slag.

External desulphurising of hot metal in transfer ladles using lime, calcium carbide, and/or magnesium is a commonly used practice, however in addition to the cost of the fluxing materials, the additional stage reduces process efficiency and the separation of the produced slag and remaining hot metal naturally results in a reduction of yield due to the loss of iron in the slag.

A reduction in slag basicity could be used to reduce slag viscosity, improving gas distribution through the furnace, whilst a reduction in slag volume of 10 kg/tHM can reduce the coke rate by 2 kg/tHM [15]. Using the example scenario in Section 9.3, it is possible to estimate a lowering of the coke rate corresponding to maintaining constant hot metal sulphur by lowering the slag volume, as described in Equation 9.6.

Using the assumptions that the initial conditions were 60% sulphur volatilisation, original slag volume, n_1 was 250 kg/tHM, the sulphur distribution ratio, L_S, remained constant at 50, and that the target hot metal sulphur $[S]$ remained constant, Table 9.4 can be produced.

Table 9.4: Effect of coal sulphur volatilisation on required slag volume

Material	S volatilisation / %	S load / kg/tHM	Required slag volume / kg/tHM
Coal C	60	0.624	250
	80	0.572	227.5
	100	0.520	205

As demonstrated in the table, a 20% increase in the volatilisation of coal sulphur from the raceway can have a large effect on the required slag volume based upon Equation 9.4. A 22.5 kg/tHM reduction in the slag volume would lower the required coke rate by 4.5 kg/tHM, which in a blast furnace producing 10,000 tonnes of hot metal per day, would equate to a reduction of 45 tonnes of coke per day, which is a substantial saving. Once again, this calculation is based upon several assumptions and uses relationships that occur "in a vacuum". The benefits of lowering the slag volume are likely offset by factors such as reduced residence time of the hot metal in the slag. However, even a 2.5 kg/tHM reduction in slag volume could result in a 5 tonnes per day reduction in coke rate in a blast furnace producing 10,000 tonnes of hot metal.

An additional consideration of reduced sulphur load is the potential for producing hot metal with lower levels of silicon. The use of high basicity slag (with low viscosity) and a low slag volume facilitates the production of low-silicon hot metal. However, due to Equation 9.10, suitable desulphurisation is not possible until silicon in the hot metal is at a high enough level [15]. By lowering the sulphur load, the required level of silicon in the hot metal is reduced.

$$[FeS] + (CaO) + 0.5[Si] \rightarrow (CaS) + 0.5(SiO_2) + [Fe] \qquad (9.10)$$

The lowering of hot metal silicon would result in possible savings later in the steelmaking process, where basic oxygen steelmaking times can potentially be shortened. Silicon is removed during basic oxygen steelmaking, however as the exothermic oxidation of silicon contributes to the heat required to melt any scrap used in the process, significant reductions in hot metal silicon may not be wholly beneficial.

As suggested in this section, it appears that the opportunities for more substantial savings arise from the modification of blast furnace operations as a reaction to lower sulphur loads, as produced from increased sulphur volatilisation in the raceway, as opposed to the savings resulting directly from the reduction of endothermic desulphurising reactions occurring between the hot metal and slag. If the overall gaseous sulphur fixation capacity of the blast furnace burden could be accurately estimated, it would allow for better management of slag chemistry based upon a more accurate calculation of the sulphur load.

9.3.2 Further considerations for process optimisation

Whilst savings may be possible resulting from the increased volatilisation of sulphur in the raceway, there are some considerations that should be made when modifying process parameters to increase the volatilisation of sulphur.

The volatilisation of sulphur has been shown to be closely associated with the coal burnout in the raceway. Coal burnout can be in increased by:

- Using coals with high volatile matter contents.
- Enriching the hot blast with oxygen.
- Increasing the hot blast temperature.
- Decreasing the particle size of the injected coal.

Whilst the use of high volatile matter coals increases coal burnout, the devolatilisation reactions are endothermic and lead to a reduced raceway flame temperature. The lowering of the flame temperature can hamper raceway combustion and the melting of the ore burden. High volatile coals generally have lower calorific values than medium volatile or low volatile coals, this affects the coke replacement ratio and the stability of the furnace. The increased volatile matter content creates a greater volume of gas in the raceway, increasing blast momentum and raceway depth. This leads to higher pressures in the raceway, which increases the coal gasification rate. The chars of high volatile matter coals are generally more reactive, increasing the rate of burnout. Higher volatile matter coals have been linked with increased coke fine formation, and without sufficient oxygen enrichment, incomplete combustion of the volatilised gases can lead to soot formation, both of which can negatively affect blast furnace permeability. High volatile matter coals produce more H_2 gas which is utilised in iron ore reduction. This is favourable to reduction via CO as the regeneration of H_2 via Equation 9.11 is less endothermic and occurs more quickly than the regeneration of CO by the reverse Boudouard reaction [114–118] .

$$H_2O + C \rightarrow CO + H_2 \tag{9.11}$$

Enriching the hot blast with oxygen increases the rate of combustion in the raceway, reducing the amount of unburnt char leaving the raceway. This helps to compensate for the cooling effect of coal injection, with greater oxygen enrichment being required to maintain the flame temperature with increasing volatile matter content. The upper limit of oxygen enrichment is determined by the flame temperature and maintaining a sufficient top gas temperature. Too high a flame temperature can lead to burden descent becoming erratic. As oxygen is increased, the gas mass flow within the blast furnace decreases, decreasing heat flow to the upper region of the furnace. Oxygen enrichment can be paired with top gas recycling for large energy savings. The availability and cost of oxygen enrichment limits its application [114–118] .

An alternative to oxygen enrichment is increasing the hot blast temperature. This is usually more cost-effective as it allows a lower consumption of oxygen [114–118] . Higher blast temperatures increase the rate of devolatilisation of the coal particles. It also lowers the required coke rate; with savings of 10kg/tHM per 100°C possible [15].

Reducing the particle size of injected coal leads to intensification of its combustion due to the increase in total surface area of the coal, however the additional grinding increases costs from extra energy consumption, reduced mill productivity, and worsened pneumatic transport of the coal [15].

As can be deduced from this section, the extra volatilisation of coal sulphur is sometimes a secondary benefit of the methods used to optimise blast furnace operations. However, the savings introduced by increasing sulphur volatilisation by using a high volatile matter coal could quite potentially be offset by the reduction in raceway flame temperature, for example. Ultimately, the conditions that provide the greatest sulphur volatilisation, and therefore lowest sulphur load in the hearth of the furnace, may not be the optimal conditions for the overall operation of the furnace. Conditions that provide the greatest burnout of injected coal whilst maintaining stable and cost-effective furnace operation would be the optimum.

9.3.3 Suggestions for industrial application

As has been discussed, the optimisation of blast furnace operation for maximised sulphur volatilisation in the blast furnace raceway may not be preferable to the stable running of the blast furnace. The most useful application of this study is likely to be in the determination of the sulphur load and therefore changing slag chemistry and volume accordingly. The sulphur balance of blast furnaces is often produced with only the hot metal and slag sulphur being measured, an additional measurement of the blast furnace top gas sulphur would allow for accurate calculation of the sulphur load. Accurate calculation of the sulphur load may prevent excess slag volume or basicity, improving blast furnace efficiency and reducing required the coke rate. This can likely be done at a relatively low cost, the price of a robust gas analyser or sampling method, with the potential savings realised in a short period.

9.4 The use of alternative fuels

The use of alternative fuels as a replacement for injected coal may be a method for reducing the costs or overall emissions of the ironmaking process, however considerations such as availability of local material, security of supply, and the effect of diverting material from other applications should all be made. For example, the use of left over agricultural produce, such as straw, may seem attractive, but would this affect the supply of straw used for local animal husbandry, leading to the import of materials? Conversely, is the use of a wood based biochar that is sourced from the Americas of more environmental benefit to a European user than using a locally sourced coal, or does the transport of this material nullify the benefits? The use of life cycle assessments are therefore crucial in the application of alternative fuels. The greatest benefits obviously come from the use of local material with a low cost and little market demand.

The presence of undesirable elements in alternative fuels will play a massive role in their suitability for use in the blast furnace. The introduction of excess alkali elements or phosphates, which can be associated with biomass materials, can negatively impact furnace production, removing any benefits generated by offsetting a portion of the injection coal.

The production of H_2 is also a subject for discussion. Some plants in Europe, such as those discussed in Chapter 2, have begun ironmaking operations with grey hydrogen, produced by steam methane reforming. These plants may be adapting for the implementation of a green hydrogen network, but until this is realised, the use of hydrogen remains intrinsically linked to the use of fossil fuels. Where compromises may be found is in the gasification of waste materials to produce CO/H_2 syngases, that may be utilised in DRI or modified BF processes.

What this study showed is that the use of these alternative fuels, whether solid or gaseous, can affect the burnout and sulphur volatilisation of coals and coal blends in the DTF. This would likely be replicated in the raceway of the blast furnace. How this affects the overall operation of the furnace and whether any potential savings are offset by poorer blast furnace operation must therefore be considered when selecting alternative fuels.

Chapter 10

Conclusions and further work

10.1 Conclusions

This thesis has studied the fate of sulphur introduced from coal injection within the blast furnace. Through the study of existing literature, a hypothesis was produced. Objectives were produced to validate this hypothesis. These have been addressed via the experimental work and subsequent analysis produced in this thesis.

Literature showed that the blast furnace is already a well understood technology. The fate of the sulphur entered into the furnace via the coke and burden is well understood, with the interactions between sulphides, sulphates, slag, and the hot metal being managed to ensure the desulphurisation of the hot metal. The fate of sulphur introduced from pulverised coal injection was found to be less well studied. It has been shown by blast furnace operational data that much of the sulphur entered into the blast furnace leaves via the slag, but the source of the 2-5% of the sulphur balance that leaves the blast furnace through the top gas was not identified. This thesis therefore attempted to identify the route through which sulphur entered into the blast furnace via coal injection exits the furnace and whether any coal or process parameters have an effect on this route.

Literature provided a strong base of understanding of coal sulphur: the association of organic sulphur in coal with coal rank; the relative thermal stabilities of coal sulphurs; and the accelerant, retardant, and fixative properties of elements on coal sulphur have all been well studied. This knowledge was applied to the theoretical understanding of the blast furnace, the raceway region in particular, to produce a hypothesised route of sulphur introduced via coal injection through the blast furnace.

In order to study the volatilisation of coal sulphur in the raceway, four blast furnace injection coals were studied via use of a drop tube furnace in Chapter 6. The key conclusions were:

- The greatest contributing factor to the volatilisation of coal sulphur was found to be the burnout of the char. The rate of burnout increased with increasing coal volatile matter content.
- The volatilisation of sulphur from a coal appeared to occur in a two stage process. During the combustion of the volatile matter content of a coal, less thermally stable sulphur compounds in the coal decompose, volatilising the sulphur. More thermally stable compounds do not decompose until the combustion of the remaining non-volatile coal macromolecule. The sulphur forms existing in the initial coal samples can therefore give an indication of the sulphur forms that could be found in any unburnt char.

With one eye on the short term future of blast furnace ironmaking, the suitability of alternative injectants was studied in Chapter 7. Alternative solid fuel injectants for blast furnace co-injection with reference to the effects on burnout and sulphur volatilisation were studied using blends of the alternative solid fuel and Coal C.

- Burnout remained the major factor in sulphur volatilisation, with the sulphur volatilisation of each material following the same trend as the char burnout. However, differences likely arose from the introduction of different sulphur forms in differing quantities to Coal C. The relative thermal stability of those sulphur compounds would play a large role in the volatilisation of sulphur from the blend. It would therefore be a requirement of fuel selection to not only consider total sulphur, but the form of sulphur present in the fuel.

- The use of waste or recycled materials, such as sewage sludge or tyres, can lead to the introduction of undesirable elements or compounds into the injectant blend. The presence of these materials could inadvertently lead to increased coke rates, offsetting any potential savings introduced by the use of the alternative solid fuels.

The effects of H_2 and CO_2 addition on the burnout and sulphur volatilisation of four injection coals was studied by the manipulation of the gaseous atmosphere of the DTF.

- It was shown that the addition of H_2 produced results concurrent with recent literature. The burnout of the chars initially increased, which has been attributed in literature to the increased volatilisation and combustion of the coal's volatile matter. The final burnouts were decreased in comparison to the reference atmosphere, which in literature has been attributed to the localised depletion of O_2 around the char particle due to the preferential combustion of the H_2. The sulphur volatilisation may have been slightly affected by the addition of hydrogen, with the relative sulphur volatilisation in comparison to the burnout increasing for Coals A and C, which may be due to the presence of sulphur forms in the coals that are more readily hydrolysed.

- It was shown that the addition of CO_2 affected both the burnout and sulphur volatilisation of the studied coals. In Coal A and Coal C, the introduction of CO_2 led to a reduction in burnout. This could be as a result of the low gasification reactivity of these chars or possibly as a result of the cooling effect of the reverse Boudouard reaction. However, whilst burnout fell, sulphur volatilisation did not fall as greatly. This could be due to the effect of CO_2 on promoting the scission of C-S bonds and lowering the temperature at which sulphur is volatilised. In Coals B and D, the burnouts were also affected by the addition of CO_2. Whilst Coal B initially showed a higher burnout in the CO_2:Air atmosphere at 100 ms, both coals produced 350 ms chars with reduced burnouts before producing 700 ms chars with burnouts equivalent to the reference atmosphere. This may suggest a relationship with the higher volatile matter contents or possibly the higher char gasification reactivities. The relative sulphur volatilisation in the CO_2:Air atmosphere was also slightly higher in Coals B and D, once again supporting the literature findings.

The relative sulphur fixation capacities of blast furnace charge materials were investigated in Chapter 8. The key findings were:

- The iron bearing materials showed a strong sulphur fixation capacity, with the pellet fixing more than double the amount of sulphur at 450°C and 600°C than the other blast furnace materials.

- The strong sulphur fixation by the iron bearing materials at 900°C suggests that any gaseous sulphur fixed by the iron bearing burden in the blast furnace would remain in the burden throughout the dry portion of the furnace. This would likely result in this sulphur making its way into the hot metal and consequently being removed from the blast furnace by the slag.
- Coke was shown to have a negligible effect on the sulphur fixation of blast furnace gas. This suggests that sulphur may not be volatilised from coke under the conditions in the stack of the blast furnace. This would be a strong indication that the majority of sulphur leaving the blast furnace through the top gas is produced in the raceway.

The application of the knowledge gained in this study to current industrial practice has been discussed in Chapter 9.

- Descriptions of the volatilisation of sulphur in the raceway and the route of sulphur through the blast furnace were produced and discussed.
- The effect of increased raceway sulphur volatilisation on coke rate and slag chemistry requirements have been discussed. Considerations of other affected blast furnace conditions were made. It has been concluded that the optimisation of blast furnace operation for maximised sulphur volatilisation in the blast furnace raceway may not be preferable as this may affect the stable running of the blast furnace.
- The most useful application of this study is likely to be in the determination of the sulphur load and therefore changing slag chemistry and volume accordingly. The sulphur balance of blast furnaces is often produced with only the hot metal and slag sulphur being measured, an additional measurement of the blast furnace top gas sulphur would allow for accurate

calculation of the sulphur load. Accurate calculation of the sulphur load may prevent excess slag volume or basicity, improving blast furnace efficiency and reducing required the coke rate.

10.2 Suggestions for further work

This study has produced a theoretical understanding of the fate of sulphur originating from coal injection within the blast furnace, however there are several areas where this work can be improved or expanded upon.

- The repeatability of the experiments in Chapter 8 can be questioned due to the poor performance of the repeatability testing undertaken. Whilst this could possibly be explained by human error introduced during this testing, further investigation of the repeatability would be prudent to confirm the findings of the main body of experiments.

- The laboratory experiments undertaken in this work provides snapshots of conditions in specific locations in the blast furnace. The sulphur fixation capacity of the blast furnace dry section could be more accurately estimated by using a scaled simulator of the blast furnace, where coke, pellets, and sinter could be charged and heated with a temperature profile across the vertical range with a sulphur containing gas injected at the bottom of the furnace. A gas analyser on the top gas exhaust of this simulator would then be able to provide the data required to assess the sulphur fixation capacity of the simulator.

- The conclusions of this thesis make the assumption that any sulphur in the unburnt char leaving the raceway makes its way into the hot metal or slag in the hearth of the furnace alongside any sulphur in the charged coke. This assumption is based upon the sulphur balance of the blast furnace, where 80-90% of the sulphur entered into the blast furnace is then removed from the furnace via the slag. The accuracy of this assumption could be assessed by an experiment measuring the gaseous products of coke and char decomposition within liquid hot metal or slag. A similar experiment measuring the sulphur fixation capacity of the area below the cohesive zone by bubbling a sulphur containing syngas through molten hot metal or slag could also help to quantify the amount of volatilised raceway sulphur fixed in the immediate vicinity of the raceway before it reaches the dry section of the furnace.

- Whilst data has been produced in a laboratory setting, validation with blast furnace data would confirm the findings of this thesis. The measurement of gaseous sulphur forms such as H_2S and SO_2 in blast furnace top gas and correlating this with injection coal data would examine the suggestion that the majority of top gas sulphur originates from the raceway. This could then be followed with simulations and trials modifying the flux charging relating to more accurate calculation of the furnace sulphur load.
- This work has focused on the fate of sulphur within the blast furnace, however the knowledge gained could potentially be utilised in other parts of an integrated steelworks. Further work could investigate how this knowledge could be applied to cokemaking, sintermaking, or steelmaking to facilitate further optimisation of the processes. For example, the selection of coals containing a greater proportion of less thermally stable sulphurs would be preferable in cokemaking as the sulphur would then be less likely to find its way into the blast furnace.

References

[1] Geerdes, M., Chaigneau, R., and Kurunov, I. (2015) Modern Blast Furnace Ironmaking: An Introduction (Third Edition, 2015), IOS Press, Amsterdam.

[2] Ishii, K., (ed.) (2000) Advanced Pulverized Coal Injection Technology and Blast Furnace Operation, Elsevier, Oxford.

[3] Liao, J., Qing, G., and Zhao, B. (2023) Phase Equilibrium Studies of the CaO-MgO-Al2O3-SiO2 System for Iron Blast Furnace Slag: A Review. *Metals,* **13**(4), 801.

[4] Calkins, W. H. (1987) Investigation of Organic Sulfur-Containing Structures in Coal by Flash Pyrolysis Experiments. *Energy & Fuels,* **1**(1), 59–64.

[5] Miura, K., Mae, K., Shimada, M., and Minami, H. (2001) Analysis of Formation Rates of Sulfur-Containing Gases during the Pyrolysis of Various Coals. *Energy & Fuels,* **15**(3), 629–636.

[6] Wang, M., Liu, L., Wang, J., Chang, L., Wang, H., and Hu, Y. (2015) Sulfur K-Edge XANES Study of Sulfur Transformation during Pyrolysis of Four Coals with Different Ranks. *Fuel Processing Technology,* **131**, 262–269.

[7] Müller, M., Schnell, U., and Scheffknecht, G. (2013) Modelling the Fate of Sulphur During Pulverized Coal Combustion under Conventional and Oxy-Fuel Conditions. *Energy Procedia,* **37**, 1377–1388.

[8] BS 1016-106.5:1996, ISO 157:1996 Methods for Analysis and Testing of Coal and Coke. Ultimate Analysis of Coal and Coke. Determination of Forms of Sulfur in Coal. (1996).

[9] Speight, J. G. (2012) The Chemistry and Technology of Coal, Third Edition, CRC Press, Boca Raton.

[10] Iron and Steel – Analysis. https://www.iea.org/reports/iron-and-steel.

[11] Patisson, F. and Mirgaux, O. (2020) Hydrogen Ironmaking: How It Works. *Metals,* **10**(7), 922.

[12] Iron and Steel Technology Roadmap – Analysis - IEA. https://www.iea.org/reports/iron-and-steel-technology-roadmap.

[13] Herbet, J. (2019) The Effects of Mineral Matter from Pulverised Coal Injection on the Blast Furnace Raceway PhD thesis Cardiff University School of Engineering Cardiff.

[14] Hutton, G., Rhodes, C., Ward, M., and Bolton, P., (2023) UK Steel Industry: Statistics and Policy. Technical report, .

[15] Babich, A., Senk, D., Gudenau, H. W., and Mavrommatis, K. T. (2008) Ironmaking, Mainz, Aachen.

[16] webmaster@defra gsi gov uk Department for Environment, F. a. R. A. D. Overview of Greenhouse Gases - Defra, UK. https://naei.beis.gov.uk/overview/ghg-overview.

[17] Hydrogen Sulfide & Health — California Air Resources Board. https://ww2.arb.ca.gov/resources/hydrogen-sulfide-and-health.

[18] World Steel in Figures 2022. https://worldsteel.org/steel-topics/statistics/world-steel-in-figures-2022/.

[19] Fact Sheets. https://worldsteel.org/publications/fact-sheets/.

[20] Iron and Steel – Analysis. https://www.iea.org/reports/iron-and-steel.

[21] tec-science Blast Furnace Process. https://www.tec-science.com/material-science/steel-making/blast-furnace-process/ (2018).

[22] Osborne, D., (ed.) (2013) The Coal Hanbook Towards Cleaner Production Volume 2: Coal Utilisation, Number 51 in Woodhead Publishing Series in EnergyWoodhead Publishing Limited, Cambridge.

[23] Berkowitz, N. (1979) An Introduction to Coal Technology, Academic Press, New York.

[24] Steer, J., Greenslade, M., and Marsh, R. (2021) A Comparison of Laboratory Coal Testing with the Blast Furnace Process and Coal Injection. *Metals,* **11**, 1476.

[25] Carpenter, A. M. (2006) Use of PCI in Blast Furnaces, IEA Clean Coal Centre, London.

[26] Steer, J. M., Marsh, R., Sexton, D., and Greenslade, M. (2018) A Comparison of Partially Burnt Coal Chars and the Implications of Their Properties on the Blast Furnace Process. *Fuel Processing Technology,* **176**, 230–239.

[27] Morrison, G. F. (1986) Understanding Pulverised Coal Combustion, IEA Coal Research, London.

[28] About Midrex. https://www.midrex.com/about-midrex/.

[29] Yang, Y., Raipala, K., and Holappa, L. (2014) Chapter 1.1 - Ironmaking. In Seetharaman, S., (ed.), *Treatise on Process Metallurgy*, pp. 2–88 Elsevier Boston.

[30] Circored™ Hydrogen-Based Reduction. https://www.mogroup.com/portfolio/circored-hydrogen-based-reduction/.

[31] HYBRIT. A New Revolutionary Steelmaking Technology.. https://www.ssab.com/en-gb/fossil-free-steel/hybrit-a-new-revolutionary-steelmaking-technology.

[32] Timeline for HYBRIT and Fossil-Free Steel. https://www.ssab.com/en/company/sustainability/sustainable-operations/hybrit-phases.

[33] Hydrogen-Based Steelmaking to Begin in Hamburg — ArcelorMittal. https://corporate.arcelormittal.com/media/case-studies/hydrogen-based-steelmaking-to-begin-in-hamburg/.

[34] ArcelorMittal Commissions Midrex to Design Demonstration Plant for Hydrogen Steel Production in Hamburg. https://www.midrex.com/press-release/arcelormittal-commissions-midrex-to-design-demonstration-plant-for-hydrogen-steel-production-in-hamburg/.

[35] Midrex and Paul Wurth Selected by H2 Green Steel. https://www.midrex.com/press-release/midrex-and-paul-wurth-selected-by-h2-green-steel/.

[36] Öhman, A., Karakaya, E., and Urban, F. (2022) Enabling the Transition to a Fossil-Free Steel Sector: The Conditions for Technology Transfer

for Hydrogen-Based Steelmaking in Europe. *Energy Research & Social Science,* **84**, 102384.

[37] Zhang, C., Vladislav, L., Xu, R., Sergey, G., Jiao, K., Zhang, J., Li, T., Aleksei, T., Wang, C., and Wang, G. (2022) Blast Furnace Hydrogen-Rich Metallurgy-Research on Efficiency Injection of Natural Gas and Pulverized Coal. *Fuel,* **311**, 122412.

[38] Ren, M., Liu, W., Zhao, J., Zou, C., Ren, L., Wu, H., and Zhao, J. (2022) Effects of Hydrogen Fraction in Co-Injection Gas on Combustion Characteristics of the Raceway in Low Carbon Emission Blast Furnace. *International Journal of Hydrogen Energy,*.

[39] Li, J., Kuang, S., Jiao, L., Liu, L., Zou, R., and Yu, A. (2022) Numerical Modeling and Analysis of Hydrogen Blast Furnace Ironmaking Process. *Fuel,* **323**, 124368.

[40] Ueki, Y., Yoshiie, R., Naruse, I., and Matsuzaki, S. (2017) Effect of Hydrogen Gas Addition on Combustion Characteristics of Pulverized Coal. *Fuel Processing Technology,* **161**, 289–294.

[41] Yilmaz, C., Wendelstorf, J., and Turek, T. (2017) Modeling and Simulation of Hydrogen Injection into a Blast Furnace to Reduce Carbon Dioxide Emissions. *Journal of Cleaner Production,* **154**, 488–501.

[42] Wang, Q., Wang, E., An, Q., and Chionoso, O. P. (2022) CFD Study of Bio-Syngas and Coal Co-Injection in a Blast Furnace with Double Lance. *Energy,* p. 125906.

[43] Zhuo, Y., Hu, Z., and Shen, Y. (2021) CFD Study of Hydrogen Injection through Tuyeres into Ironmaking Blast Furnaces. *Fuel,* **302**, 120804.

[44] Moriya, K., Takahashi, K., Murao, A., Sato, T., and Fukada, K. (2020) Effect of Large Amount of Co-injected Gaseous Reducing Agent on Combustibility of Pulverized Coal Analyzed with Non-Contact Measurement. *ISIJ International,* **60**(8), 1662–1668.

[45] Wang, H., Chu, M., Guo, T., Zhao, W., Feng, C., Liu, Z., and Tang, J. (2016) Mathematical Simulation on Blast Furnace Operation of Coke Oven Gas Injection in Combination with Top Gas Recycling. *steel research international,* **87**(5), 539–549.

[46] Liu, Z., Chu, M., Guo, T., Wang, H., and Fu, X. (2016) Numerical Simulation on Novel Blast Furnace Operation of Combining Coke Oven Gas Injection with Hot Burden Charging. *Ironmaking & Steelmaking,* **43**(1), 64–73.

[47] Li, Z., Qi, Z., Wang, Z., Zhang, L., Liang, D., and Dong, Q. (2022) Numerical Investigation of Coke Oven Gas (COG) Injection into an Ironmaking Blast Furnace (BF). *International Journal of Hydrogen Energy,* **47**(73), 31109–31128.

[48] Bailera, M. (2023) Comparing Different Syngas for Blast Furnace Ironmaking by Using the Extended Operating Line Methodology. *Fuel,* **333**, 126533.

[49] Li, J., Li, C., Zhang, W., Zhang, J., and Xue, Z. (2022) Material, Energy and Exergy Flows of the Oxygen Blast Furnace Process with Sintering Flue Gas Injection. *Journal of Cleaner Production,* **371**, 133294.

[50] Yeh, C.-P., Du, S.-W., Tsai, C.-H., and Yang, R.-J. (2012) Numerical Analysis of Flow and Combustion Behavior in Tuyere and Raceway of Blast Furnace Fueled with Pulverized Coal and Recycled Top Gas. *Energy,* **42**(1), 233–240.

[51] Ye, L., Zhang, J., Wang, G., Wang, C., Mao, X., Ning, X., Zhang, N., Teng, H., Li, J., and Wang, C. (2023) Feasibility Analysis of Plastic and Biomass Hydrochar for Blast Furnace Injection. *Energy,* **263**, 125903.

[52] Seinfeld, J. H. and Pandis, S. N. (2006) ATMOSPHERIC CHEMISTRY AND PHYSICS From Air Pollution to Climate Change, John Wiley & Sons, Inc., Hoboken, New Jersey 2nd edition.

[53] Fioletov, V. E., McLinden, C. A., Krotkov, N., Li, C., Joiner, J., Theys, N., Carn, S., and Moran, M. D. (2016) A Global Catalogue of Large SO2 Sources and Emissions Derived from the Ozone Monitoring Instrument. *Atmospheric Chemistry and Physics,* **16**(18), 11497–11519.

[54] Krotkov, N. A., McLinden, C. A., Li, C., Lamsal, L. N., Celarier, E. A., Marchenko, S. V., Swartz, W. H., Bucsela, E. J., Joiner, J., Duncan, B. N., Boersma, K. F., Veefkind, J. P., Levelt, P. F., Fioletov, V. E., Dickerson, R. R., He, H., Lu, Z., and Streets, D. G. (2016) Aura OMI Observations of Regional SO_2 and NO_2 Pollution Changes from 2005 to 2015. *Atmospheric Chemistry and Physics,* **16**(7), 4605–4629.

[55] IEA Data & Statistics. Available at https://www.iea.org/data-and-statistics [Accessed: 01/04/2020].

[56] Amann, M., Klimont, Z., and Wagner, F. (2013) Regional and Global Emissions of Air Pollutants: Recent Trends and Future Scenarios. *Annual Review of Environment and Resources,* **38**(1), 31–55 _eprint: https://doi.org/10.1146/annurev-environ-052912-173303.

[57] Gutowski, T. G., Allwood, J. M., Herrmann, C., and Sahni, S. (2013) A Global Assessment of Manufacturing: Economic Development, Energy Use, Carbon Emissions, and the Potential for Energy Efficiency and Ma-

terials Recycling. *Annual Review of Environment and Resources,* **38**(1), 81–106 _eprint: https://doi.org/10.1146/annurev-environ-041112-110510.

[58] Hasanbeigi, A., Khanna, N., and Price, L., (March, 2017) Air Pollutant Emissions Projections for the Cement and Steel Industry in China and the Impact of Emissions Control Technologies. Technical Report LBNL–1007268, Lawrence Berkeley National Lab.

[59] Karr, C. (1978) Analytical Methods for Coal and Coal Products, Vol. 1, Academic Press, INC. (London) Ltd., London united kingdom edition edition.

[60] Xu, L., Yang, J., Li, Y., and Liu, Z. (2004) Behavior of Organic Sulfur Model Compounds in Pyrolysis under Coal-like Environment. *Fuel Processing Technology,* **85**(8-10), 1013–1024.

[61] Wang, M., Jia, T., Wang, J., Hu, Y., Liu, F., Wang, H., and Chang, L. (2016) Changes of Sulfur Forms in Coal after Tetrachloroethylene Extraction and Theirs Transformations during Pyrolysis. *Fuel,* **186**, 726–733.

[62] Casagrande, D. and Siefert, K. (1977) Origins of Sulfur in Coal: Importance of the Ester Sulfate Content of Peat. *Science,* **195**(4279), 675–676.

[63] Kostova, I., Marinov, S., Stefanova, M., Markova, K., and Stamenova, V. (2005) The Distribution of Sulphur Forms in High-S Coals of the Maritza West Basin, Bulgaria. *Bulletin of Geosciences,* **80**(1), 23–32.

[64] Wang, M., Hu, Y., Wang, J., Chang, L., and Wang, H. (2013) Transformation of Sulfur during Pyrolysis of Inertinite-Rich Coals and Correlation with Their Characteristics. *Journal of Analytical and Applied Pyrolysis,* **104**, 585–592.

[65] Ward, C. R. and Gurba, L. W. (1998) Occurrence and Distribution of Organic Sulphur in Macerals of Australian Coals Using Electron Microprobe Techniques. *Organic Geochemistry,* **28**(11), 635–647.

[66] Ward, C. R., Li, Z., and Gurba, L. W. (2006) Variations in Elemental Composition of Macerals with Vitrinite Reflectance and Organic Sulphur in the Greta Coal Measures, New South Wales, Australia. *International Journal of Coal Geology,* **69**, 205–219.

[67] Speight, J. G. (2005) Handbook of Coal Analysis, John Wiley & Sons, Hoboken, New Jersey.

[68] Raask, E. (1985) Mineral Impurities in Coal Combustion: Behavior, Problems, and Remedial Measures, Hemisphere Publishing Corporation, London.

[69] Ma, X. M., Zhang, M. X., and Min, F. F. (2015) A Study of Organic Sulfur Analysis in Coal Using Non-Destructive Techniques. *Energy Sources, Part A: Recovery, Utilization, and Environmental Effects,* **37**(24), 2716–2723 _eprint: https://doi.org/10.1080/15567036.2012.736916.

[70] McMurry, J. (2008) Organic Chemistry, Thomson Brooks/Cole, Belmont, CA.

[71] Hill, J., McCreary, T., and Kolb, D. (2015) Chemistry for Changing Times, Pearson, London.

[72] Liu, F., Xie, L., Guo, H., Xue, M., Hu, R., and Hu, H. (2014) Sulfur Release and Transformation Behaviors of Sulfur-Containing Model Compounds during Pyrolysis under Oxidative Atmosphere. *Fuel,* **115**, 596–599.

[73] Gu, Y., Yperman, J., Reggers, G., Carleer, R., and Vandewijngaarden, J. (2016) Characterisation of Volatile Organic Sulphur Compounds Release during Coal Pyrolysis in Inert, Hydrogen and CO2 Atmosphere. *Fuel,* **184**, 304–313.

[74] Deng, J., Ma, X., Zhang, Y., Li, Y., and Zhu, W. (2015) Effects of Pyrite on the Spontaneous Combustion of Coal. *International Journal of Coal Science & Technology,* **2**(4), 306–311.

[75] Davidson, R. M. (1993) Organic Sulphur in Coal, IEA Coal Research, London.

[76] Suárez-Ruiz, I. and C. Crelling, J., (eds.) (2008) Applied Coal Petrology, Elsevier, Oxford.

[77] Gu, Y., Yperman, J., Vandewijngaarden, J., Reggers, G., and Carleer, R. (2017) Organic and Inorganic Sulphur Compounds Releases from High-Pyrite Coal Pyrolysis in H2, N2 and CO2: Test Case Chinese LZ Coal. *Fuel,* **202**, 494–502.

[78] Liu, F., Li, B., Li, W., Bai, Z., and Yperman, J. (2010) Py-MS Study of Sulfur Behavior during Pyrolysis of High-Sulfur Coals under Different Atmospheres. *Fuel Processing Technology,* **91**(11), 1486–1490.

[79] Mullens, S., Yperman, J., Carleer, R., Bozdemir, T., Durusoy, T., and Yürüm, Y. (2005) Sulfur Analysis of Bolu-Mengen Lignite before and after Microbiological Treatment Using Reductive Pyrolysis and Gas Chromatography/Mass Spectrometry. *Energy & Fuels,* **19**(3), 1029–1036.

[80] Tang, L., Chen, S., Gui, D., Zhu, X., He, H., and Tao, X. (2020) Effect of Removal Organic Sulfur from Coal Macromolecular on the Properties of High Organic Sulfur Coal. *Fuel,* **259**, 116264.

[81] Shen, Y., Wang, M., Hu, Y., Kong, J., Wang, J., Chang, L., and Bao, W. (2019) Transformation and Regulation of Sulfur during Pyrolysis of Coal Blend with High Organic-Sulfur Fat Coal. *Fuel,* **249**, 427–433.

[82] Liang, P., Jiang, W.-M., Zhang, Y.-Q., Wang, X.-H., and Zhu, J.-L. (2016) Effect of Circulating Ash on Sulfur Conversion Characteristics in the Coal Polygeneration Process. *Fuel Processing Technology,* **150**, 16–22.

[83] Marinov, S., Tyuliev, G., Stefanova, M., Carleer, R., and Yperman, J. (2004) Low Rank Coals Sulphur Functionality Study by AP-TPR/TPO Coupled with MS and Potentiometric Detection and by XPS. *Fuel Processing Technology,* **85**(4), 267–277.

[84] Mullens, S., Yperman, J., Reggers, G., Carleer, R., Buchanan, A. C., Britt, P. F., Rutkowski, P., and Gryglewicz, G. (2003) A Study of the Reductive Pyrolysis Behaviour of Sulphur Model Compounds. *Journal of Analytical and Applied Pyrolysis,* **70**(2), 469–491.

[85] Rocha, J. D., Brown, S. D., Love, G. D., and Snape, C. E. (1997) Hydropyrolysis: A Versatile Technique for Solid Fuel Liquefaction, Sulphur Speciation and Biomarker Release. *Journal of Analytical and Applied Pyrolysis,* **40-41**, 91–103.

[86] Wang, X., Guo, H., Liu, F., Hu, R., and Wang, M. (2016) Effects of CO2 on Sulfur Removal and Its Release Behavior during Coal Pyrolysis. *Fuel,* **165**, 484–489.

[87] Yang, N., Guo, H., Lei, Y., Zhang, Y., Wang, M., Liu, F., Hu, R., and Hu, Y. (2019) XAS Combined with Py-GC Study on the Effects of Temperatures and Atmospheres on Sulfur Release and Its Transformation Behavior during Coal Pyrolysis. *Fuel,* **250**, 373–380.

[88] Jurado, N., Darabkhani, H. G., Anthony, E. J., and Oakey, J. E. (2014) Oxy-Combustion Studies Into the Co –Firing of Coal and Biomass Blends: Effects on Heat Transfer, Gas and Ash Compositions. *Energy Procedia,* **63**, 440–452.

[89] Zhang, Y., Liang, P., Jiao, T., Wu, J., and Zhang, H. (2017) Effect of Foreign Minerals on Sulfur Transformation in the Step Conversion of Coal Pyrolysis and Combustion. *Journal of Analytical and Applied Pyrolysis,* **127**, 240–245.

[90] Stanger, R. and Wall, T. (2011) Sulphur Impacts during Pulverised Coal Combustion in Oxy-Fuel Technology for Carbon Capture and Storage. *Progress in Energy and Combustion Science,* **37**(1), 69–88.

[91] Yan, R., Gauthier, D., Flamant, G., and Badie, J. (1999) Thermodynamic Study of the Behaviour of Minor Coal Elements and Theiraffinities to Sulphur during Coal Combustion. *Fuel,* **78**(15), 1817–1829.

[92] Carpenter, A. M. and Skorupska, N. M. (1993) Coal Combustion - Analysis and Testing, IEA Coal Research, London.

[93] Steer, J. M., Marsh, R., Morgan, D., and Greenslade, M. (2015) The Effects of Particle Grinding on the Burnout and Surface Chemistry of Coals in a Drop Tube Furnace. *Fuel,* **160**, 413–423.

[94] Steer, J. M., Marsh, R., Greenslade, M., and Robinson, A. (2015) Opportunities to Improve the Utilisation of Granulated Coals for Blast Furnace Injection. *Fuel,* **151**, 40–49.

[95] Sexton, D. C., Steer, J. M., Marsh, R., and Greenslade, M. (2018) Investigating Char Agglomeration in Blast Furnace Coal Injection. *Fuel Processing Technology,* **178**, 24–34.

[96] Davies-Smith, C. A., Steer, J. M., Marsh, R., and Morgan, D. (2022) A study of the volatilisation of coal sulphur during combustion under conditions similar to a blast furnace raceway. *Fuel,* **330**, 125552.

[97] Shen, Y., Hu, Y., Wang, M., Bao, W., Chang, L., and Xie, K. (2021) Speciation and Thermal Transformation of Sulfur Forms in High-Sulfur Coal and Its Utilization in Coal-Blending Coking Process: A Review. *Chinese Journal of Chemical Engineering,* **35**, 70–82.

[98] Schwab, G.-M. and Philinis, J. (1947) Reactions of Iron Pyrite: Its Thermal Decomposition, Reduction by Hydrogen and Air Oxidation. *Journal of the American Chemical Society,* **69**(11), 2588–2596.

[99] Maes, I. I., Yperman, J., Mullens, J., and Poucke, L. C. V. (1995) Study of Coal-Derived Pyrite and Its Conversion Products Using Atmospheric Pressure Temperature-Programmed Reduction. *Energy & Fuels,* (9), 950–955.

[100] Bergholm, A., (1995) Oxidation of Pyrite. Technical Report 95-389, U.S. Geological Survey Boulder, Colorado.

[101] Siow, K., Britcher, L., Kumar, S., and Griesser, H. (2018) XPS Study of Sulfur and Phosphorus Compounds with Different Oxidation States. *Sains Malaysiana,* **47**(8), 1913–1922.

[102] Li, P.-S., Hu, Y., Yu, W., Yue, Y.-N., Xu, Q., Hu, S., Hu, N.-S., and Yang, J. (2009) Investigation of Sulfur Forms and Transformation during the Co-Combustion of Sewage Sludge and Coal Using X-ray Photoelectron Spectroscopy. *Journal of Hazardous Materials,* **167**(1), 1126–1132.

[103] Li, W., Shen, Y., Guo, J., Kong, J., Wang, M., and Chang, L. (2021) Effects of Additives on Coke Reactivity and Sulfur Transformation dur-

ing Co-pyrolysis of Long Flame Coal and High-Sulfur Coking Coal. *ACS Omega,* **6**(50), 34967–34976.

[104] Sexton, D. C. (2019) Coal Agglomeration in Blast Furnace Injection Coals PhD thesis Cardiff University School of Engineering Cardiff.

[105] Karunadasa, K. S. P., Manoratne, C. H., Pitawala, H. M. T. G. A., and Rajapakse, R. M. G. (2019) Thermal Decomposition of Calcium Carbonate (Calcite Polymorph) as Examined by in-Situ High-Temperature X-ray Powder Diffraction. *Journal of Physics and Chemistry of Solids,* **134**, 21–28.

[106] McIntosh, R. M., Sharp, J. H., and Wilburn, F. W. (1990) The Thermal Decomposition of Dolomite. *Thermochimica Acta,* **165**(2), 281–296.

[107] Valverde, J. M., Perejon, A., Medina, S., and Perez-Maqueda, L. A. (2015) Thermal Decomposition of Dolomite under CO2: Insights from TGA and in Situ XRD Analysis. *Physical Chemistry Chemical Physics,* **17**(44), 30162–30176.

[108] Fantauzzi, M., Elsener, B., Atzei, D., Rigoldi, A., and Rossi, A. (2015) Exploiting XPS for the Identification of Sulfides and Polysulfides. *RSC Advances,* **5**(93), 75953–75963.

[109] Demri, B. and Muster, D. (1995) XPS Study of Some Calcium Compounds. *Journal of Materials Processing Technology,* **55**(3-4), 311–314.

[110] Grosvenor, A. P., Kobe, B. A., Biesinger, M. C., and McIntyre, N. S. (2004) Investigation of Multiplet Splitting of Fe 2p XPS Spectra and Bonding in Iron Compounds. *Surface and Interface Analysis,* **36**(12), 1564–1574.

[111] XPS Spectra. http://www.casaxps.com/help_manual/manual_updates/xps_spectra.pdf.

[112] Osokina, A. A., Zhuravleva, N. V., Potokina, R. R., Ismagilov, Z. R., Lazarevskiy, P. P., Romanenko, Y. E., and Tsiple, O. L. (2017) Products of Coal Pyrolysis. *Coke and Chemistry,* **60**(12), 476–484.

[113] Xia, X., Zhao, X., Zhou, P., Feng, T., Ma, C., and Song, Z. (2020) Reduction of SO2 to elemental sulfur with carbon materials through electrical and microwave heating methods. *Chemical Engineering and Processing - Process Intensification,* **150**, 107877.

[114] Sarna, S. K. Coal for Pulverized Coal Injection in Blast Furnace – IspatGuru. https://www.ispatguru.com/coal-for-pulverized-coal-injection-in-blast-furnace/.

[115] Sarna, S. K. Non Coking Coal for Iron Production – IspatGuru. https://www.ispatguru.com/non-coking-coal-for-iron-production/.

[116] Sarna, S. K. Pulverized Coal Injection in a Blast Furnace – IspatGuru. https://www.ispatguru.com/pulverized-coal-injection-in-a-blast-furnace/.

[117] Sarna, S. K. Understanding Blast Furnace Ironmaking with Pulverized Coal Injection – IspatGuru. https://www.ispatguru.com/understanding-blast-furnace-ironmaking-with-pulverized-coal-injection/.

[118] Sarna, S. K. Understanding Pulverized Coal Injection in Blast Furnace – IspatGuru. https://www.ispatguru.com/understanding-pulverized-coal-injection-in-blast-furnace/.